Momentum transfer of laser radiation to inhomogeneous dielectrics

Author:
Lawrence, Vincent Ferrer

Publication Date:
1978

DOI:
https://doi.org/10.26190/unsworks/7381

MOMENTUM TRANSFER OF LASER RADIATION TO INHOMOGENEOUS DIELECTRICS

VINCENT FERRER LAWRENCE, B.Sc. (Hons) U.N.S.W

Thesis submitted for the degree of

DOCTOR OF PHILOSOPHY

in the Faculty of Science,

University of New South Wales.

March, 1978

TABLE OF CONTENTS

Abstract

This thesis explores the transfer of laser light radiation into inhomogeneous dielectrics. We assume that the dielectric interacts initially with a laser prepulse to form a specified initial plasma density profile. The main pulse of laser radiation will then impinge on the plasma. The motivation of this thesis is to study, explore and understand the development of the laser light radiation into the plasma especially at times shorter than the electron ion thermal equilibration time when the transfer of energy is due to the nonlinear force which is the immediate electrodynamic interaction.

The mechanics of the plasma are governed by conservation laws of continuity, momentum and energy. The state of the plasma may be described as a two temperature, one fluid model where electron-ion thermalisation and implicit temperature solutions of the energy equations are taken into account. A one dimensional finite differencing scheme is employed to simulate the velocities, densities, ion and electron temperatures of the plasma and the electromagnetic energy density of the laser pulse in the plasma.

To transfer large amounts of laser energy into the plasma, low reflectivity of the plasma is required. The inhomogeneous Rayleigh profile satisfies this requirement The reason for work done with the Rayleigh profile was twofold. The low reflectivity of that profile and the available exact solutions for the electromagnetic fields.

It was hoped to use the Rayleigh profiles with exact solutions for approximations of the density profile instead of linear step approximations. In the course of work it was discovered that discrepancies occurred between the exact and high order approximations of reflections, a paradox which is seen as similar to Osterberg's generation of local reflectivity and a radiation law for plane waves was suggested.

The approximation of plasma density by the Rayleigh profiles together with the exact solutions add further problems to the complex simulation of laser plasma interactions and as the plasma densities vary with time, small step linear approximations though not exact were adequate to describe the interactions.

The finite difference scheme solves the conservation equations including the effects of the nonlinear force and the nonlinear change of the optical constants depending on intensity. The fully dynamical nonlinear scheme at times shorter than the electron ion thermalisation time displayed the following.

The generation of instabilities as well as the supression of instabilities by varying the initial density profile. The formation of standing waves at the cut off density was observed. By varying the value of α the existence of block like motion of plasma was verified due to the nonlinear force from a solitary electromagnetic energy wave called a soliton.

The ablating plasma generated by the soliton showed the existence of a density minimum called a caviton occurring at times of picoseconds corresponding to experimental evidence observing cavitons ablating at times of nanoseconds.

The behaviour of the absorption of laser light at different temperatures due to collisional effects was demonstrated.

Efficient nonthermalised transfer of energy was seen by the development of the soliton into the plasma, so that the nonlinear force scheme makes possible compression of plasma by nonthermal dynamically collisionless absorption of radiation. Intensity thresholds at 10^{13}-10^{14} W/cm^2 for Nd glass lasers appeared for both changes in gradients of the electron temperatures and the nonlinear transfer of energy, corresponding to the predominance of the nonlinear force over thermokinetic force. Evaluation was made of the transfer of energy E_k into the plasma for different intensities I expressing a nonlinear relationship for the range of intensities from 5×10^{15} W/cm^2 to 10^{18} W/cm^2 resulting in $E_k \alpha I^{1.8}$

Confirmation was made of recently observed experiments satisfying the relationship $I^2\lambda$ where λ is the wave length of laser light radiation. The gas dynamic model is inadequate to explain the experimentally observed phenomena. The inclusion of the nonlinear force verifies the wave length intensity dependence.

Acknowledgement

Sincere appreciation and gratitude to Professor Heinrich Hora who has been far more than a thesis adviser but a friend and companion who always found the time to give help and advice to me.

Discussions with E.L. Kane, Dr. M.B. Nicholson-Florence, M.N. Novak P.S.Ray, R. Castillo, M. Read, J. Adler, J. Ho, R. Sutherland, A.Professor J. Oitmaa, J. Shepanski, Dr. D.N. Lowy, are gratefully acknowledged. Sincere thanks go to all members of the School of Physics, U.N.S.W., who have made the effort of creating an environment both pleasant and condusive for research. Special thanks to Miro Novak and Ed Kane, travelling companions who put up with my cooking while away on conferences. Credit goes to Deidre Watt for the excellent typing done on this manuscript.

For the love and patience, shown to me all these years I thank my parents, Mr. and Mrs. W.M. Lawrence.

The work done on the thesis was supported by the Australian Research Grants Commission grant no. B75/15538.

Chapter 1 Introduction

The increasing energy requirements of the world and the diminishing supply of petroleum means that there must be an alternative for the supply of the world's energy needs. One of these alternatives is the compression of plasmas by lasers, releasing energy by thermonuclear reactions such as

$$H + {}^{11}B \rightarrow 3\ {}^{4}He + 8.9\ \text{Mev}$$ [1]

$$D + D \rightarrow {}^{3}He + n + 3.27\ \text{Mev}$$ [2]

$$\searrow T + p + 4.03\ \text{Mev}$$

$$D + T \rightarrow {}^{4}He + n + 17.8\ \text{Mev}$$

Basov and Krokhin[3] were the first to publish a paper on the production of a high density, high temperature plasma by the interaction of laser radiation with a pellet of solid Hydrogen, predicting thermonuclear reactions. Further calculations appeared by Dawson[4] and the first optimized reaction yields were due to Hora[4]. Afanasyev and Krokhin[5] analysed laser plasma interactions based on gas dynamic equations. Incident laser intensity flux densities in the range of 10^6 W/cm^2 to 10^9 W/cm^2 predicted two separate mechanisms. At the low range of flux densities, the material vaporised by the laser beam expands as a centred rarefaction wave, corresponding to an isentropic expansion of gas in a vacuum. At the high range of flux densities the thermal pressure causes the material to expand and becomes transparent to incident radiation. Subsequent research on laser plasma interactions were described by such a gas dynamic scheme where the plasma interacting with laser radiation behaved as vaporised matter. Nuckolls[6] numerically simulated spherical implosions of plasma by laser pulses shaped in time and obtained very high compressions of plasma. The generated compression of plasma by thermal pressure is due to a collision produced absorption of laser light. The compression of plasma is compensated by a density decreasing monotonically as a thermokinetic expansion of plasma. The energy dissipated by the scheme due to ablation of plasma, thermalisation and reflection of neodymium laser light transfers 5% of the incident laser energy into the plasma.

At low levels of laser intensities, less than 10^{10}W/cm^{2} for Nd glass lasers inverse bremsstrahlung was the basic mechanism of absorption of laser light. Experimental measurements of absorption[7] of laser light at higher flux densities showed that this mechanism fails to predict absorption levels at the higher intensities. The optical constants are affected by nonlinear effects at the higher laser intensities, proportional to the inverse of the intensity to the power of three halves as derived by Rand[8] and Hora[9] from different considerations. Nonlinear effects together with the change of the optical constant partially solves the observed dilemma.

It has long been known that the decay of photons into a homogeneous plasma can form plasma waves (plasmons or Langmuir waves) or ion waves. Scattering of these waves may lead to Raman or Brillouin scattering instabilities. Each specific instability occurring at their individual characteristic intensity threshold can be described as occurring due to the nonlinear force of a purely electrodynamic interaction between the laser field and the plasma.

F.F. Chen[10] derived the parametric instabilities on the basis of the nonlinear force only and accounts for induced anomalous high frequency resistivity.

Other nonlinear processes are exhibited in other ways, namely

- the nonlinear change of the collision frequency[11]
- relativistic correction to the plasma frequency[12]
- coupling of transverse mode waves with longitudinal waves[13]
- self focussing at low power threshold[14]
- self focussing at high relativistic intensity[15]
- two stream instabilities[16]
- anomalous absorption at the cut off density[17]
- high energy x radiation and directly back scattered radiation[18]

Each of the above anomalies occurs at its specific power threshold or at high incident flux densities from 10^{13} to 10^{16} W/cm^2 for Nd glass lasers. Some processes can occur within a time of picoseconds as the generation of fast plasmas with ion energies of the order of Mev[19].

The inclusion of the nonlinear force into the gas dynamic scheme, results in the generation of self steepening of the density profile and generation of density minima in the ablating plasma discovered first numerically by Shearer, Kidder and Zink[20]. This corresponded to observations made by microwave experiments by Wong and Stenzel[21]. Further laser plasma experimental observations of density minima by Zakharenkov[22], Azechi[23], Fedosejevs[24], described the mechanism as due to the nonlinear force.

Acting at times shorter than the electron ion thermal equilibration time, by suitable choice of an initial density profile reducing reflectivity, the nonlinear force scheme can transfer a large percentage of the laser energy into the plasma. The inhomogeneous Rayleigh plasma exhibits low reflectance of laser radiation and by suitable arrangement of the density profile fifty percent of the laser energy may be transferred to the compressed block of plasma. By conservation of momentum fifty percent of the energy is lost through the ablating block of plasma. The dynamic description and simulation of the plasma in this thesis including the equations governing the gas dynamic scheme together with the nonlinear force and the nonlinear corrections to the optical constants verifies that fifty percent of the laser energy can be transferred to the plasma at times less than the electron ion thermal equilibration time.

The fusion reaction gain G based on numerically optimised calculations at optimum temperatures using empirical data on nuclear reaction cross sections and simplified assumptions without secondary processes such as reheat is given by[25]

$$G = \left(\frac{E_o}{E_{b\bar{e}}}\right)^{1/3} \left(\frac{n_o}{n_s}\right)^{2/3}$$

where E_o is the input energy, E_{be} the breakeven energy n_o is the initial ion density and n_s the solid state density. A change in E_o for the input laser energy increasing in efficiency of transfer from 5 to 50% due to the different schemes corresponds to an equivalent fusion gain of 1000 times less laser energy.

In this thesis we explore the transfer of momentum into the plasma from a laser pulse of varying intensities by a one dimensional plane wave code allowing for electron and ion thermal equilibration. This is necessary especially at short times when the two temperatures of the ions and electrons are different, justifying the use of a two temperature model. We assume a one fluid model where Debye shielding effects guarantee quasineutrality of the plasma. The usual gas dynamic scheme and the hydrodynamic equations include the nonlinear force and the corrections to the optical constants by the nonlinear force.

The importance of the action of the nonlinear force, especially for short laser pulses consists of the possibility of a non thermalising transfer of optical energy into kinetic energy of plasma for compression, which has a minimum of entropy production and is therefore highly efficient.

In chapter 2 investigations are made of the occurrence of low reflectivities of inhomogeneous plasma especially for Rayleigh like density profiles by analytical and approximate methods. The resulting inaccuracy of the step approximation compared with that of using the Rayleigh profile for the exact analytical results was seen to be futile for the approximation of absorption in laser plasma simulation. Nevertheless it was shown that discrepancies between exact results and step wise approximations exists. This approximation method allows estimation of local generation of reflectivities.

The discussion of the nonlinear force follows in chapter 3. The derivation of the nonlinear force and the formation of solitons and cavitons due to the nonlinear force by theoretical calculations and experimental observations are discussed. The characteristics of those observations are reproduced by the code in the results section. In chapter 4 we analyse the theory of the optical constants by various methods and note that the collision frequency and hence the absorption coefficient of a plasma are nearly equivalent whether we use a classical or quantum mechanical approach. The optical constants are replaced to include nonlinear effects due to intense laser radiation. In chapter 5 we discuss the assumptions of the model and describe the equations governing the change of velocities, densities, electron and ion temperatures, derived from conservation laws. The nonlinear optical constants and nonlinear force terms are included in the one dimensional plane wave gas dynamic code as described.

By the use of a Rayleigh density profile with the property of having low reflectivities near the cut off density, will suppress standing wave patterns. The soliton so formed will force block like motion of plasma, as suggested from implications of the nonlinear force, causing a high percentage of energy transferred into the plasma. The simulations seen initially in chapter 6 at times of 10^{-13}sec verify that blocks of non-thermalised plasmas are compressed. The general code was then extended to times of picoseconds and the results of the interactions with generalisation of energy transfer by the nonlinear force scheme and interactions at different laser light wavelengths were compared confirming very recent experimental results.

CHAPTER 2 REFLECTIVITIES

The numerical work of laser interactions with plasmas is involved with the problems of solving electromagnetic waves in inhomogeneous media. It is well known that experimental data of the reflectivity of laser irradiated targets scatter over orders of magnitudes from 0.1% to 60%, occurring at irradiances[1] for which the usually assumed nonlinear effects and parametric instabilities may not be effective. If not, self-focussing[2] is the reason for the confusing variety of the experimental results. Numerical calculations, assuming one dimensional geometry of plane incidence of the radiation, arrive at reflectivities of 70% and more[1,3] where a direct solution of the Maxwellian equations or an approximation by step-like (homogeneous) layers is being used.

The problem of the non-existence of a local generation of reflectivity within the inhomogeneous medium has been discussed very generally by Osterberg[4], where the use of only two solutions of the wave equation, one for the penetrating and one for the reflected wave with a constant ratio of their amplitudes excluded the aspect of "local generations of reflectivity". The same result has been derived before by discussing the special case of a medium with a Rayleigh-like density profile[5]. One of these results, the very low reflectivity generated at the continuous connection of a homogeneous medium with a Rayleigh profile as well as Osterberg's non-existence of a local generation of reflectivity will be of interest for discussing the measured values of low reflectivity from laser produced plasmas.

Before using the mentioned methods of low reflectivity in numerical codes, we have discussed some very simple, Rayleigh-like cases which permit very transparent, mathematically exact results.

The comparison of numerical calculations with stepwise approximation and exact calculations of reflectivity at the interfaces results in a much higher reflectivity for a small number of steps. Computing the case for a large number of steps will result in values close to exact calculations, however, there is still some discrepancy which can only be considered as a paradox as numerical inaccuracies and instabilities have been excluded.

I The Inhomogeneous Rayleigh Profile

Let us first describe an inhomogeneous plasma by what we shall call a Rayleigh density profile, whose complex refractive index $\underline{n}$ is given by

$$\underline{n} = \frac{1}{1 + \underline{a}\, x} \tag{1}$$

where $\underline{a}$ is any complex number and x the depth of a one dimensional medium. Allowing $\underline{a}$ to be equal to $\alpha + i\beta$ where α, β are real quantities we obtain

$\underline{n} = n + iK$ where

$$n = \frac{\alpha x + 1}{(\alpha x+1)^2 + \beta^2 x^2} \qquad K = \frac{-\beta x}{(\alpha x+1)^2 + \beta^2 x^2} \tag{2}$$

n, K are known as the refractive index and absorption coefficient respectively. If $\beta = 0$ then n reduces to $\frac{1}{1 + \alpha x}$ and K reduces to 0, which is the description for a collisionless plasma. It is known that for a collisionless plasma where the collision frequency ν is equal to 0 we have

$$n = \left(1 - \frac{\omega_p^2}{\omega^2}\right)^{\frac{1}{2}} \tag{3}$$

Equating expression (3) with the expression of the Rayleigh profile (2) allowing $\beta = 0$ we obtain

$$\omega_p^2 = \omega^2 \left(1 - \left(\frac{1}{1 + \alpha x}\right)^2\right) \tag{4}$$

which corresponds to an electron density n_e,

$$n_e = n_{ec} \left(1 - \left(\frac{1}{1 + \alpha x}\right)^2\right) \tag{5}$$

since the plasma frequency ω_p is given by

$$\omega_p^2 = \frac{4\pi e^2 n_e}{m_e} \tag{6}$$

where e is the electron charge, m_e the electron mass, n_{ec} the cut off density (the electron density n_e in eq. (6) corresponding to $\omega = \omega_p$). Let us now look at a one dimensional, collisionless, inhomogeneous plasma with a Rayleigh like profile given by

$$n = \frac{1}{1 + \alpha x} \tag{7}$$

whose electron density corresponds to equation (5). The propagation of electromagnetic waves in inhomogeneous plasma is described in terms of the electric vector $\underline{E}$, the magnetic vector $\underline{H}$, the dielectric constant ε, the magnetic permeability μ and the electrical conductivity Θ by

Maxwell's equations, (assuming $\Theta = 0$)

$$\nabla \times \underline{E} = -\mu\mu_o \frac{\partial \underline{H}}{\partial t} \tag{8a}$$

$$\nabla \times \underline{H} = \varepsilon\varepsilon_o \frac{\partial \underline{E}}{\partial t} \tag{8b}$$

We are limiting the case to propagation only in the x direction at perpendicular incidence so that the x component of the high frequency part of $\underline{E}$ and $\underline{H}$ are zero. We can describe the electromagnetic fields with frequency ω as

$$\underline{E}\ (x) = E_Y\ (x) \exp\ (-i\omega t) \tag{9a}$$

$$\underline{H}\ (x) = H_z\ (x) \exp\ (-i\omega t) \tag{9b}$$

Because of perpendicular incidence [6] we can have

$$\text{div}\ (\varepsilon\varepsilon_o \underline{E}) = 0 \tag{9c}$$

$$\text{div}\ (\mu\mu_o \underline{H}) = 0 \tag{9d}$$

From equation (8a) and (8b) we have (assume $\mu = 1$)

$$-\frac{\partial}{\partial x} E_y(x) = \pm\ i\omega\mu_o H_z(x) \tag{10a}$$

$$-\frac{\partial}{\partial x} H_z(x) = \pm\ i\omega\varepsilon\varepsilon_o E_y(x) \tag{10b}$$

combining eqs. (10a) and (10b) we obtain

$$\frac{\partial^2}{\partial x^2} E_y(x) + \omega^2\mu_o\ \varepsilon_o\ \varepsilon\ E_y\ (x) = 0 \tag{10c}$$

For the Rayleigh profile case, the dielectric constant is given by

$$\varepsilon(x) = \frac{1}{(1 + \alpha x)^2}$$

so that (10c) reduced to

$$\frac{d^2}{dx^2} E_y\ (x) + \frac{\omega^2}{c^2\ (1 + \alpha x)^2}\ E_y\ (x) = 0 \tag{11}$$

Let $\zeta = 1 + \alpha x$ and $\frac{k^2}{4} = \frac{\omega^2 \varepsilon}{c^2\ \alpha^2}$, then eq. (11) reduces to an Euler differential equation

$$\zeta^2 \frac{d^2 E_y(\zeta)}{d\zeta^2} + \frac{k^2}{4} E_y(\zeta) = 0 \tag{11a}$$

with a solution $E_y(x) = (1 + \alpha x)^{\lambda}$ we obtain

$$E_y(x) = (1 + \alpha x)^{\frac{1}{2}} \exp\left(\pm i \ln(1 + \alpha x) \sqrt{\frac{\omega^2}{c^2\alpha^2} - \frac{1}{4}}\right) \tag{12}$$

using (10a) we obtain for the magnetic field

$$H_z(x) = \pm \left(\sqrt{\frac{\varepsilon_o}{\mu_o} - \frac{\alpha^2}{4\omega^2\mu_o^2}} - \frac{i\alpha}{2\omega\mu_o} \right) (1 + \alpha x)^{-\frac{1}{2}}$$

$$\exp\left(\pm i \ln(1 + \alpha x) \sqrt{\frac{\omega^2}{c^2\alpha^2} - \frac{1}{4}}\right) \tag{13}$$

II The Rayleigh like plasma between two homogeneous media

The solutions (12) and (13) have a singularity at $x = -\frac{1}{\alpha}$. We can use these Rayleigh like solutions to describe both propagating and reflected waves depending on the ± sign. The + sign will be for a propagating wave and the - sign for the reflected wave. Calculations can then be made with appropriate complex amplitudes (integration constants) of the Reflection coefficients at a vacuo-inhomogeneous plasma barrier described by the Rayleigh density profile, Figure 1.

We have the following conditions for Figure 1.

Medium I	$x \leq 0$	$n = n_v = 1$	(14a)
Medium II	$0 < x < D$	$n = \frac{1}{1 + \alpha x}$	(14b)
Medium III	$D \leq x$	$n = \text{constant} = \frac{1}{1 + \alpha D}$	(14c)

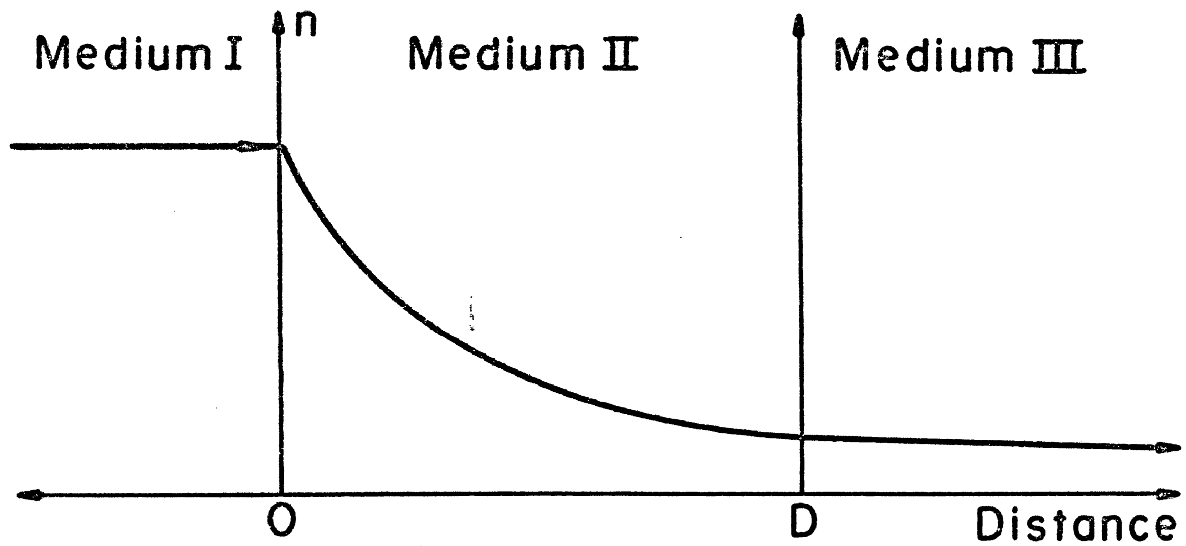

Fig. 1

The schematic dependence on distance x of the refractive index n for connections of homogeneous media I and III with an inhomogeneous Rayleigh like density profile.

In Medium III we can describe the components of the electric and magnetic fields by plane waves so that

$$E_3 = C_{3+} \exp\left(i(n_3 \frac{\omega}{c} x - \omega t)\right) + C_{3-} \exp\left(-i(n_3 \frac{\omega}{c} x + \omega t)\right) \quad (15a)$$

$$H_3 = C_{3+} \left(\frac{\varepsilon_o}{\mu_o}\right)^{\frac{1}{2}} n_3 \exp\left(i(n_3 \frac{\omega}{c} x - \omega t)\right)$$

$$- C_{3-} \left(\frac{\varepsilon_o}{\mu_o}\right)^{\frac{1}{2}} n_3 \exp\left(-i\,(n_3 \frac{\omega}{c} x + \omega t)\right) \quad (15b)$$

where the subscript denotes the medium and the constants C_+, C_- the transmission and reflection coefficients respectively. At $x = D$ we describe only the transmitted waves and not reflected waves in Medium III by specifying $C_{3+} = 1.0$, $C_{3-} = 0.0$, we then have for Medium III $(t = 0)$

$$E_3 = \exp\left(i n_3 \frac{\omega}{c} D\right) \quad (16)$$

$$H_3 = \left(\frac{\varepsilon_o}{\mu_o}\right)^{\frac{1}{2}} n_3 \exp i \frac{\omega}{c} n_3 D \quad (17)$$

In Medium II from equations (12) and (13) the components of the E and H fields are $(t = 0)$

$$E_{2+} = C_{2+} (1 + \alpha x)^{\frac{1}{2}} \exp\left(i\left(\frac{\omega^2}{c^2\alpha^2} - \frac{1}{4}\right)^{\frac{1}{2}} \ln(1 + \alpha x)\right) \quad (18)$$

$$E_{2-} = C_{2-} (1 + \alpha x)^{\frac{1}{2}} \exp\left(-i\left(\frac{\omega^2}{c^2\alpha^2} - \frac{1}{4}\right)^{\frac{1}{2}} \ln(1 + \alpha x)\right) \quad (19)$$

$$H_{2+} = C_{2+} (1 + \alpha x)^{-\frac{1}{2}} \left(\left(\frac{\varepsilon_o}{\mu_o} - \frac{\alpha^2}{4\omega^2 \mu_o^2}\right)^{\frac{1}{2}} - \frac{i\alpha}{4\omega\mu_o} \right)$$

$$\exp\left(i \left(\frac{\omega^2}{c^2} - \frac{1}{4}\right)^{\frac{1}{2}} \ln (1 + \alpha x)\right) \quad (20)$$

$$H_{2-} = C_{2-} (1 + \alpha x)^{-\frac{1}{2}} \left(- \left(\frac{\varepsilon_o}{\mu_o} - \frac{\alpha^2}{4\omega^2 \mu_o^2}\right)^{\frac{1}{2}} + \frac{i\alpha}{2\omega\mu_o} \right)$$

$$\exp\left(-i\left(\frac{\omega^2}{c^2} - \frac{1}{4}\right)^{\frac{1}{2}} \ln (1 + \alpha x)\right) \quad (21)$$

The boundary conditions at the interfaces can be derived for $t = 0$. At the junctions of Medium II and III we have for $x = D$

$$E_{2+} + E_{2-} = E_3 \tag{22a}$$

$$H_{2+} + H_{2-} = H_3 \tag{22b}$$

It is then algebraically possible to solve for the reflection and transmission coeffieients of Medium II, C_{2+} and C_{2-}. For waves in Medium I where n = 1.

$$E_1 = C_{1+} \exp\left(i\left(\frac{\omega}{c} n_1 x - \omega t\right)\right) + C_{1-} \exp\left(-i\left(\frac{\omega}{c} n_1 x + \omega t\right)\right) \tag{23}$$

$$H_1 = C_{1+} n_1 \left(\frac{\varepsilon_o}{\mu_o}\right)^{\frac{1}{2}} \exp\left(i\left(\frac{\omega}{c} n_1 x - \omega t\right)\right)$$

$$- C_{1-} n_1 \left(\frac{\varepsilon_o}{\mu_o}\right)^{\frac{1}{2}} \exp\left(-i\left(\frac{\omega}{c} n_1 x + \omega t\right)\right) \tag{24}$$

At the junction of Medium I and Medium II where x = 0 at t = 0

$$E_1 = C_{1+} + C_{1-} \tag{25}$$

$$H_1 = C_{1+} n_1 \left(\frac{\varepsilon_o}{\mu_o}\right)^{\frac{1}{2}} - C_{1-} n_1 \left(\frac{\varepsilon_o}{\mu_o}\right)^{\frac{1}{2}} \tag{26}$$

$$E_2 = C_{2+} + C_{2-} \tag{27}$$

$$H_2 = C_{2+} \left(\left(\frac{\varepsilon_o}{\mu_o} - \frac{\alpha^2}{4\omega^2 \mu_o^2}\right)^{\frac{1}{2}} - \frac{i\alpha}{2\omega\mu_o}\right)$$

$$+ C_{2-} \left(-\left(\frac{\varepsilon_o}{\mu_o} - \frac{\alpha^2}{4\omega^2 \mu_o^2}\right)^{\frac{1}{2}} + \frac{i\alpha}{2\omega\mu_o}\right) \tag{28}$$

Equating

$$E_1 = E_2 \tag{29}$$

$$H_1 = H_2 \tag{30}$$

we obtain

$$R = \frac{(\frac{\varepsilon_o}{\mu_o})^{\frac{1}{2}} E_2 - H_2}{(\frac{\varepsilon_o}{\mu_o})^{\frac{1}{2}} E_2 + H_2} \tag{31}$$

where R is the reflection coefficient of the amplitudes as an exact solution depending on both α and D. This result is equivalent to the general result obtained by Wait[8] using a different method.

III Approximation by Steps of Homogeneous media

We are now approximating the case of Figure 1 by a series of homogeneous media with a stepwise decreasing refractive index n in the Rayleigh Medium II. With reference to Figure 1 and the same restrictions of equation (14), equations (15) to (17) remain the same for Medium III. In Medium II, however, using plane wave approximations at t = 0 we obtain in the first order single step approximation with $n_2 = (n_1 + n_3)/2$

$$E_2 = C_{2+} \exp (in_2 \frac{\omega}{c} x) + C_{2-} \exp (-in_2 \frac{\omega}{c} x) \tag{32}$$

$$H_2 = C_{2+}n_2 (\frac{\varepsilon_o}{\mu_o})^{\frac{1}{2}} \exp (in_2 \frac{\omega}{c} x)$$

$$- C_{2-}n_2 (\frac{\varepsilon_o}{\mu_o})^{\frac{1}{2}} \exp (-in_2 \frac{\omega}{c} x) \tag{33}$$

For higher approximations we can use $n_2^i = (n_2^{i+1} + n_2^i)/2$ where i denotes the homogeneous slab number depending on the number of steps. It is then possible to calculate the reflectivity from the conditions of Medium III back to

Medium I where the refractive index $n_2(x)$ in Medium II is given by the Rayleigh case. It is necessary to note that in using step approximations the refractive index varies depending on number of steps used. For each step beginning at distance D we calculate the values of C_{2+}, C_{2-} and use these as a basis for the next step approximation till $x = 0$.

We write here the analytical result of the first approximation. For Medium I we have for $n = 1$, $t = 0$;

$$E_1 = C_{1+} \exp\left(i \frac{\omega}{c} x\right) + C_{1-} \exp\left(-i \frac{\omega}{c} x\right) \tag{34}$$

$$H_1 = C_{1+} \left(\frac{\varepsilon_o}{\mu_o}\right)^{\frac{1}{2}} \exp\left(i \frac{\omega}{c} x\right) - C_{1-} \left(\frac{\varepsilon_o}{\mu_o}\right)^{\frac{1}{2}} \exp\left(-i \frac{\omega}{c} x\right) \tag{35}$$

At the junction of Medium I and Medium II where $x = 0$, $n = 1$ and $t = 0$

$$C_{1+} + C_{1-} = C_{2+} + C_{2-} \tag{36}$$

$$C_{1+} - C_{1-} = n_2 C_{2+} - n_2 C_{2-} \tag{37}$$

so that

$$R = \frac{C_{1+}}{C_{1-}} = \frac{(1 + n_2)\, C_{2+} + (1 - n_2)\, C_{2-}}{(1 - n_2)\, C_{2+} + (1 + n_2)\, C_{2-}} \tag{38}$$

IV Numerical Results

The following calculations were performed for a set of cases, where the Rayleigh parameter α was set constant (for a wavelength $\lambda = 1.06$ μm corresponding to the wavelength of neodymium glass laser radiation) and the thickness D of the Rayleigh medium was varied. Figure 2

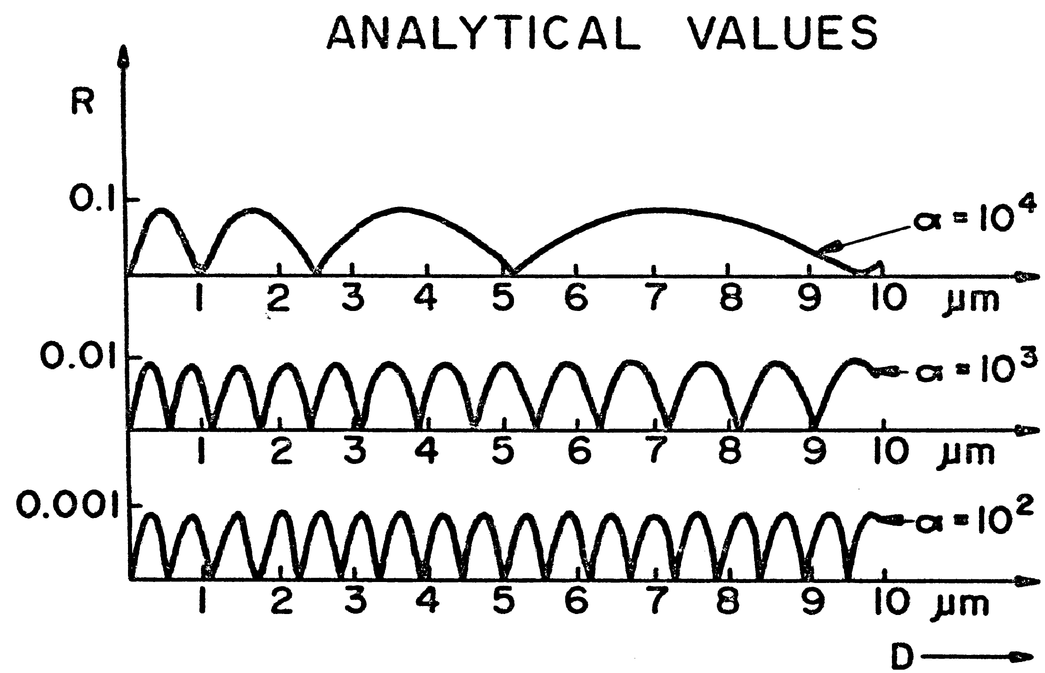

Fig. 2

Reflectivity R depending on the distance D of the Rayleigh like plasma interface between homogeneous plasmas, described in figure 1. The parameter α determines the refractive index n from eq. (7). The computed values of analytical solutions for the reflectivity, eq. (31) is shown for the decreasing refractive index as α increases.

shows the results, where the abscissa gives D in cm and the ordinate the reflectivity. It is obvious, that we find an oscillation of the reflectivity R with zero values at such thicknesses D where the phases of the incident and reflected waves in the Rayleigh medium are just cancelling the reflection as known from the interference at the transmission of light through parallel plates. It is evident, that for higher α we have a higher reflectivity. At $\alpha = \frac{2\omega}{c} = 1.18 \times 10^5\ cm^{-1}$ we have total reflection at the discontinuity between the profile and the vacuum,(though the waves are perpendicularly incident) as discussed before[5]. The case of $\alpha \geq \frac{2\omega}{c} = 1.18 \times 10^5 cm^{-1}$ has been excluded in this paper. For cases of higher α, we find a more stretched sequence of the zero points of reflectivity which is immediately evident, as the Medium III has a smaller refractive index at the same distances D for higher α, and therefore a much larger effective wave-length, than for smaller α.

It is remarkable that the maxima of R are of the same height. This is related to the fact that we have no absorption and the reflection is determined only at $x = 0$ and $x = D$. As we know from the Rayleigh case[5] in agreement with the general result of Osterberg[4], the reflection is only determined by α, therefore the maxima are of constant value, though the refractive index of Medium III is monotonically decreasing with increasing D.

For the step-wise approximation, we find for a small number of steps, corresponding minima but increasing maxima with medium thickness D, by orders of magnitudes larger than the exact case. This can be understood from the crude approximation of the refractive index n, which shows the insufficiency of the approximation with few steps. This is hardly surprising as large number of steps imply the use of small mesh sizes which increases the accuracy of calculations.

The numerical calculations with large number of steps (one hundred or one thousand) Figure 3, converges to the exact case. We find then the same reflectivity as in the exact case, the same constancy of the maxima and the corresponding distances of zero reflectivities. On closer observation, however, we find a slight difference: zero reflectivity distances increase for the step wise approximation. Such a "wave-length" effect is of a basic nature. It has been excluded that any numerical inaccuracies or instabilities are involved so we have a definite paradox in the discrepancy of the approximation.

Leaving aside, for the moment, the abovementioned paradox, we can discuss the Osterberg problem in the following manner. It is a mathematical fact that there are two exact linearly independent solutions in the homogeneous medium, whose ratios are the reflectivity determined by the boundaries to the homogeneous media. The condition of only penetrating waves, that is, only transmitted waves in Medium III (no standing waves) and depending on the thickness D determines the phase. This is originally reproduced by the stepwise approximation (apart from the paradox). However, we can follow in the

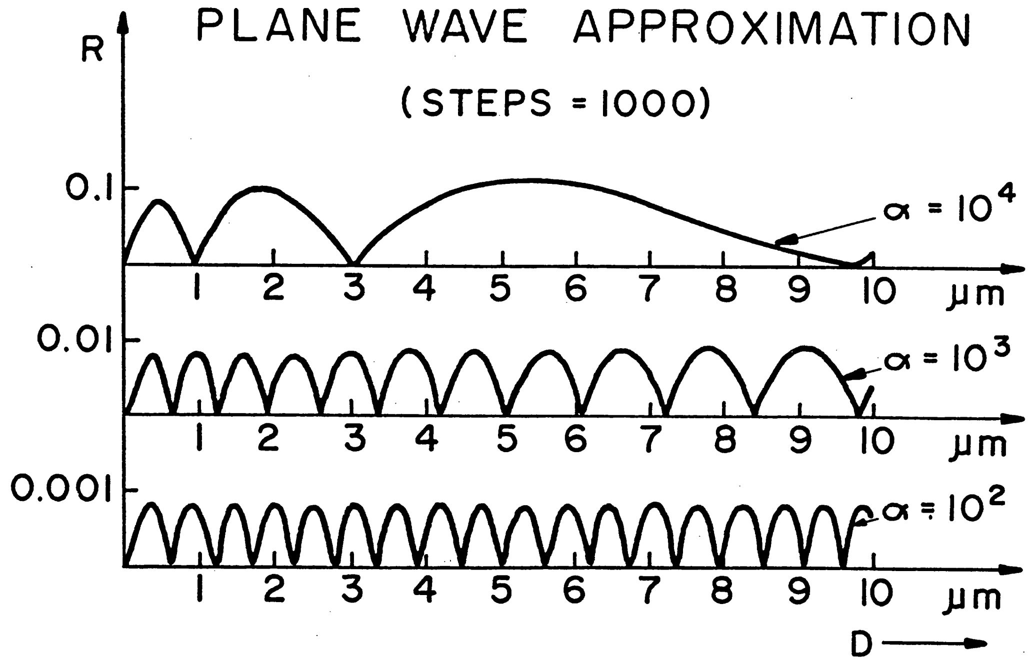

Fig. 3

The plane wave stepwise approximation using 1000 steps for the corresponding calculations of reflectivity R as in figure 2. Both figures have varying refractive indices dependent on α.

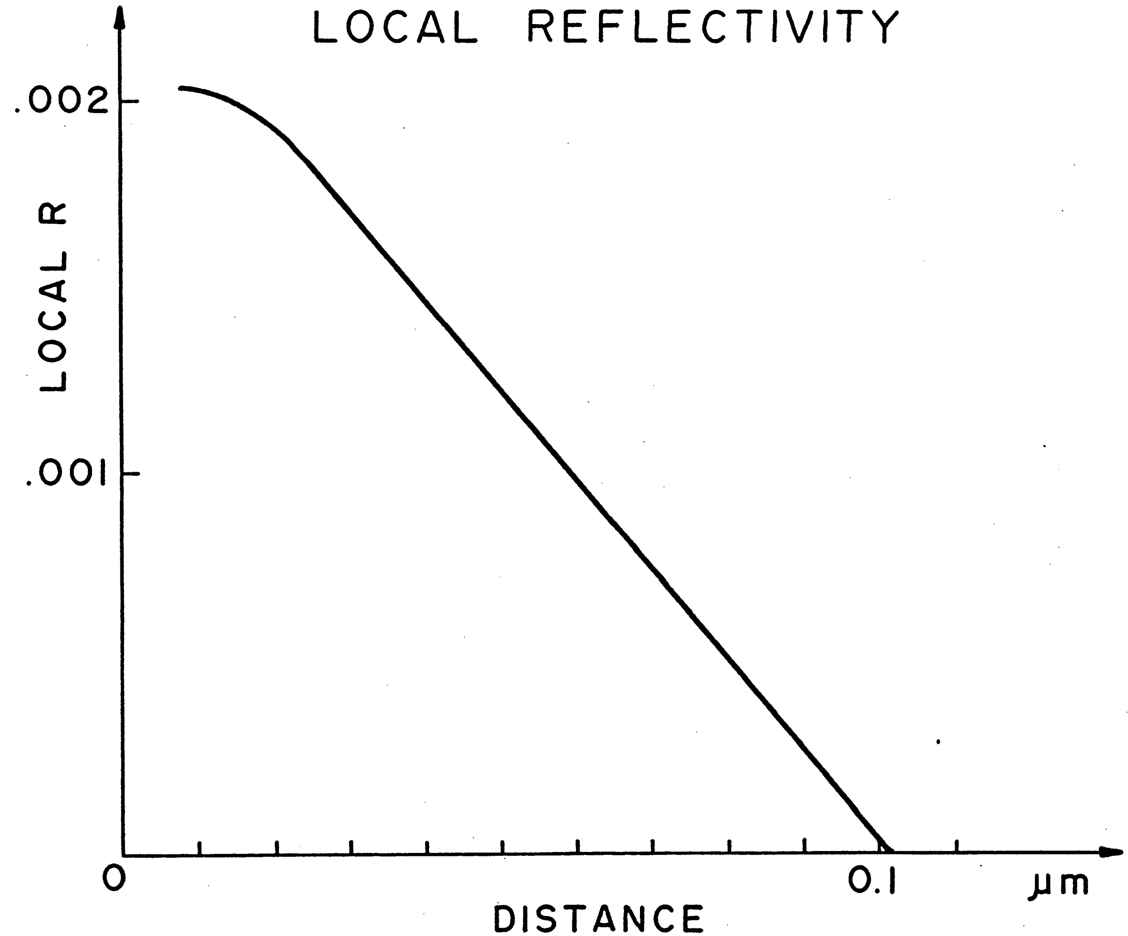

Fig. 4

Variation of the reflection on the coefficient R of the plane wave approximation with distance in Medium II representing a local reflection.

case of the approximation, how the reflection coefficient of the plane waves within the steps decreases from Medium I to III, Figure 4. Therefore we can conclude that both results, Osterberg "non-reflectivity" and the plane wave "local reflectivity" are not contradicting each other.

The problem is, how are the solutions for the inhomogeneous medium to be determined. The only condition is similar to that of Sommerfeld's spherical radiation condition (at large distance r, the amplitude has to decrease as $\frac{1}{r}$) expressed here for plane waves: when $x \to +\infty$, the solution is approximately that of a homogeneous medium with only forward propagating waves and no standing waves, while any approximation of the exact case by fine steps for other x will produce in effect, internal reflection or standing waves. The exact solution does not exhibit reflection properties and the stepwise approximation is - so to say - a probe for mathematically detecting local reflectivity.

V Use of the Rayleigh Profile

The exact solution of the wave equation for an inhomogeneous medium requires a high number of stepwise approximations of the refractive index for comparable results. In the example of approximating a Rayleigh density profile even with a high order approximation, a discrepancy appeared in the interference minima for the inhomogeneous slab approximated analytically.

The Osterberg problem of "no local generation of reflection" can be explained as a mathematical solution while a sufficiently accurate stepwise approximation acts as a mathematical probe to determine the local generation of reflection. The necessity of very high order stepwise approximation for a sufficient agreement with the exact case (even for the relatively uncomplicated case of the Rayleigh profile) acknowledges that a critical view is necessary for the use of approximations. In the case of laser plasma interactions an approximation of plasma density by a series of analytical profiles of the Rayleigh or Airy[7] type are recommended for the calculation of absorption of radiation. In theory more accurate predictions may be made by suitable choices of approximations by varying values of the constant α to fit the density profile of the plasma. It is however impractical to use such analytical approximations as laser plasma interactions are dynamic processes and initial density profiles will deviate from both analytical approximations of the Rayleigh profile or a linear profile. For practical purposes and as long as step sizes are small, reflectivities of the plasma differs little from approximations made by analytical methods.

The Rayleigh density profiles display properties of low reflection of laser light. Reflection at the kink of the density profile between the Rayleigh density and the vacum is less than 10% following the exact wave optical treatment seen here for values of α less than $10^5 cm^{-1}$. Similarly for small step sizes the approximations by plane wave methods appear sufficient for accurate predictions. The resulting reflectivity of less than 10% for $\alpha = 10^4 cm^{-1}$ means at least 90% of the laser energy is transmitted into the plasma.

CHAPTER 3 NONLINEAR FORCE

I General description

From a general description of stress tensors in an electromagnetic field[1] the stress tensor for the electric field was for nondispersive media only,

$$\sigma_{ik} = - p_o\ (\rho,T)\ \delta_{ik} - \frac{E^2}{8\pi} (\varepsilon - \rho(\frac{\partial \varepsilon}{\partial \rho})_T)\ \delta_{ik} + \frac{\varepsilon E_i E_k}{4\pi} \quad (1)$$

where p_o is the pressure found in the medium in the absence of a field for given values of density ρ and temperature T. Where ε is the electric permittivity and δ_{ik} the Kronecker delta function. Similarly the magnetic stress tensor with $B = \mu H$ is

$$\sigma_{ik} = - p_o\ (\rho T) - \frac{H^2}{8\pi} (\mu - \rho(\frac{\partial \mu}{\partial \rho})_T)\ \delta_{ik} + \mu \frac{H_i H_k}{4\pi} \quad (2)$$

where μ is the magnetic permeability. By summing the two stress tensors, eqs. (1) and (2) we obtain the stress tensor for an electromagnetic field if $\mu = 1$.

$$\sigma_{ik} = - p_o\ (\rho,T) - (\frac{E^2}{8\pi}(\bar{n}^2 - \rho(\frac{\partial \bar{n}^2}{\partial \rho})_T + \frac{H^2}{8\pi})\ \delta_{ik} + \bar{n}^2 \frac{E_i E_k}{4\pi} + \mu \frac{H_i H_k}{4\pi} \quad \ldots\ldots\ldots \quad (3)$$

where the electric permittivity ε is defined as the complex refractive index $\bar{n}^2$. The generalisation of eq. (1) for the dispersive plasma was shown by Hora[15] indirectly by algebraical identification with the generalised first Schluter[16] equation which predicted a correct result for oblique incidence of the laser radiation. Since

$$\rho = \bar{m}_i\ n_i = \bar{m}_i\ Z\ n_e \quad (4)$$

where $\bar{m}_i$ is an averaged ion mass and $n_{i,e}$ are the ion and electron densities and Z is the charge then

$$\rho \frac{1}{\partial \rho} = n_e \frac{\partial}{\partial n_e} \quad (5)$$

so that $$\rho \frac{\partial \bar{n}^2}{\partial \rho} = n_e \frac{\partial \bar{n}^2}{\partial n_e} \quad (6)$$

By definition the refractive index for an absorbing plasma where $\nu \neq 0$ is given by

$$\bar{n}^2 = 1 - \frac{n_e}{n_{ec}} \left(\frac{1}{1-i\nu/\omega}\right) \tag{7}$$

then
$$\frac{\partial \bar{n}^2}{\partial n_e} = -\frac{1}{n_{ec}} \left(\frac{1}{1-i\nu/\omega}\right) \tag{8}$$

$$n_e \frac{\partial \bar{n}^2}{\partial n_e} = -\frac{n_e}{n_{ec}} \left(\frac{1}{1-i\nu/\omega}\right) = \bar{n}^2 - 1 \tag{9}$$

that is
$$\rho \frac{\partial \bar{n}^2}{\partial \rho} = \bar{n}^2 - 1 \tag{10}$$

Inserting eq. (10) into eq. (3) results in the electromagnetic stress tensor as

$$\sigma_{ik} = - p_0 (\rho, T) - \frac{E^2 + H^2}{8\pi} \delta_{ik} + \bar{n}^2 \frac{E_i E_k}{4\pi} + \frac{H_i H_k}{4\pi} \tag{11}$$

similar to eq. (7) using

$$\bar{n}^2 = 1 - \frac{\omega_p^2}{\omega^2 (1-i\nu/\omega)} \tag{12}$$

using
$$\omega_p^2 = \frac{4\pi e^2 n_e}{m_e} \; ; \quad \omega^2 = \frac{4\pi e^2 n_{ec}}{m_e} \tag{12a}$$

then eq. (11) becomes

$$\sigma_{ik} = - p(\rho, T) - \frac{E^2 + H^2}{8\pi} \delta_{ik} + \frac{H_i H_k}{4\pi} + \frac{E_i E_k}{4\pi} - \frac{\omega_p^2}{4\pi(\omega^2 + \nu^2)} \times E_i E_k \left(1 + i \frac{\nu}{\omega}\right) \quad \ldots\ldots\ldots \tag{13}$$

Taking the terms individually

$$-\frac{E^2+H^2}{8\pi} \delta_{ik} = \frac{1}{4\pi} \begin{bmatrix} -\frac{1}{2}(E_x^2+E_y^2+E_z^2+H_x^2+H_y^2+H_z^2) & 0 & 0 \\ 0 & -\frac{1}{2}(E_x^2+E_y^2+E_z^2+H_x^2+H_y^2+H_z^2) & 0 \\ 0 & 0 & -\frac{1}{2}(E_x^2+E_y^2+E_z^2+H_x^2+H_y^2+H_z^2) \end{bmatrix} \tag{14}$$

Similarly

$$\frac{E_i E_k}{4\pi} + \frac{H_i H_k}{4\pi} = \frac{1}{4\pi} \begin{bmatrix} E_x^2 + H_x^2 & E_x E_y + H_x H_y & E_x E_z + H_x H_z \\ E_x E_y + H_x H_y & E_y^2 + H_y^2 & E_y E_z + H_y H_z \\ E_x E_z + H_x H_z & E_y E_z + H_y H_z & E_z^2 + H_z^2 \end{bmatrix} \tag{15}$$

Summing eq. (14) and (15) gives

$$-\frac{E^2+H^2}{8\pi}\delta_{ik}+\frac{E_iE_k}{4\pi}+\frac{H_iH_k}{4\pi}=\frac{1}{4\pi}\times$$

$$\begin{bmatrix} \frac{1}{2}(E_x^2-E_y^2-E_z^2+H_x^2-H_y^2-H_z^2) & E_xE_y+H_xH_y & E_xE_z+H_xH_z \\ E_xE_y+H_xH_y & \frac{1}{2}(-E_x^2+E_y^2-E_z^2+H_y^2-H_x^2-H_z^2) & E_yE_z+H_yH_z \\ E_xE_z+H_xH_z & E_yE_z+H_yH_z & \frac{1}{2}(-E_x^2-E_y^2+E_z^2-H_x^2-H_y^2+H_z^2) \end{bmatrix} \quad (16)$$

we can define the right hand side of eq. (16) as T_{ik} then eq. (13) transforms to

$$\sigma_{ik}=-p(\rho,T)+T_{ik}-\frac{\omega_p^2}{(\nu^2+\omega^2)}\frac{1}{4\pi}(1+i\nu/\omega)\,E_iE_k \quad (17)$$

By definition the force $\underline{f}$ per unit volume can be calculated from the stress tensor σ_{ik} the momentum flux density which includes the momentum of both matter and the electromagnetic field. By relativistic invariance the energy flux of an electromagnetic wave in a dielectric given by c $(\underline{E}\times\underline{H}/4\pi)$, to be the same as before except for a factor $1/c^2$, This force is used in the dielectric with a variable electromagnetic field so that

$$f_i=\frac{\partial\sigma_{ik}}{\partial x_i}-\frac{\partial}{\partial t}\frac{(\underline{E}\times\underline{H})i}{4\pi c} \quad (18)$$

Using eq. (17) in eq. (18) leads us to the required force as

$$\underline{f}=-\underline{\nabla}\cdot\underline{P}+\underline{\nabla}\cdot(\underline{T}-\frac{\omega_p^2}{\omega^2+\nu^2}\frac{1}{4\pi}(1+i\nu/\omega)\underline{E}\ \underline{E})-\frac{\partial}{\partial t}\frac{\underline{E\times H}}{4\pi c} \quad (19)$$

eq. (19) is the general force density equation.

If we assume perpendicular incidence of a plane wave propagating in the x direction on a stratified plasma with linear polarisation of E in the y direction. We can assume

$$\frac{\partial}{\partial y} = \frac{\partial}{\partial z} = 0; \qquad E_x = E_z = 0; \qquad H_x = H_y = 0 \tag{20a}$$

and $i_x . i_y = i_x . i_z = i_y . i_z = 0$ (20b)

The gradient of the stress tensor $\underline{T}$ is written as

$i_x \frac{\partial}{\partial x} + i_y \frac{\partial}{\partial y} + i_z \frac{\partial}{\partial z} \cdot \underline{T}$ where the $\underline{\nabla}$ function and $\underline{T}$ with assumptions (20) reduce to

$$i_x \frac{\partial}{\partial x} \cdot \frac{1}{4\pi} \begin{bmatrix} -\frac{1}{2}(E_y{}^2+H_z{}^2) i_x i_y & 0 & 0 \\ 0 & -\frac{1}{2}(E_y{}^2-H_z{}^2) i_y i_y & 0 \\ 0 & 0 & \frac{1}{2}(-E_y{}^2+H_z{}^2) i_z i_z \end{bmatrix} \tag{21}$$

from (20b)

$$\underline{\nabla} \cdot \underline{T} = -\frac{i_x}{8\pi} \frac{\partial}{\partial x} (E_y{}^2+H_z{}^2) \tag{22}$$

Similarly $\nabla \cdot (\frac{1}{4\pi} \frac{\omega_p^2}{\omega^2+\nu^2} (1 + i\nu/\omega)\ EE)$ reduces to

$$i_x \frac{\partial}{\partial x} \frac{\omega_p^2}{4\pi(\omega^2+\nu^2)} (1 + i\ \nu/\omega) \cdot$$

$$\begin{aligned} (& i_x i_x E_x E_x + i_x i_y E_x E_y + i_x i_z E_x E_z \\ & + i_y i_x E_y E_x + i_y i_y E_y E_y + i_y i_z E_y E_z \\ & + i_z i_x E_z E_x + i_z i_y E_z E_y + i_z i_z E_z E_z) \end{aligned} \tag{23}$$

Using assumptions (20a) this reduces further to

$$i_x \frac{\partial}{\partial x} \frac{\omega_p^2}{4\pi(\omega^2+\nu^2)} (1 + i\nu/\omega) \left[i_y i_y E_y{}^2 \right] \tag{24}$$

but $i_x i_y = 0$ so this term is zero.

Then

$$\underline{f} = - \underline{\nabla} \cdot \underline{p} - \frac{i_x}{8\pi} \frac{\partial}{\partial x} (E_y{}^2 + H_z{}^2) - \frac{\partial}{\partial t} \frac{\underline{E} \times \underline{H}}{4\pi c} \qquad (25a)$$

The Poynting term can similarly be reduced so that

$$\underline{f} = -\nabla \cdot \underline{p} - \frac{i_x}{8\pi} \frac{\partial}{\partial x} (E_y{}^2 + H_z{}^2) - \frac{\partial}{\partial t} \frac{E_y H_z}{4\pi c} i_x \qquad (25b)$$

For a dispersive medium we use the average value of the force density during one period of the laser light. The switch on process of the laser light wave is very slow in comparison with the frequency of the laser light so we can neglect the Poynting term $\frac{\underline{E} \times \underline{H}^{\cdot}}{4\pi c}$ in eq. (25b) by the reasoning below

For a quantitative view of $\frac{\partial}{\partial t} \frac{\underline{E} \times \underline{H}}{4\pi c}$

$\partial t = \Delta t = 10^{-12}$ secs.

At intensities of 10^{16}W/cm^2 E = 3 x 10^9V/cm = 10^7cgs; H is of the same value = 10^7 Gauss so that

$$\frac{1}{\Delta t} \frac{\underline{E} \times \underline{H}}{4\pi c} = \frac{1}{10^{-12}} \times \frac{10^7 \times 10^7}{4 \times \pi \times 3 \times 10^{10}} = 2.65 \times 10^{14}$$

whereas

$$\frac{\partial}{\partial x} (E^2 + H^2) = \frac{1}{\Delta x} (10^{14} + 10^{14}) = \frac{1}{10^{-3}\text{cm}} \times 2 \times 10^{14}$$

$$= 2 \times 10^{17}\text{cgs}$$

and $\quad 2 \times 10^{17} >> 2.65 \times 10^{14}$

II Collisionless Nonlinear Force

The time averaged nonlinear force for linearly polarsied perpendicular light incident is given by $\frac{1}{8\pi} \nabla (\overline{E}^2 + \overline{H}^2)$

Using a collisionless WKB approximation where

$$E^2 = E_v^2/2|\bar{n}| \exp(\pm kx) \tag{26a}$$

$$H^2 = E_v^2|\bar{n}|/2 \exp(\pm kx) \tag{26b}$$

than $\frac{1}{8\pi} \nabla (\bar{E}^2 + \bar{H}^2) = \frac{1}{16\pi} \nabla E_v^2 (\frac{1}{|\bar{n}|} + |\bar{n}|)$ since $k = 0$ for collisionless plasma. For perpendicular incidence (propagation in the x direction:)

$$\bar{f}_{nl} = \frac{E_v^2}{16\pi} \frac{\partial}{\partial x} \frac{1+|\bar{n}|}{|\bar{n}|^2}$$

$$= \frac{E_v^2}{16\pi} \frac{n\ (2\bar{n})-(1+\bar{n}^2)}{|\bar{n}|} \frac{\partial \bar{n}}{\partial x}$$

since $n^2 = 1 - \frac{\omega_p^2}{\omega^2}$.

$$\bar{f}nl = - \frac{E_v^2}{16\pi} \frac{\omega_p^2}{\omega^2} \frac{\partial}{\partial x} \frac{1}{|\bar{n}|} \tag{27}$$

Formally eq. (19) can be rewritten [2] by use of the Maxwells equations (C.G.S. units).

$$\text{Curl } \underline{E} = - \frac{1}{c} \frac{\partial H}{\partial t} \tag{28a}$$

$$\text{Curl } \underline{H} = \frac{4\pi \underline{j}}{c} + \frac{1}{c} \frac{\underline{E}}{t} \tag{28b}$$

and by defining the current density $\underline{j}$ with ion velocity v_i as

$\underline{j} = en_e\ (\underline{v}_e - Zv_i)$ giving [15]

$$f_{tot} = -\nabla\cdot\underline{p} + \frac{1}{c}\ \underline{j} \times \underline{H} + \frac{1}{4\pi}\ \underline{E}\ \underline{\nabla}\cdot\underline{E} - \frac{1}{4\pi} \frac{\omega_p^2}{\omega^2+\nu^2}(1+i\nu/\omega)\underline{E}\ \underline{\nabla}\cdot\underline{E}$$

$$- \frac{1}{4\pi} \frac{\omega_p^2}{\omega^2+\nu^2}\ (1+i\nu/\omega)\underline{E}\cdot\underline{\nabla}\ \underline{E} - \frac{1}{4\pi}\ \underline{E}\ \underline{E}\cdot\underline{\nabla} \frac{\omega_p^2}{\omega^2+\nu^2}(1+i\nu/\omega)$$

...... (29)

The last four terms of eq. (29) drop out for perpendicular incidence from previous assumptions on a stratified plasma so that the nonlinear force is determined by $\frac{1}{c}\,\underline{j} \times \underline{H}$. For oblique incidence all terms of eq. (29) are required.

By substitution of the WKB approximation for E and H into eq. (29) we see for perpendicularly incident light

$$\underline{E}_{wkb} = \underline{i}_y \frac{E_v}{\bar{n}^{\frac{1}{2}}} \exp(iF) \exp(\pm k(x)\, x/2) \qquad (30)$$

$$\underline{H}_{wkb} = \underline{i}_z E_v \bar{n}^{\frac{1}{2}} \exp(iF) \exp(\pm k(x)\, x/2) \qquad (31)$$

where $F = \omega(t \pm \int^x re(\bar{n}(\xi)d\xi/c)$; $k(x)=\omega/(xc)\int^x Im(\bar{n}(\xi)\,d\xi$ ... (32)

so that after averaging over one period $^1/_\omega$ and substituting this into

$$f_{nl} = \frac{1}{c}\,\underline{j} \times \underline{H} \qquad (33)$$

we obtain

$$\bar{f}_{nl} = -i_x \frac{E_v^{\;2}}{16\pi} \frac{\omega_p^2}{\omega^2} \frac{\partial}{\partial x} \frac{1}{|\bar{n}|} \qquad (34)$$

which is equivalent to eq. (27)

The microscopic quivering motion of the electron can couple with the macroscopic properties of the plasma:

We assume a WKB approximation with electric and magnetic fields defined by equations (30),(31) and (32) and eq. (20) so that

$$\dot{v}_y = \frac{e}{m_e} E_y \qquad (35)$$

$$\dot{V} = i_y \frac{e}{m_e} V_y \times H \qquad (36a)$$

and eq. (36a) defines the Lorentz force so that

$$\dot{V}_x = \frac{e}{cm_e} V_y \; |\underline{H}| \tag{36b}$$

From (35)

$$V_y = \frac{E_v}{|\bar{n}|^{\frac{1}{2}}} \frac{c\,e}{\omega m_e} \sin F \tag{37}$$

Then eq. (36b) becomes

$$\dot{V}_x = \frac{e^2}{\omega m_e^{\,2}} \frac{E_v}{|\bar{n}|^{\frac{1}{2}}} \sin F \left[\frac{c}{2\omega} \frac{E_v}{|\bar{n}|^{\frac{3}{2}}} \frac{d\bar{n}}{dx} \sin F - E_v \, \bar{n}^{\frac{1}{2}} \cos F \right] \tag{38}$$

Time averaging eq. (38) gives

$$< \dot{V}_x > = \frac{e^2 c}{2\omega^2 m_e^{\,2}} \frac{E_v}{|\bar{n}|^{\frac{1}{2}}} \frac{d\bar{n}}{dx} < \sin^2 F > \tag{39a}$$

$$< \dot{V}_x > = \frac{e^2 c}{4\omega^2 m_e^{\,2}} \frac{E_v^{\,2}}{|\bar{n}|^{\frac{1}{2}}} \frac{d|\bar{n}|}{dx} \cdot \tfrac{1}{2} \tag{39b}$$

The time averaged nonlinear force density is defined macroscopically as

$$f_{nl} = \overline{n_e m_e \dot{V}_x} \tag{40}$$

so inserting (39b) into (40) gives

$$\bar{f}_{nl} = n_e m_e \frac{e^2 c}{4\omega^2 m_e^{\,2}} \frac{E_v^{\,2}}{|\bar{n}|^2} \frac{d|\bar{n}|}{dx} \tag{41}$$

recalling $\omega_p^2 = \dfrac{4\pi e^2 n_e}{m_e}$ and that the force is in the x direction

$$\bar{f}_{nl} = i_x \frac{1}{16\pi} \frac{\omega_p^2}{\omega^2} \frac{E_v}{|\bar{n}|^2} \frac{d|\bar{n}|}{dx} \tag{42}$$

which is precisely eq. (34) and (27). The quivering motion of the electrons due to the electromagnetic field is transferred into a macroscopic force motion equation which is justified by use of the Maxwellian stress tensor eq. (19). This justifies the use of the nonlinear force in a macroscopic model.

III Predominance of the nonlinear force over thermal kinetic (gas dynamic) force.

From eq. (26), allowing for a dispersive medium and the discussed deletion of the Poynting term we have

$$\underline{f} = -\underline{\nabla} n_e k\ T + \frac{1}{8\pi}\ \underline{\nabla}(\underline{E}^2 + \underline{H}^2) \qquad (43)$$

where the pressure vector is replaced by $n_e k\,T$ whose gradient is the gas dynamic force. Eq. (43) can be rewritten as[15]

$$\underline{f} = \underline{\nabla}\left(-n_e k\ T + \frac{1}{8\pi}(\underline{E}^2 + \underline{H}^2)\right) \qquad (44)$$

The nonlinear force term will than be larger than the gas dynamic force when

$$n_e k\ T \leq \frac{1}{8\pi}\left[(E^2 + H^2) - (E_v^{\ 2} + H_v^{\ 2})\right] \qquad (45)$$

assuming $E^2 = E_v^{\ 2}/\bar{n}(k,T)$ for $n < \cdot 1$ then

$$n_e k\ T \leq \frac{1}{8\pi}\,\frac{E_v^{\ 2}}{\bar{n}(n_e,T)} \qquad (46)$$

From considerations of the oscillation energy the maximum value of $\frac{1}{\bar{n}} = \frac{T^{\frac{3}{4}}}{a}$ where for 1.06μm wavelength light[4]

$a = (2ev)^{\frac{3}{2}}$

so that $n_e k\ T \leq \frac{E_v^{\ 2}}{8\pi}\ \frac{T^{\frac{3}{4}}}{a}$

Then for the collisionless case the predominance of the nonlinear force over the thermal kinetic force is given by

$$I \geq I^* = 2.08 \times 10^{14}\,\mathrm{W/cm^2}\ (\mathrm{Ruby})\ T^{\frac{1}{4}} \quad \text{where } T \text{ is in ev}$$

$$7.5 \times 10^{13}\ (\mathrm{Nd\ glass}) \qquad (47)$$

Including the oscillation energy to the calculations of Stienhauer and Ahlstrom[3] results in similar threshold intensities described by eq. (47) only if the nonlinear intensity dependence of the refractive index has been included[4].

IV Nonlinear force with absorption in plasma

Equations (27), (34) and (42) expresses the nonlinear force in terms of the refractive index $|\bar{n}|$. For a WKB approximation averaged over time including collisions we use equations (26a) and (26b) with $k \neq 0$ then

$$\bar{E}^2 = E_v^2/2|\bar{n}| \exp(\pm kx) \tag{48a}$$

$$\bar{H}^2 = H_v^2|\bar{n}|/2 \exp(\pm kx) \tag{48b}$$

Then the nonlinear force is given by

$$f_{nl} = \frac{1}{8\pi} \underline{\nabla} (\underline{E}^2 + \underline{H}^2) = \frac{1}{16\pi} \cdot E_v^2 (\frac{1}{|\bar{n}|} + |\bar{n}|) \exp(\pm kx) \quad \ldots. \tag{49}$$

For perpendicularly incident laser light (assumption 20a)

$$f_{nl} = - \frac{1}{16\pi} \frac{\partial}{\partial x} E_v^2 (\frac{1}{|\bar{n}|} + |\bar{n}|) \exp(\pm kx) \tag{50}$$

then $$f_{nl} = \frac{E_v^2}{16\pi} (\frac{1-|\bar{n}|^2}{|\bar{n}|^2}) \frac{\partial \bar{n}}{\partial x} \exp(\pm kx)$$

$$\pm \frac{E_v^2}{16\pi} (\frac{1+|\bar{n}|^2}{|\bar{n}|^2}) k \exp(\pm kx) \quad \ldots\ldots \tag{51}$$

where k is the absorption constant defined as

$$k = \frac{2\omega}{c} \mathrm{Im}(\bar{n}) \tag{52}$$

For the collisionless case, $k = 0$ and equation (12) reduces to $n = 1 - \frac{\omega_p^2}{\omega^2}$, so the nonlinear force equation (51) becomes equation (27) with a singularity at $n = 0$ when $\omega_p^2 = \omega^2$. The first term of equation (51) forces plasma from high density to low density depending on the gradient of the refractive index. The second term shows that the force can be in the same direction as the laser light.

If the direction of laser light is reversed then the sign of the second term also reverses. In either case the force is in the direction of the laser light whose magnitude depends on the value of the optical constant. The force acts as radiation pressure of light due to the collisions of photons with the electrons, acting always in the same direction as the laser light.

V Solitons

The properties of the nonlinear force lie in the gradient of the electromagnetic energy density, $\nabla (E^2 + H^2)$. In figure 1 is the case of a symmetric electron density profile $n_e(x)$ of a collisionless plasma,. The corresponding penetrating laser beam satisfies the WKB condition where the density maximum is less than the cut off density n_{ec}. The electromagnetic energy density can be described for the WKB conditions, equations (26a) and (26b) then

$$E^2 + H^2 = E_v^{\,2} \left(\frac{1}{n} + n\right)/2 \tag{52}$$

when E and H describes the electric and magnetic fields, E_v is the vacuum value of the electric field and n the refractive index. If n is small the electromagnetic field swells as $1/_n$. This is also seen via the conservation of energy flux where if the group velocity is V_g and ϕ the illuminated area is related to E by

$$E^2 V_g \ \phi = \text{constant} \tag{53}$$

Then with smaller values of the refractive index, the group velocity falls implying a rise in the amplitude of the electric field denoted by swelling.

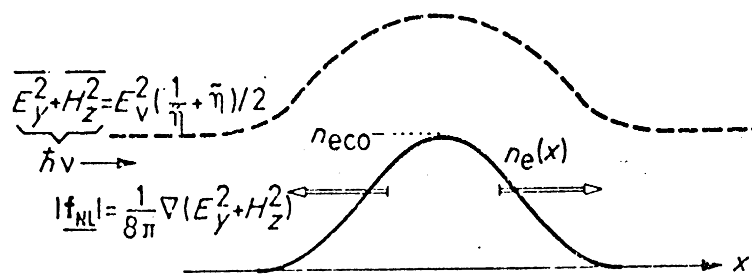

Fig.1The electron density profile of a collisionless plasma with maximum density slightly less than n_{ec}. The penetrating laser beam satisfying the WKB condition and exists as a solitary electromagnetic wave, from Hora[4]

The variation in $E^2 + H^2$ gives magnitude to the nonlinear force f_{nl} in figure 1, due to the gradient of $E^2 + H^2$. The nonlinear force therefore forces plasma from regions of high densities to low densities. The term soliton describes the solitary electromagnetic wave in figure 1.[4]

Similarly for a monotonically increasing electron density profile, figure 2, the corresponding approximation for the electromagnetic energy density is shown. The WKB approximation is possible even for densities exceeding the cut off density n_{ec}. The value of the electromagnetic energy density, after approaching n_{ec}, decreases exponentially due to collisional absorption in the plasma.

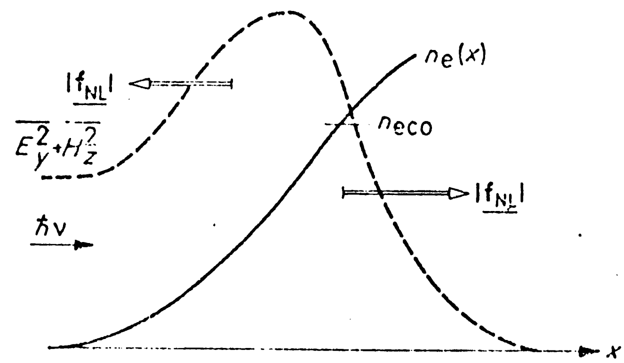

Fig 2 A density profile increasing above the cut off density shows the formation of a soliton which is critically damped at the cut off intensity. Not to be confused with soliton formations in the results section where laser light is incident from the right.

Assuming that the totally penetrating laser beam is collisionally damped at the cut off density, the electromagnetic energy density can be constructed which also displays a solitary electromagnetic energy density where the swelling of the intensity, electric field and wave length are effectively given by

$$I = \frac{I_{vac}}{|\bar{n}|} \quad ; \quad E = \frac{E_{vac}}{|\bar{n}|^{\frac{1}{2}}} \quad ; \quad \lambda = \frac{\lambda vac}{|\bar{n}|} \qquad (54)$$

The above WKB approximation describes a single wave maximum known as a soliton.

VI Generation of Density Minumum

The gas dynamic compression of plasma is associated with the thermokinetic expansion of plasma which ablates towards the incoming laser light as a monotonically decreasing profile. Gas dynamic compression models[5] based on equations of continuity, conservation of momentum and energy conservation without the inclusion of nonlinear force terms have shown that the thermokinetic expansion of plasma (ablation) is towards the laser light. It acts as a compensation from the conservation of momentum where the monotonically decreasing density profile from near the cut off density balances the density profile from areas of compression driven by collision produced absorption of laser light. Figure 3.

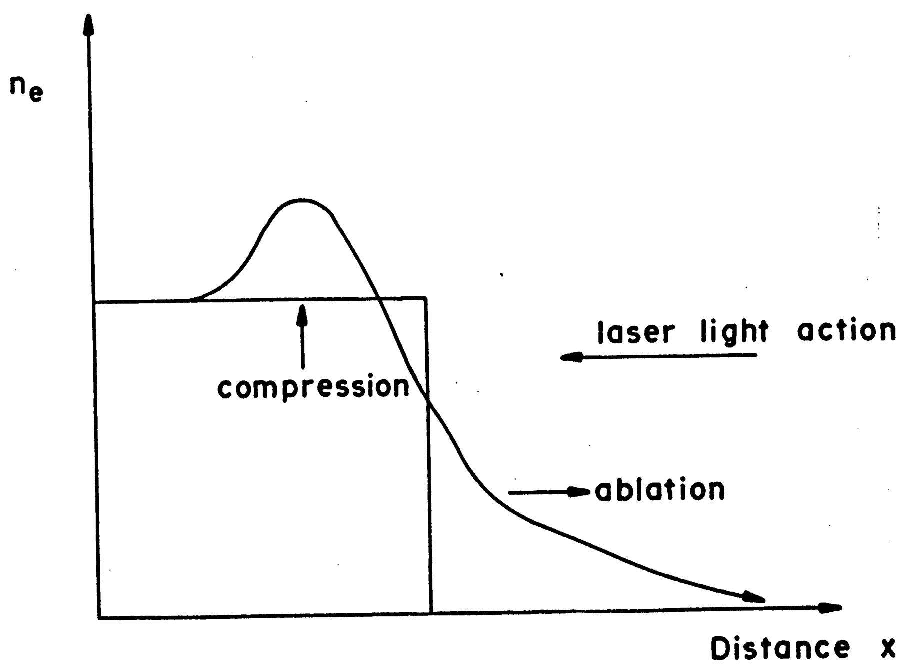

Fig 3 Schematic description of action of laser light on plasma in a gas dynamic scheme, with compression of plasma by collisional processes and the subsequent ablation of plasma.

One describes the nonlinear force as the immediate electrodynamic interaction, the gas dynamic interaction occuring after thermalisation of the radiation and heating of the ions.

The inclusion of the nonlinear force in the model of the interaction will generate a density minimum appearing in the ablating plasma. This was first seen numerically by Shearer Kidder and Zink,[6] figure 4. The density minimum appearing at a time of 33 psecs and at the later time of 92.9 psec the density maximum associated with the caviton.

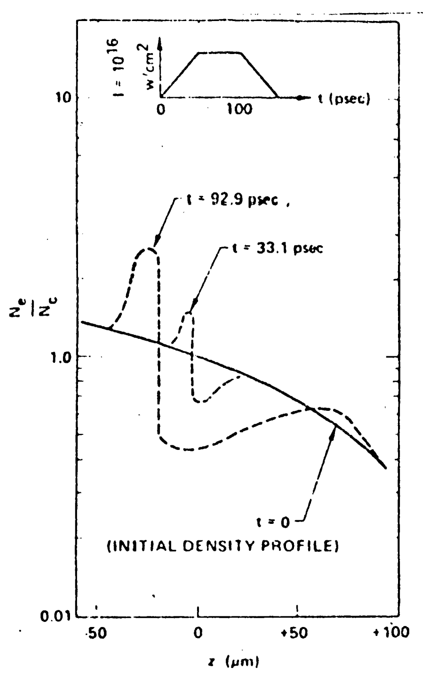

Fig. 4 Density profile at different times for a laser intensity described in the upper part of the figure. The low density maximum is generated initially by the nonlinear force.[6] The term caviton describes the generated density minimum.

Other numerical evaluations of plasma yielded both solitons and cavitons. The one dimensional simulation of plasma by large numbers of single electrons and ions yielded figures 5a and 5b from Valeo and Kruer[7].

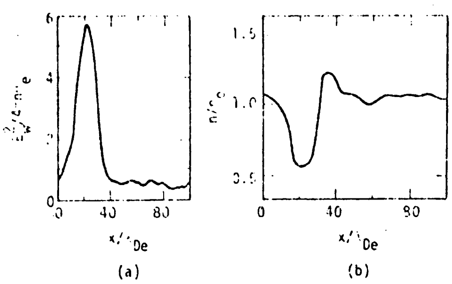

Fig. 5 Spatial dependence of the electric field intensity and ion density observed in a one dimensional computer simulation from Valeo and Kruer[7].

Figure 5a describes a soliton and figure 5b the corresponding caviton generated by a one dimensional electrostatic computer similation. Similarly Brueckner[8] simulated the caviton (figure 6).

Experimental evidence of ion density cavitons created as a result of ion expulsion driven by the non-linear force was seen for microwave pulse sources in figure 7 from Wong and Stenzel[9] at times of 6 μsecs.

Several microseconds after the electromagnetic pulse shows the presence of a large ion current just outside the resonant area due to ions with energies much higher than ambient. This current peak is followed by a density depression due to the expulsion of ions from

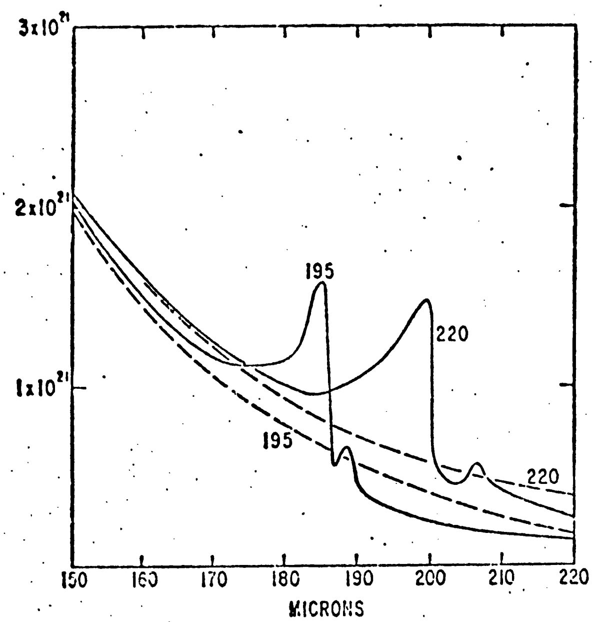

Figure 6

Density profile in the vicinity of n_{ec} at $10^{21}cm^{-3}$ for 1 μm radiation. Brueckner's[8] simulation without the radiation pressure gave the dashed curve and times in psecs.

the resonant region. As the ion structure travels down the density profile, the peak consisting of a wide range of ion velocities quickly dispenses while the caviton composed of background ions maintains its shape as a nonlinear pertubation for a much longer time. The explanation of the result lies in the nonlinear force action on the electrons driving electrons from regions of high to low densities. As the electrons are accelerated they pull the ions with them by self consistent fields thus preserving space charge neutrality. The electron response to the electric field is much faster than the ions so that ion motion in figure 7 occurs

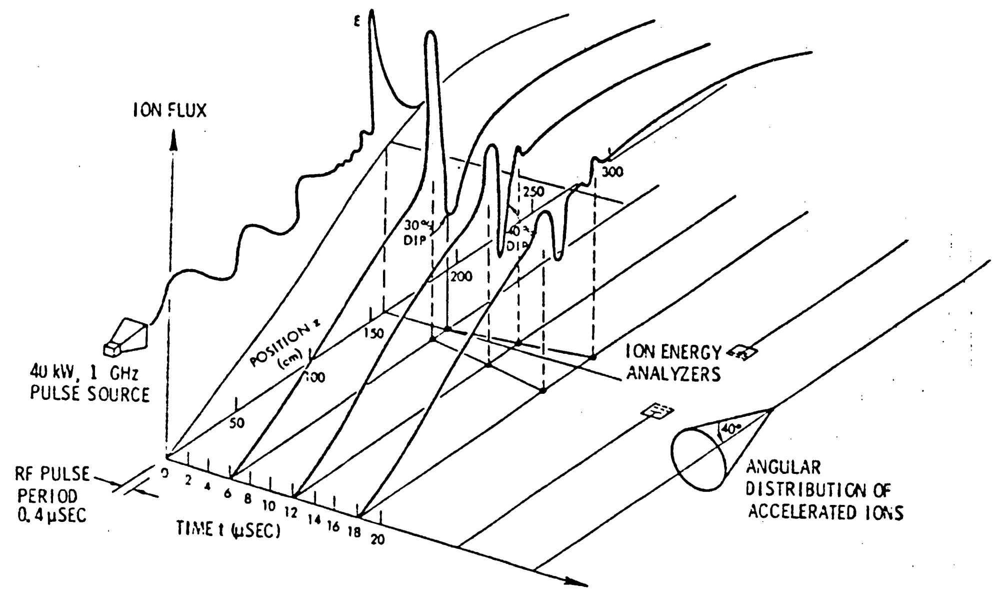

Figure 7

Density cavities as a result of ion expulsion for microwave interactinns with plasma observed experimentally by Wong and Stenzel[9].

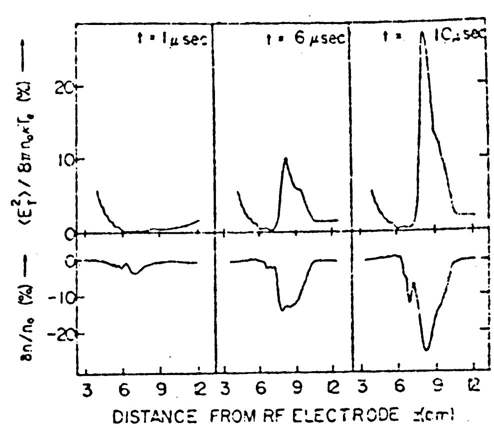

Figure 8

Experimental observations by Kim et al.[10] for microwave interaction verifying the coexistence of solitons and cavitons.

at later times in the order of μsecs. Experiments by Kim, Stenzel and Wong[10] verified the co-existence of solitons and cavitons in the microwave region, Fig. 8.

In laser plasma interaction experiments by Zakharenkov et al.[11] The plasma profile was determined by analysis of inteferograms for electron densities in the range of 10^{18} to 2×10^{19} cm^{-3}. The result is seen in figure 9.

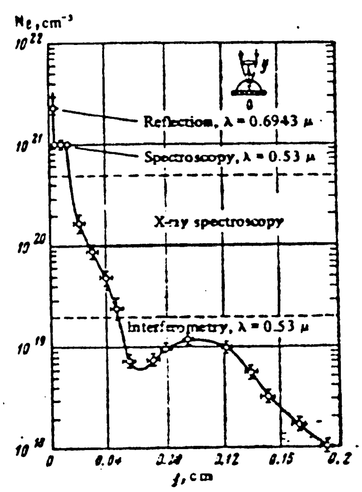

Figure 9

Electron density profile for laser plasma interaction at 2 nsec, observed by different methods. The target was aluminium with incident laser intensity of 3×10^{14} W/cm^2. The Nd glass laser interaction displays the existence of a density caviton experimentally verified by Zakharenkov et al.[11]

Measurements of the density profile in figure 9 for densities greater than 5×10^{18} cm^{-3} during the first 2 nanoseconds are impossible due to the formation of the opacity zone due to refraction or insufficient time resolution or depolarisation as discussed by Zakharenkov et al. Nevertheless the existence of the caviton was experimentally verified for times of 2 nsecs with a velocity $\approx 5 \times 10^{7}$ cm/sec for laser light intensities of 3×10^{14} W/cm^2 .

Experimental results showing density steepening and the density cavity is seen in figure 10. Experimental results of Azechi et al.[12] for Nd glass laser of intensities of 10^{16} W/cm^2 displayed the caviton existing at .37 nsecs after laser irradiation.

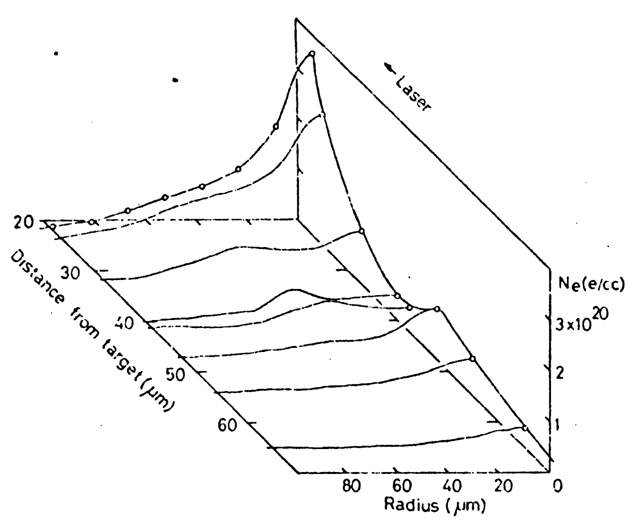

Figure 10

Radial density profile observed at 370 psec after the Nd glass laser irradiation at intensities of 10^{16} W/cm^2 observed by Azechi et al.[12]

Similarly from interferometric measurements for a CO_2 laser pulse with a peak power of 10^{14} W/cm^2 the resultant radial electron density profiles seen in figure 11 from Fedosejev et al.[13] for times of .6 nsecs and .32 nsecs.

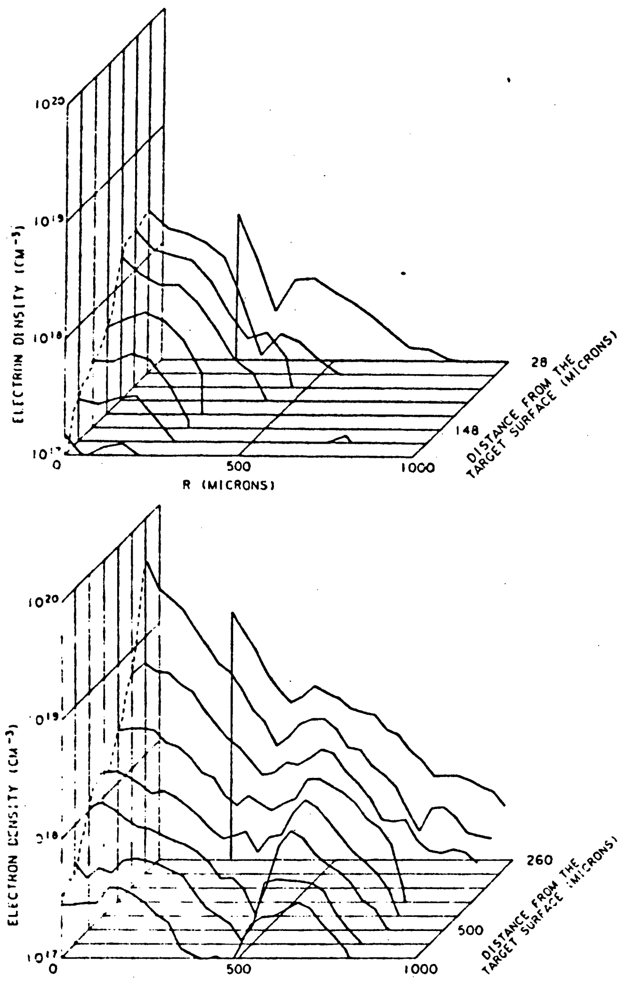

Figure 11

Radial electron density distribution of plasma[13] produced on a solid aluminium target by a 30-J CO_2 laser pulse at (a) .6 nsec and (b) 3.2 nsec.

In figure 11 the same steepening of the density profile appears with the associated caviton. Once again the nonlinear force is the dominant factor in determining the density profile and if this remains true at higher irradiances then the plasma intensity should be largely governed by the incident intensity rather than the wavelength of the radiation. Density cavities and cavities in x-ray emissivity profiles were recorded for CO_2 lasers by Donaldson et al.[14] as seen in figure 12 measured from x-ray pinhole photographs at later times of 25 nsecs.

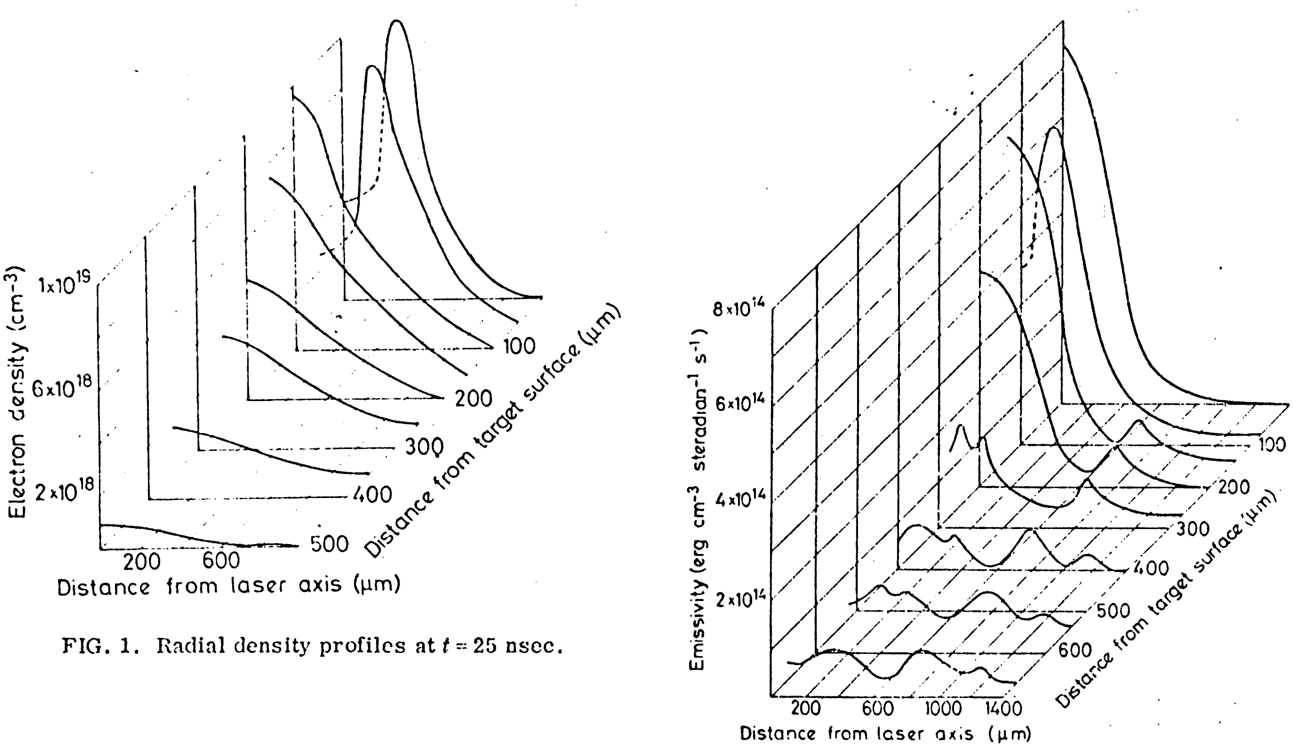

FIG. 1. Radial density profiles at $t = 25$ nsec.

Figure 12

Observation of radial density profiles and x-ray emissivity for CO_2 laser irradiation from Donaldson et al.[14]

The plasma dynamics for the interaction of high intensity laser radiation with solid targets and the instantaneously generated plasma, can be determined by the nonlinear force which is the immediate electrodynamic interaction, and then by the gas dynamic pressure occurring after thermalisation of the radiation and heating of the ions. The important consequence of the nonlinear force, especially for short laser pulses in the order of picoseconds, consists of the possibility of a nonthermalising transfer of optical energy into kinetic energy of plasma for compression, which has a minimum of entropy production and is therefore highly efficient.

CHAPTER 4 ABSORPTION OF LASER LIGHT

I Dispersion Relations

From Euler's equations of hydrodynamics the macroscopic behaviour of the electrons and ions in the plasma due to electromagnetic forces may be definied by a two species energy equation where e and i subscripts denote electron and ion species separately:

For ions with Z = 1

$$m_i n_i \frac{\partial \underline{v}_i}{\partial t} = e\underline{E} + \frac{e}{c} \underline{v}_i \times \underline{H} + m_i n_i \nu(\underline{v}_i - \underline{v}_e) + \nabla n_i kT_i + f_i \quad \ldots . \quad (1)$$

For electrons

$$m_e n_e \frac{\partial \underline{v}_e}{\partial t} = -e\underline{E} - \frac{e}{c} \underline{v}_e \times \underline{H} - m_e n_e \nu(\underline{v}_i - v_e) + \nabla n_e k T_e + f_e \quad \ldots . \quad (2)$$

where $m_{i,e}$ are the masses of the species, $n_{i,e}$ the densities, e the charge, $\underline{E}$ and $\underline{H}$ the electric and magnetic field vectors, c the velocity of light, $v_{i,e}$ the velocities, ν the collision frequency given by Spitzer,[16] k is Boltzmann's constant, $T_{i,e}$ the temperature and $f_{i,e}$ any external force.

The equations above may be rewritten in terms of a single fluid model[1] where the nett velocity of the plasma $\underline{v}$ and the current density $\underline{j}$ are written as

$$\underline{v} = \frac{m_i \underline{v}_i - m_e \underline{v}_e}{m_i + m_e} \quad (3)$$

$$\underline{j} = \frac{e(n_i \underline{v}_i - n_e \underline{v}_e)}{n_i + n_e} \quad (4)$$

subtracting equation (1) from (2) and using definitions (3) and (4), given in cgs units

$$\frac{m_e}{e^2 n_e}\left(\frac{\partial \underline{j}}{\partial t} + \nu \underline{j}\right) = \underline{E} + \frac{\underline{v}}{c} \times \underline{H} + \frac{1}{c_e n_c}\, \underline{j} \times \underline{H} + \frac{1}{e\, n_e c} \nabla p_e \qquad (5)$$

where p_e is the electron pressure corresponding to the term $n_e k\ T_e$ in equation (2). This is the diffusion equation or the generalised Ohm's Law. For periodic time dependence we may write

$$j = j_o \exp\,(-\, i\omega t + \theta) \qquad (6a)$$

$$E = E_o \exp\,(-\, i\omega t) \qquad (6b)$$

These give rise to the identities

$$j = \frac{i}{\omega}\ \frac{\partial}{\partial t}\ j \qquad (7a)$$

$$E = -\,\frac{1}{\omega^2}\,\frac{\partial}{\partial t^2}\ E \qquad (7b)$$

We can neglect the gradient of the pressure in equation (5) since it is dominated by other terms for intensities above 10^{13} W/cm^2, for Nd glass lasers. (See nonlinear force chapter). The justification for neglecting the Lorentz and Hall terms follows.

The value of E is much larger than $|\frac{v}{c}| \times \underline{H}$ where-ever $|\underline{v}| << c$. Since we are not dealing with relativistic velocities the Lorentz term may be neglected.

The Hall term equivalent to $\frac{1}{en_e zc}\, \underline{j} \times \underline{H}$ requires values of $|j|$ and $|H|$ to be determined.

Using $\frac{m_e}{e^2\, n_e}\left(\frac{\partial \underline{j}}{\partial t} + \nu\, \underline{j}\right) = \underline{E}'$

and equation (7a) we obtain

$$\underline{j} = \frac{e^2\, n_e}{\omega\, m_e}\ |\underline{E}|$$

Using $|E| \simeq |H|$ and $z = 1$ then

$$\frac{1}{en_e c} \quad |\underline{j}| \times |\underline{H}| = \frac{e^2 n_e}{m_e \omega_e n_e c} |E|^2$$

$$= \frac{e}{m_e c\omega} \quad |E|^2$$

$$\simeq \frac{10^5}{\omega} \quad |E|^2$$

Therefore the Hall term can be neglected depending on frequency of laser light when

$$\frac{10^5}{\omega} \quad |E|^2 << |E|$$

For Nd glass laser with $\omega \simeq 10^{15}$

$$|E| << 10^{10} \text{ cgs units}$$

That is $\qquad |E| << 3 \times 10^{12}\ \text{V/cm}^2$

which corresponds to an intensity flux of about 10^{22} W/cm²

So for non relativistic velocities and intensity fluxes of less than 10^{22} W/cm² and larger than 10^{13}W/cm² we may ignore the pressure , Lorentz and Hall terms in equation (5).

Using the identity for the plasma frequency $\omega_p^2 = \dfrac{4\pi e n_e}{m_e}$ in eq. (5) and using eq. (7)

$$\frac{4\pi}{\omega_p^2} \left(\frac{\partial \underline{j}}{\partial t} + i\frac{\nu}{\omega} \frac{\partial \underline{j}}{\partial t}\right) = - \frac{1}{\omega^2} \frac{\partial}{\partial t^2} \quad \underline{E} \tag{8}$$

Substituting this into a Maxwellian wave equation where

$$\underline{\nabla}^2 \ \underline{E} = \frac{1}{c^2} \ \frac{\partial^2}{\partial t^2} \ \underline{E} + \frac{4\pi}{c^2} \ \frac{\partial \underline{j}}{\partial t} \tag{9}$$

from the use of Maxwell's equations

$$\underline{\nabla} \times \underline{E} = - \mu\mu_0 \dot{\underline{H}} \tag{9a}$$

$$\underline{\nabla} \times \underline{H} = \sigma\, \underline{E} + \varepsilon\, \varepsilon_0\, \dot{E} \tag{9b}$$

$$\text{Then } \underline{\nabla}^2\, \underline{E} = \frac{1}{c^2}\frac{\partial^2}{\partial t^2}\, \underline{E} - \frac{\omega_p^2}{c^2\omega^2(1 + i\nu/\omega)}\, \frac{\partial^2 E}{\partial t^2} \tag{10}$$

$$\text{that is } \underline{\nabla}^2\, \underline{E} - \frac{1}{c^2}\left(1 - \frac{\omega_p^2}{\omega^2(1 + i\nu/\omega)}\right) \frac{\partial^2 E}{\partial t^2} = 0 \tag{11}$$

This gives the dispersion relation where the complex refractive index $\underline{n}$ is defined as

$$\bar{n}^2 = 1 - \frac{\omega_p^2}{\omega^2(1 + i\nu/\omega)} \tag{12}$$

The real part of $\bar{n}$ is the refractive index n and the imaginary part of $\bar{n}$ is the absorption coefficient k given by

$$n = \sqrt{\tfrac{1}{2}\left(1 - \frac{\omega p^2}{\omega^2+\nu^2}\right) + \tfrac{1}{2}\left(\left(1- \frac{p}{\omega^2+\nu^2}\right)^2 + \left(\frac{\nu}{\omega}\, \frac{\omega p^2}{\omega^2+\nu^2}\right)^2\right)^{\frac{1}{2}}} \tag{13}$$

$$k = \sqrt{-\tfrac{1}{2}\left(1 - \frac{\omega p^2}{\omega^2+\nu^2}\right) + \tfrac{1}{2}\left(\left(1- \frac{\omega_p^2}{\omega^2+\nu^2}\right)^2 + \left(\frac{\nu}{\omega}\, \frac{\omega p^2}{\omega^2+\nu^2}\right)^2\right)^{\frac{1}{2}}} \tag{14}$$

Then the absorption constant k is given by

$$K = \frac{2\omega}{c}\, k \tag{15}$$

For collisionless cases we assume that the collision frequency ν is very much less than the incoming laser light frequency ω then ν may be neglected and the refractive index n from eq. (13) is rewritten as

$$n = \sqrt{1 - \frac{\omega_p^2}{\omega^2}} \tag{16a}$$

and the absorption coefficient k will be zero. In terms of the electron densities the refractive index n may be written as

$$n = \sqrt{1 - \frac{n_e}{n_{ec}}} \tag{16b}$$

The phase velocity of the light wave in the plasma is v_p given by

$$v_p = \frac{c}{|\bar{n}|} \tag{17a}$$

and the group velocity v_g is

$$v_g = c|\bar{n}| \tag{17b}$$

II Collision frequency

Coulombic collisions between charged particles in the plasma state are dominated by electron-ion collisions. A crude approximation of the electron-ion collision frequency follows:

The coulombic force existing between the electron and Z number of ionised ions is given by

$$F = -\frac{Ze^2}{r^2} \tag{18}$$

This force acts during a time given by

$$t \simeq \frac{r_o}{v} \tag{19}$$

where r_o is the distance of closest approach called the impact parameter. The change in momentum of the electron is given by

$$Ft \simeq \frac{Ze^2}{r_o v} \tag{20}$$

The cross section for large angle collisions where an electron is deflected by more than 90^0 the change of momentum is of the order of the momentum itself that is

$$Ft \simeq m_e v = \frac{Ze^2}{r_o v} \tag{21}$$

then

$$r_0 = \frac{Ze^2}{m_e v^2} \tag{21a}$$

the cross section is given by χ where

$$\chi = \pi r_0^2 = \frac{Z^2 \pi e^4}{m_e^2 v^4} \tag{22}$$

the electron ion collision frequency is defined as

$$\nu_{ei} = n_i \chi v \tag{23a}$$

since $n_i = n_e/Z$

then $$\nu_{ei} = \frac{Z n_e \pi e^4}{m_e^2 v^3} \tag{23b}$$

The average value of the velocity v in a plasma at equilibrium can be corrected to the temperature T_e of the electrons where

$$\frac{m}{2}e\, v^2 = \frac{3}{2} k\, T_e \tag{24}$$

substitution of eq. (24) into eq. (23b) gives

$$\nu_{ei} = \frac{Z n_e \pi e^4 3^{-\frac{3}{2}}}{m_e^{\frac{1}{2}} (k\, T)^{\frac{3}{2}}} \tag{25a}$$

Spitzer's expression[2] for the electron-ion collision frequency is given by

$$\nu = \frac{n_e \pi e^4 m_e}{(m_e k\, T_e)^{\frac{3}{2}}} \ln \Lambda sp \tag{25b}$$

where Λsp is Spitzer's ratio of the maximum (debye lengths) to minimum impact paremeter. The difference between eq. 25a and 25b is a constant and the log term. Over the large range of temperatures and electron densities the difference is not significant.

Estimations of collisional absorption of laser light in many derivations use Kirchoff's law enforcing thermodynamic equilibrium between absorption and emission separately for each individual frequency. In the microwave region Oster[3] had calculated the absorption coefficient of a plasma for both classical and quantum limits. In the classical limit Oster obtained for the emission coefficient per unit volume ε_ω assuming a Maxwellian electron velocity distribution which was the same result as Schuer[4] for collective collisions of electrons and ions. The gist of the theory both for microwaves and later for light waves is the estimation of the coefficient of absorption from thermodynamic equilibrium when absorption and emission balances out separately for each frequency. This is effectively Kirchoff's Law related by Planck's function

$$p_\omega = \varepsilon_\omega = k_\omega b_\omega \tag{26}$$

where b_ω is Planck's function; the universal function of equilibrium temperature, and k_ω is the absorption coefficient for frequency ω.

On the basis of a classical microscopic theory Dawson and Oberman[5] calculated the absorption coefficient of a plasma at high frequencies obtaining

$$k = \frac{8\pi z^2 e^6 n_i n_e}{\mu c(2\pi mkT)^{\frac{3}{2}}\omega^2} \quad \ln\left(\frac{k^2 maxu_0{}^2}{2\pi^2\nu^2} - \nu\right) \tag{27}$$

For a value of $k_{max} = \frac{kT}{Ze^2}$ the value of k is close to microwave predictions of Schuer.

By applying Snell's Law, Dawson[6] included the refractive index into the absorption coefficient by using Kirchoff's Law. He obtained a correction factor for the absorption constant $\mu = \left(1 - \frac{\omega_p^2}{\omega}\right)^{\frac{1}{2}}$ which accounts for the reduction of the group velocity of the wave in the region where the plasma is nearly overdense.The factor μ in eq.27 restricts the validity of that equation to the plasma frequency less than ω.Inserting Spitzer's electron ion collision frequency into eq.27 and using the condition for quasineutrality $n_e = n_i = n$ gives

$$k \;\alpha\; \frac{\nu}{nc\mu} \; \frac{\omega^2}{\omega} \; \ell nC \qquad (28)$$

where C is the ratio of the log terms of Spitzer and Dawson,Oberman.Eq.28 expresses the direct proportionality between the collision frequency and the absorption coefficient.Comparison of the crude approximation,eq. (25a) and eq. (25b) with a quantum mechanical[8] treatment shows values of the collision frequencies differing only by a constant and the log terms.The importance of the difference over the large magnitudes of densities and temperatures is not significant.An important assumption arises and is discussed in a paper by Green[9],that for a plasma at temperatures above 10^4 ^{0}K,a Quantum mechanical model can be replaced by a purely classical model.

III Nonlinear Optical Constants

Experimental results[7] have shown that absorption of laser radiation differs from predictions by inverse bremsstahlung mechanisms at higher intensities.At intensities when the oscillation energy of the electron due to the laser light is larger than the thermal energy equivalent to the random motion of the electron,then non-linear mechanisms enhance absorption due to the decaying processes of the light in the plasma.

When the oscillation energy is comparable or larger than the thermal energy of the electron then the temperature of the electron is increased by

$$T = T_{th} + E_{os}/k \tag{29}$$

where T_{th} is the thermal temperature of the electron, E_{os} is the oscillation energy of the electron and k is the Boltzmann's constant. Since the velocity of the electron in the form of an oscillation, due to the electric field E in vacuum, is given by

$$v_i = eE/m\omega \tag{30}$$

then the oscillation energy of the electron is

$$E_{os} = e^2E^2/2m\omega^2 \tag{31}$$

comparison of E_{os} to $m_c{}^2$ derives the laser intensity for which relativistic effects[10] are taken into account. For Nd glass laser the relativistic threshold intensity is 3.7×10^{18} W/cm². If $E_{os} << mc^2$ Spitzer's collision frequency ν in eq. (25b) may be rewritten including eq. (29) as

$$\nu = \frac{n_e \pi e^4 m_e}{n_e^{\frac{3}{2}}(kT_{th} + E_{os})^{\frac{3}{2}}} \ln \Lambda \tag{32}$$

and the nonlinear absorption constant is obtained from eq. (27) as

$$k = \frac{8\pi z^2 e^6 n_i n_e \quad \ln \Lambda}{c\omega^2 (2\pi m_e)^{\frac{3}{2}} \; (kT_{th} + E_{os}/k)^{\frac{3}{2}}} \quad \frac{1}{\sqrt{1-\omega_p{}^2/\omega^2}} \tag{33}$$

which is valid for intensities less than 3.7×10^{18}W/cm² and where $\omega_p < \omega$.

When the oscillation energy of the electron is much larger than the thermal energy of the electron and the relationship between the electric field amplitude E and the intensity of the laser field I is given by

$$E = \sqrt{8\pi\ I/c} \quad \text{(cgs)} \tag{42}$$

we obtain the nonlinear collision induced absorption coefficient by classical inverse bremsstrahlung for high intensities as

$$k_{nl} = \frac{8\pi Z^2 e^3 n_e n_i \ln\Lambda c^{\frac{1}{2}}\omega}{(8\pi\ I)^{\frac{3}{2}}} \tag{43}$$

on comparison with a fully quantum mechanical multiphoton treatment[8], one sees only a difference in constants and logarithm terms. Both Rand's[8] treatment and the one described above, show the nonlinear absorption coefficient as proportional to the frequency of laser light ω and inversely proportional to the three halves of the intensity of the laser beam. The refractive index of the plasma is included in eq. (43) to give

$$k_{nl} = \frac{8\pi Z^2 e^3 n_e n_i \ln\Lambda c^{\frac{1}{2}}\ \omega}{(8\pi^2 I)^{\frac{3}{2}}\ \sqrt{1-\omega_p{}^2/\omega^2}} \tag{44}$$

which is valid for $kT >> h\ \nu$; $E_{os} >> k\ T_{th}$; $\omega_p < \omega$ where no account is made for relativistic effects and $I < 3.7 \times 10^{18}\ W/cm^2$. The absorption coefficient increases as ω_p approaches ω which is near the cut off density n_e.

IV Dynamic collisionless absorption

We have dealt with the absorption of laser light by the processes of inverse bremsstrahlung and the correction to absorption at high intensities, when the oscillation energy of the electron due to the radiation is larger than the electrons thermal energy. As a consequence of change neutrality (Debye shielding) ions are carried along by electrons and are adiabatically compressed and expanded so that any change in the temperature of the ions in short time is not due to ionic absorption of radiation, but due only to absorption of radiation via the electrons. As a consequence of the oscillation energy, macroscopically the quivering motion of the electrons means a change in the plasma frequency acting as a collision induced absorption of radiation by electrons.

As in the chapter on nonlinear forces, we neglect the case of oblique incidence of radiation. We note that there exists an optimum angle[11] for which there is maximum absorption of radiation at $\omega_p \simeq \omega$. Coherent energy incident at the optimum angle is resonant with plasma oscillations. If the electron ion collision frequency is small compared to the wavelength then the oscillations build up to large amplitudes. If collisions limit the size of amplitude thermal electrons are formed. If not the oscillations grow till they break in phase space and hot electrons are produced describing a resonance absorption mechanism.

Large amounts of energy transfer of laser light to plasma can occur due to instability processes occuring at each specific intensity threshold. In some cases[12] higher harmonics and half numbered harmonics have been observed in backscattered radiation due to Raman, Brillouin type instabilities generating large transfers of energy into the plasma with a corresponding anomalous backscatter of radiation.

Each instability manifests itself at their individual characteristic intensity threshold. Many instabilities may be associated with the threshold growth of the nonlinear force. The nonlinear force in an anomalous manner generates macroscopic motion of the plasma. It is a direct transfer of optical energy into mechanical energy in the plasma. The mechanical energy changes density gradients and in this way increases dynamic absorption nonlinearly without collisions. Density profiles with low reflectivities, such as the Rayleigh profile will exhibit dynamic absorption without collisions thus allowing large transfer of energy into the plasma. For completeness absorption via inverse bremsstrahlung must be included to the macroscopic dynamic collisionless abosrption whose predominance however, is one of the results from the following calculations.

It should be mentioned that the inclusion of the decay instabilities producing "effective collision frequencies" as Dubois proposed[12] should have been included into this treatment. However, though the basic theory of these instabilities has been developed extensively[14] the theory of saturation is not yet finished. While the use of the instabilities is very important for diagnostics, eg. by the second harmonics generation, their importance for the dynamics may be relatively small as Wong[15] indicated due to the fact that the back scattered harmonics are of small intensity compared with the initially incident radiation. This highly complex question may be considered as not completely settled.

CHAPTER 5 LASER PLASMA INTERACTION MODEL

I Equation of State

In this model electrons and ions act as separate species and we assume that they are monatomic gases and that quasineutrality holds so that the number of ions n_i equals the number of electrons n_e, that is $n_e = n_i = n$. At temperatures of 100eV and at the Nd glass laser cut off density of $10^{21}cm^{-3}$ we can assume that the perfect gas law holds and then the equations of state for the separate species are

$$p_i = n_i \, k \, T_i \tag{1}$$

$$p_e = n_e \, k \, T_e \tag{2}$$

where p_i, p_e are the pressures of the ions and electrons respectively T_i, T_e the temperatures of the ions and electrons, k is Boltzmann's constant, Z the ion charge. The energies $E_{i,e}$ of the species are given in general by E where

$$E = \frac{p}{\rho(\gamma-1)} \tag{3}$$

where γ is the ratio of specific heat and for a monatomic gas[1] $\gamma = {}^5/_3$ so that

$$E = \frac{3}{2} \cdot \frac{p}{\rho} \tag{4}$$

where ρ is the density in terms of ions and electrons the energies are

$$E_i = \frac{3}{2} \frac{kT_i}{m_i} \tag{5}$$

$$E_e = \frac{3}{2} \frac{kT_e}{m_e} \tag{6}$$

where m_i, m_e are the masses of the ions and electron.

II Heat Conduction

Separate thermal conductivity coefficients are specified for each individual species from Spitzer[2].

$$K_{ii} = K_i = 5/85 \times 10^{11}\sqrt{m_e/m_i}\,(T_i/1.1605 \times 10^7)^{\frac{5}{2}} \qquad (7)$$

$$K_{ee} = K_e = 5.85 \times 10^{11}\,(T_e/1.1605 \times 10^7)^{\frac{5}{2}} \qquad (8)$$

where $K_{i,e}$ are the thermal conductivities of the ions and electrons respectively. Flux limitations on the electrons as defined by Shearer[13] are not justified by the electron temperatures experienced in our model and is not included.

Heat transfer between species is denoted by $Q_{ie} = -Q_{ei}$ where

$$Q_{ie} = \frac{3}{2} k \,(T_i - T_e)/\tau \qquad (9)$$

the time required for the transfer of energy between species is represented by τ (Spitzer's relaxation time)

$$\tau = \frac{3m_i m_e}{8\sqrt{2\pi}} \frac{\left[\frac{kT_i}{m_e} + \frac{kT_e}{m_e}\right]^{\frac{3}{2}}}{e^4 Z^2 \, n \ln \Lambda} \qquad (10)$$

where e is the electron and Λ is the usual ratio of impact parameters given by

$$\Lambda = \frac{3}{2e^3} \left(\frac{k^3 T_e^{\,3}}{\pi n_e}\right)^{\frac{1}{2}} \qquad (11)$$

the coulomb logarithm is set to its maximum value equal to 10.

Since the ions are not directly heated by the laser beam, because of the mass of ion and electron ratio, energy is transferred to the ions from the electrons via collisions. The time for the collisional process to equilibrate is given by τ.

Allowing the densities $n_e = n_i = 5 \times 10^{21}$ cm^{-3} the time τ required for equilibriation of temperatures at different temperatures is calculated in table 1.

τ(sec)	T_e(^{0}K)
3.14×10^{-11}	10^6
5.34×10^{-10}	10^7
1.15×10^{-8}	10^8
2.63×10^{-7}	10^9
7×10^{-6}	10^{10}

Table 1

At a temperature of 10^7 ^{0}K the time required to reach equilibrium of species temperatures is 5.34×10^{-10} secs. For picosecond pulses of laser light one would observe (in the scale of a picosecond) differences in the temperatures of the ions and electrons. A nanosecond laser pulse would be of sufficient time for a temperature of 10^7 ^{0}K to allow equilibration of temperature of both species. This justifies the use of a two temperature fluid model for subnanosecond pulses of radiation.

III Viscosity

The contribution of viscosity to the energy equations of a plasma in one dimension may be written as Kidder, Barnes[3]

(1) Slab-like co-ordinates

$$\rho \dot{e}_{vis} = \frac{4}{3} \mu \left(\frac{\partial \dot{r}}{\partial r}\right)^2 \tag{12}$$

(2) Cylindrical co-ordinates

$$\rho \dot{e}_{vis.} = \frac{4}{3} \mu \left(\frac{\partial \dot{r}}{\partial r}\right)^2 - \left(\frac{\dot{r}}{r}\frac{\partial \dot{r}}{\partial t}\right) + \left(\frac{\dot{r}}{r}\right)^2 \qquad (13)$$

(3) Spherically symmetric co-ordinates

$$\rho \dot{e}_{vis} = \frac{4}{3} \mu \left[r\frac{\partial}{\partial r}\left(\frac{\dot{r}}{r}\right)\right]^2 \qquad (14)$$

where μ is the normal viscosity. Due to uniform compresson and/or expansion where spherically symmetrical co-ordinates imply that volume elements are undistorted means that $\dot{r}/r$ is a constant and hence the viscous contribution to the energy equation drops out in a spherically symmetric geometry. One sees the contribution of viscous terms as being zero or negligible except at shock fronts because the hydrodynamic equations are valid when the mean free path is much smaller than the characteristic length. They become invalid when the mean free path approaches the value of the characteristic length which occurs at shock fronts. Any computational stability at the shock front requires the use of an artificial viscosity term both in a slab like geometry and a spherically symmetric geometry. No requirement is made of an artificial viscosity term for expansion. We use the scheme of Richtmyer and Morton[4] where for the artifical viscosity term appears for compression (when $V_j \geq V_j + 1$)

$$QP = \begin{cases} c\rho\Delta^2 \left(\frac{\partial v}{\partial_x}\right) & \text{if } \frac{\partial v}{\partial_x} < 0 \\ 0 & \text{if } \frac{\partial v}{\partial_x} > 0 \end{cases} \qquad (15)$$

where c is a constant, ρ the density and Δ the mesh size

The argument for an artifical viscosity term lies in the Von Neumann and Richtmyer scheme[5]. When in a compressible fluid, disturbances of large amplitudes occur, waves of different wavelengths couple and energy tends to propagate from the long wavelengths to the short wavelengths. Energy will aggregate in the shortest wavelengths on a different mesh. Hence large oscillations occur between variables at adjacent mesh points. The artifical viscosity term transforms the energyof thelarge mesh oscillations into the thermal energy of the fluid velocities. The value of the ion viscosity is larger than the electron viscosity by a factor of $(m_i/m_e)^{\frac{1}{2}}$. Hence the viscosity is added only to the energy equation for the ion species.

IV Assumptions for the Code

1. Debye length - maeroscopic scalelengths.

A sphere of radius Λ_d called the Debye length would have a potential energy equal to $4\pi n_e{}^2\Lambda_D$. If the kinetic energy of a particle in the sphere is kT is much larger than this potential energy then the effect of the sphere on the motion of that particle is minimal. The Debye length Λ_D is

$$4\pi n_e{}^2 \Lambda_D{}^2 = kT \qquad (16)$$

defining $\Lambda_D = \sqrt{\frac{kT}{4 n_e{}^2}}$ (17)

When considering lengths larger than Λ_D one looks at collective assembly of plasma. Lengths smaller than Λ_D means that the microscopic interparticle effects are important. When the number of particles in a sphere of radius Λ_D (called a Debye sphere) is large, then the primary phenomena of interest are macroscopic collective effects rather than binary particle effects. Such a physical system may be described by a particle field model and the plasma acts as a fluid when the macroscopic scale length of the computational model is larger than the Debye lnngth[6]. Multiphoton processes are assumed which immediately takes into account many interactions when the entire laser field interacts with the plasma - macroscopically described by a classical model.

Condition of quasineutrality also exists when the Debye length Λ_D is much smaller than the characteristic length of density variation in the plasma.

The basis and validity of the 1 fluid plasma model stems from the more general theory of Boltzmann's equations. The basic equations in 1 fluid theory interacting with a laser field contain the mass conservation, momentum conservation and energy conservation equations which are respectively,

$$\frac{\partial \rho}{\partial t} + \underline{\nabla} \cdot \rho \, \underline{v} = 0 \tag{18a}$$

$$\rho \frac{d\underline{v}}{d_t} + \underline{\nabla} \cdot (\underline{\underline{p}} + \rho \underline{v} \, \underline{v}) = \underline{j} \times \underline{B} \tag{18b}$$

$$\rho \frac{d}{d_t} \left(\frac{1}{2} v^2 + v^2\right) + \underline{\nabla} \cdot (\underline{\underline{p}} \cdot \underline{v} + \rho \, \underline{v} \, (\tfrac{1}{2}v^2 + v) + \underline{q}) =$$

$$\text{force applied} \cdot \quad \ldots\ldots \tag{18c}$$

where $\underline{v}$ is the velocity vector, $\underline{j}$ the current density, $\underline{B}$ the magnetic fieldvector, $\underline{q}$ the viscosity vector. The equations are general and the validity of them apply from the consideration of Boltzmann's equation which is the more broad kinetic theory and Boltzmann's equation is

$$\frac{\partial f}{\partial t} + v\, \nabla_r\, f + F \cdot \nabla\, v\, f = \left(\frac{\delta f}{\partial t}\right)_{coll.} \tag{19}$$

where the left hand side represents the flow terms with force F and the right hand side represents interactions with source functions. In plasmas the right hand side is represented by Fokker Planck type source functions.

The method of expansion of f[7] is

$$f = f_o\, (1 + k_n\, Q_1 + k_n^2\, Q_2 + \ldots\quad) \tag{20}$$

Generally there is no proof of convergence for Q_i It does converge depending on the restraints. The first limit for f_o is Maxwellian and

$$k_n = \frac{\Lambda}{L} \tag{21}$$

where Λ is the mean free path and L the characteristic length determined by

$$\Lambda = \frac{|\nabla\, \underline{v}|}{|\underline{v}|} \tag{22}$$

so correct convergence is always assumed for $k_n << 1$. Similarly the constraint for k_n may be made in terms of time τ_{mfp} the mean free path time and T the characteristic time so that

$$k_n = \frac{\tau_{mfp}}{L} \tag{23}$$

The constraints on k_n allow us to assume that local Q_1, Q_2 in terms of length and time are valid and therefore the set of relations eq.(18) are also valid. One sees that k_n acts as a constraint for quasineutrality requiring that the mean free path should be replaced by the Debye length Λ_D thus neglecting microscopic interparticle effects and describing a set of macroscopic equations describing a collective assembly of plasma. We assume that the plasma equations are averaged over a Maxwellian velocity distribution.

In a two fluid model description we look at macroscopic length L and time T in relation to the microscopic length Λ_D and time τ so that

$$L >> |dr| >> \Lambda_D \tag{24a}$$

$$T >> |dt| >> \tau \tag{24b}$$

We have three basic macroscopic time scales. The electron ion scattering time scale τ_e, the ion - ion scattering time scale τ_i, and an irreversible relaxation time scale τ_ε representing the time for equilibration of temperatures between electrons and ions. We do not look at reversible time due to the magnetic field interactions. Assuming $T_e = T_i$ then [8]

$$\tau_e : \tau_i : \tau_\varepsilon = 1 : \left(\frac{m_i}{m_e}\right)^{\frac{1}{2}} : \left(\frac{m_i}{m_e}\right) = 1:43 : 1840 \tag{25}$$

The transfer of momentum from ions to electrons is of the order of τ_e hence the transfer of energy from ions to electrons is small compared to ion - ion transfer. The transfer of momentum from ion to ion is small compared to electron-ion transfer which is therefore the most important effect on the electron distribution function.

If an observers time scale is less than τ_e then the observer would see both electrons and ions behaving as particles. If the time scale is larger than τ_e but less than τ_i then an observer would see electrons acting collectively as a fluid and the ions as kinetic particles. Similarly if the observers time scale was larger than τ_i but less than τ_ε the observer would see the separate species acting as fluids establishing local equilibrium within each species before equilibrium is established between species. This has been previously discussed in the section on heat conduction where a picosecond time scale would see temperature gradients between electrons and ions but nanosecond pulses would be of sufficient time for the equilibration of temperature between species,valid for both 1 or 2 fluid models.

3 Relativistic correction to Mass

Corrections to the masses m of the plasma cells were made,where m* is the relativistic mass,v the velocity of cells

$$m^* = m/\sqrt{1-v^2/c^2} \tag{26}$$

On comparison of mass and the correction to mass affecting the energy with respect to intensity of incident laser radiation, table 2, there appears a difference occurring at an intensity of 10^{17} W/cm^2.

Intensity	$\frac{1}{2} m_v{}^2$ (J)	$\frac{1}{2} m^*_v{}^2$ (J)
10^{13} W/cm^2	$5.0\ 2116 \times 10^6$	5.02116×10^6
10^{15} W/cm^2	4.179326×10^9	4.179326×10^9
10^{17} W/cm^2	4.60476×10^{13}	4.60477×10^{13}

Table 2

Relativistic effects begin to be relevant above 10^{17} W/cm^2. Only when velocities of the plasma are of the order of 10^{10}cm/sec occurring at flux densities larger than 10^{17} W/cm^2 do relativistic corrections to the mass affect results. This is in total agreement with Masini et al.[9], who predicted that relativistic effects are minor for velocities < 10^{10} cm/sec. Relativistic[13] self focussing occurs at 3.6×10^{18} W/cm^2 when the kinetic energy of the laser beam is equal to mc^2. A one dimensional plane wave scheme does not assume self focussing which is simulated by two dimensional geometry. Below the relativistic self focussing threshold intensity that effect is neglected.

4 Bremsstrahlung

We assume that the macroscopic absorption of laser light is by collisional effects namely inverse bremsstrahlung. However we assume that there are no losses due to bremsstrahlung thus limiting the oscillation energy of the electron to less than $\hbar\omega$. At temperatures above 10^7 ^{0}K the plasma radiation energy losses not only through e - i dipole radiation but also by e - e, i - i quadropole radiation[10]. Only when relativistic effects occur that e - e, i - i radiation quadropole effects are important[11]. As all cases are non relativistic any loss of energy can only be through bremsstrahlung. We assume no losses through bremsstrahlung. Reheat, Compton scattering, self generated magnetic fields, creation of non thermal particles by strong shock, non perfect equations of state and their formulations for degree of ionisation have been neglected.

5 Retardation

The solution of the Poisson's equation at boundary conditions requires no retardation time delay, since the density of the plasma self consistently describes the electric field. Therefore for computational purposes of the boundary conditions only the speed of light is assumed to be infinite, and that the laser produces stoccato bursts of energy at times $t^{n+\frac{1}{2}}$ where

$$E_{jm+2} = \tfrac{1}{2}\left[P(t^n) + P(t^{n+1})\right] \Delta t^{n+\frac{1}{2}}$$

the laser energy E_{jm+2} is incident at the plasma boundary described by cell jm + 2 at a time n + ½ and P(t) is the temporal power output of the laser. Poisson's equation is solved separately and the consequent solution included into the E field.

V Lagrangian code

Changing the set of Eulerian equations (18 a-c) by using Lagrangian co-ordinates where cells of variable size and constant mass are used compacts the equations. Use is made of the relation

$$\frac{d}{dt} = \frac{\partial}{\partial t} + \underline{v} \cdot \underline{\nabla} \tag{27}$$

(1) Conservation of Mass

In Eulerian form

$$\frac{\partial \rho}{\partial t} + \underline{\nabla} \cdot \rho \underline{v} = 0 \tag{28}$$

that is $\frac{\partial \rho}{\partial t} + \underline{v} \cdot \underline{\nabla} p + \rho \underline{\nabla} \cdot \underline{v} = 0$ (29)

in Lagrangian form

$$\frac{d\rho}{dt} = - \rho \, \underline{\nabla} \cdot \underline{v} \tag{30}$$

Since the masses of cells are constant

$$\frac{d\rho}{dt} = 0 \quad \text{implying } \underline{\nabla}.\underline{v} = 0 \tag{31}$$

(2) Conservation of Momentum

$$\frac{\partial \rho \underline{v}}{\partial t} + \underline{\nabla} \cdot \rho \, \underline{v} \, \underline{v} = - \underline{\nabla} \, p - \underline{F} \tag{32}$$

that is

$$\rho \frac{\partial \underline{v}}{\partial t} + \underline{v} \frac{\partial \rho}{\partial t} + \rho v \cdot \underline{\nabla} \, \underline{v} + \underline{vv} \cdot \underline{\nabla} \, \rho + \rho \underline{v} \, \underline{\nabla}.\underline{v} + v \rho \underline{\nabla} \cdot \underline{v}$$

$$= - \underline{\nabla} p - \underline{F} \quad \ldots\ldots \tag{33}$$

In Lagrangian form and using convervation of mass equations this simplifies to

$$\rho \frac{d\underline{v}}{dt} = - \underline{\nabla} \, p - \underline{F} \tag{34}$$

where $\underline{F}$ are the forces interacting with the plasma. We assume that the pressure is isotropic. The nonlinear force, gravitational force, artificial viscosity and the Poisson term are included in $\underline{F}$ then

$$\rho \frac{d\underline{v}}{dt} = - \nabla \, p \pm (z_{ni} - n_e) \, \underline{E} \pm \frac{1}{8\pi} \nabla \, (E^2 + H^2) \pm F_\phi - QP \quad \ldots\ldots (35)$$

The Poisson term is solved separately then included in $\nabla (E^2 + H^2)$

$\frac{1}{8\pi} \nabla \, (E^2 + H^2)$ is the nonlinear force

F_ϕ is any extraneous force e.g. gravitational and is neglected.

QP is the artificial viscosity term which is included only when the mean free path λ is greater than or equal to the characteristic length occurring at shock fronts.

The momentum is diffused through the fluid by macroscopic particle motion denoted by the artifical viscosity term assumed to affect only the ions.

The gradient of the pressure as will be seen later is comprised of the partial pressures on the ions and the electrons so that

$$\begin{aligned} \nabla p &= \nabla(p_i + p_e) \\ &= k\nabla\, n_i T_i + k\,\nabla\, n_e T_e \end{aligned} \tag{36}$$

3 Conservation of energy equations

The energy equations for the electrons and ions are treated separately. We assume that all incident radiation energy is absorbed only by the electrons through inverse bremsstrahlung. So that we have for electrons

$$\frac{\partial}{\partial t} \int_V \rho_e E_e \, dV = - \int_A p_e \, \underline{v} \, . d\, \underline{A} - \int_A K_e \frac{\partial T_e}{\partial \underline{r}} . d\underline{A} + \int_V \rho_e \dot{E}_e \, dV \quad \ldots\ldots\ldots \tag{37}$$

for ions

$$\frac{\partial}{\partial t} \int_V \rho_i E_i \, dV = - \int_A p_i \, \underline{v} \cdot d\underline{A} - \int_A K_i \frac{\partial T_i}{\partial \underline{r}} \cdot d\underline{A} \tag{38}$$

where $\rho_{e,i}$ are the separate electron and ion densities; $E_{e,i}$ are the separate electron, ion internal energies; $p_{e,i}$ are the electron, ion pressure, $\underline{v}$ is the velocity defined as $\underline{v} = \frac{d\underline{r}}{dt}$, A the area, V the volume. $\dot{E}_e$ is rate of energy addition to the electrons by inverse bremsstrahlung. $K_{e,i}$ are the coefficients of thermal conductivity for the electrons and ions.

The power absorbed by the electron via inverse bremsstrahlung is

$$W_e = I\,K = \frac{c}{8\pi}\;E^2\,K \tag{39}$$

where I is the incident intensity, E the electric field, K the absorption coefficient when $n_e < n_{ec}$, then K is given by

$$K = \frac{4\pi^4 Z^2 n_e n_i e^4 \ln\Lambda}{c\omega^2 (2\pi m_e)^{\frac{3}{2}} (kT_e + E_{os})^{\frac{3}{2}}} \tag{40}$$

the ln Λ term is set at a maximum of 10. We include the nonlinear correction to the absorption constant by including the oscillation energy of the electron due to the laser light radiation. The amount of energy absorbed only by electrons in each cell is

$$W_j^{n+\frac{1}{2}} = E_{j+1}\quad(1 - e^{\int k\,dr}) \tag{41}$$

where E_{j+1} is the energy incident on the cell and

$$E_j = E_{j+1} - W_j^{n+\frac{1}{2}} \tag{42}$$

is the energy incident on the next innermost cell. This is repeated from the first cell on the right, JM+2, inward to the first overdense cell. Assuming a linear approximation for the density of the cell, somewhere in the overdense cell the plasma frequency is equal to the laser frequency. Reflection then occurs. The process above is then repeated in the opposite direction. The temperature T_e is assumed to be constant within each cell. Integration of the absorption coefficient for each cell requires a linear profile to ascertain the precise point when $\omega_p = \omega$. This assumption prevents errors in any cell when n_e is equal to n_{ec}.

The electron and ion energy equations are converted into finite difference form so that we solve for

$$n_e^j \frac{\partial}{\partial t} T_e^j = - p_e^j \frac{\partial Vj}{\partial t} - (K_e A \frac{\partial T_e}{\partial x})_j + (K_e A \frac{\partial T_e}{\partial x})_{j+1}$$

$$- ({}^3/_2) n_e kV \frac{\nabla T}{\tau} + n_e^j \dot{E}_e^j \quad \ldots\ldots\ (43)$$

$$n_i^j \frac{\partial}{\partial t} T_i^j = - p_i^j \frac{\partial V_j}{\partial t} - (K_i A \frac{\partial T_i}{\partial x}) + (K_e A \frac{\partial T_e}{\partial x})_{j+1}$$

$$- ({}^3/_2) n_i \frac{V\, k\nabla T}{\tau} \quad \ldots\ldots\ (44)$$

where the script j represents the cell j. This set of equations are solved implicitly. The use of an implicit differencing scheme in comparison with an explicit differencing scheme which computes the new temperature from values of previous temperatures at 3 adjacent points is this. The temperature in the explicit scheme is able to propagate at most one mass point per time cycle. In reality at areas of high conductivity the heat propagates over many cells in one time cycle. To be more precise simultaneous computations should be made for all present temperatures which gives the total physical information at each cycle. Thus allowing the temperature to propagate everywhere in the plasma without loss of information.

Collisional energy transfer between electrons and ions can save computational time if the relaxation time is isolated from the energy equations and solved separately. Dividing eqs. (43) and (44) by ${}^3/_2\, n_{e,i}\, k$ and subtracting and retaining only the temperature difference yields,

$$\frac{\partial \Delta T}{\partial t} = - (1 + z) \frac{\Delta T}{\tau} \tag{45}$$

Eq. (45) can be integrated over the time step Δt by assuming that τ is constant giving

$$\Delta T = \Delta T_o \exp - \frac{\Delta t^{n+1}}{\tau} \tag{46}$$

where ΔT_o is the temperature difference between the species at the commencement of intergration. The calculation of the temperature relaxation terms is done in two separate periods. The first between times n and n + 1, followed by implicit calculations solving the remaining energy equation terms for the temperature, followed by the second period between times n + ½ and n + 1. This method of separation is required for accuracy of τ and the coupling of separate equations required for repeated computations.

The energy equations without the relaxation terms may be solved by the method of Richtmyer and Morton[4]. We set up equations (43) and (44) so that they are in the form

$$-A_j V_{j+1} + B_j V_j - C_j V_{j-1} = D_j \tag{47}$$

and solve V_j which denotes the implicit temperature value where

$$V_j = E_j V_{j+1} + F_j \tag{48}$$

$$E_o = F_o = 0 \tag{49}$$

$$E_j = A_j / (B_j - C_j E_{j-1}) \tag{50}$$

$$F_j = (D_j + C_j F_{j-1}) / (B_j - C_j E_{j-1}) \tag{51}$$

Storing E_j and F_j in the arrays D_j and B_j saving the value of D_j for use in (51) before calculating (50).

VI Description of the Code

The overall plan of the code is divided into four sections. These are initialisation, increment in temperature, dynamical increment, updating and checking.

(A) Initialise

(1) Set constants

(2) Initialise density profile

(3) Initialise plasma properties

(4) Call laser pulse parameters

(5) Write initial condition

(B) Temperature Increment

(6) Compute added energy - CALL LASER for input power

(7) Half relaxation of electron ion energy difference

(8) Ion heat conduction solved implicitly

(9) Electron heat conduction solved implicitly

(10) Half relaxation of remaining electron-ion energy difference.

(C) Dynamical Increment

(11) Advance velocity

(12) Advance radius, velocity

(D) Update and check

(13) Update plasma properties

(14) Compute and check energy balance

(15) Write current plasma variables

(16) Check temperature, densities, time

(17) Update variables

Lagrangian Mesh

The plasma in one dimension is divided into J M cells with each cell individually indexed by j. The size of each cell is variable, the adjustment of size depending on the constraint of having an invariable mass for each cell. The densities and temperatures of the plasma reside in the center of the cells at integer times. The positions of the interfaces are observed at integer times. The velocities of the interfaces are determined at half integer times.

(a) Interfaces j of the cells are located as follows at time n, figure 1.

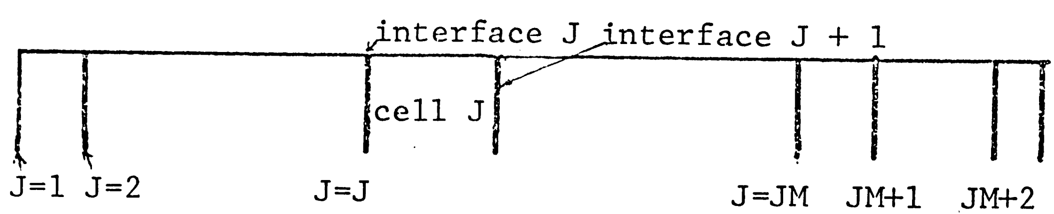

Figure 1

Plasma is divided into J m + 2 cells where the first, J = 1, cell and the last, J = J m+ 2, cell are used as dummy cells.

(b) Each interface J is advanced in time which then determines the new temperatures, velocities and densities. We can view the advancement in time by layering of the above diagram for each half and full integer time. A schematic description follows on the next page, figure 2.

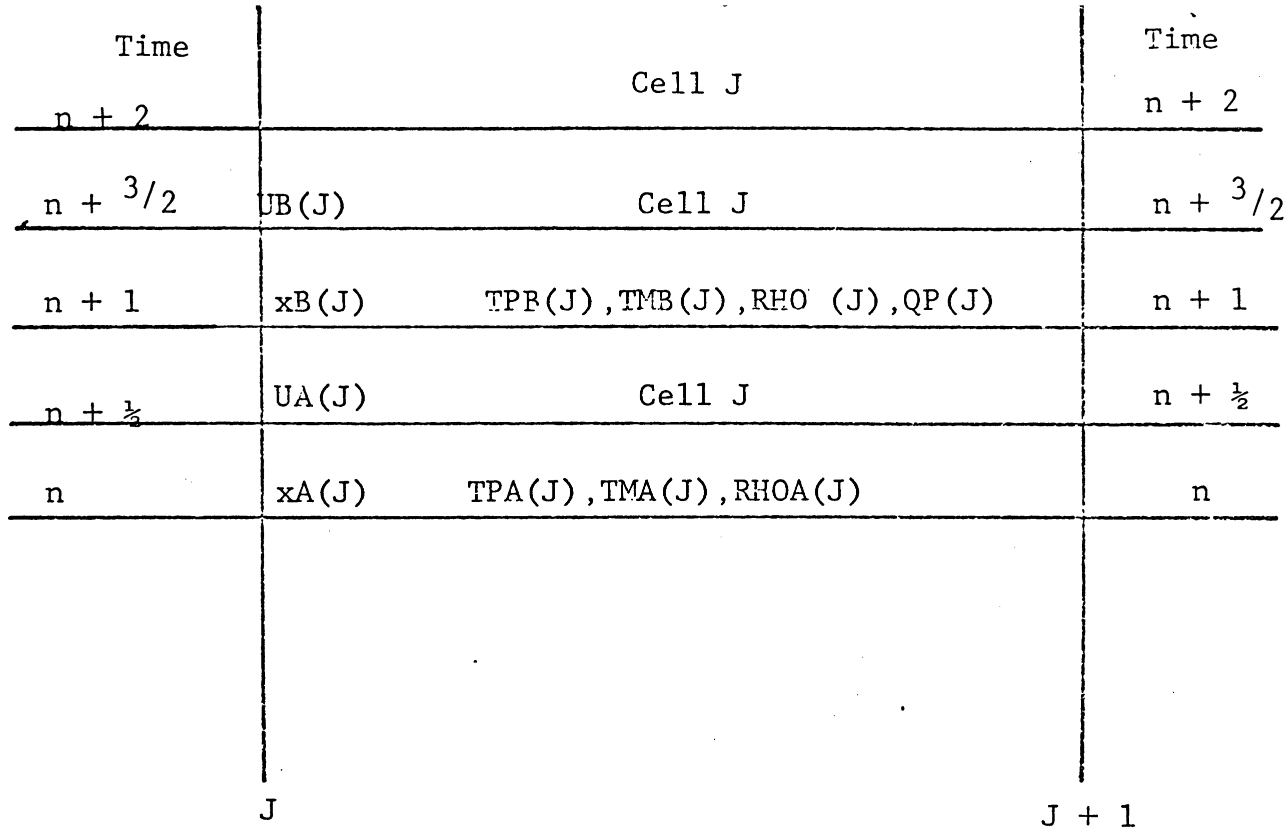

Figure 2

Schematic diagram depicting the advancement of interface J in time, determining the new temperatures, densities, velocities and temperatures in cell J.

In general if a variable ends with an A it is the earlier time step than that for a variable ending with a B. So that the position of the j^{th} interface at time n is indexed by XA(J). The position of the j^{th} interface at time n + 1 is indexed by XB(J). Similarly for temperatures of the ions TPA(J), temperatures of the electrons TMA(J) and the density of plasma RHOA(J). The velocity of the interface is determined at half integer times so that UA(J) is the velocity of the plasma at time $n + \frac{1}{2}$ and the velocity UB(J) is at time $n + {}^3/_2$. After the variables have been calculated at the new time, it is required to reset those variables for calculations at later times.

Description of Variables

XB(J) - Position of interface j at time n+1

XA(J) - Position of interface j at time n

UA(J) - Velocity of interface j at time $n + {}^1/_2$

UB(J) - Velocity of interface j at time $n + {}^3/_2$

RHOA(J) - Density of cell j between j to j+1 at time n

RHOB(J) - Density of cell j between j to j+1 at time n+1

TPA(J) - Temperature of ions in cell j at time n

TPB(J) - Temperature of ions in cell j at time n+1

TMA(J) - Temperature of electrons in cell j at time n

TMB(J) - Temperature of electrons in cell j at time n+1

DM(J) - Mass of cell j

W(J) - Specific energy absorbed in cell j between time n and n+1

QP(J) - Artificial viscous pressure in cell j at time n

ALNE(J) - Log terms of temperatures, densities for

ALNI(J) - implicit integration of energy equations.

JJ(J) - Cell number

JG(J) - Dummy cell number used as a condition for avoiding overlapping

TSI(J) -
TS2(J) -
TS3(J) -
Implicit heat conduction used for computation of A,B,C,D,E,F

A(J) -
B(J) -
C(J) -
D(J) -
E(J) -
F(J) -
Solving implicitly the heat conduction terms in the energy equations is solved by R Richtmyer R. Morton[4]

ETA(J) - Used for calculation of EM energy to be included in the absorption coefficient

XXX(J) - Used for plot routine

DTPR(20) - Used for time checks

TPRC(20) -

BETA(J) - Refractive index squared where $BETA=1-\frac{n_e}{n_{ec}}=n^2$

GAMMA(J) - Absorption coefficient calculated before and after interacting with laser light.

PR (J) - $\frac{1}{8\pi}(E^2 + H^2)$

SX(J) - Variable array for calculation of W(J)

ET(J) - Used for ETA(J) in calculating GAMMA(J)

Input Variables - all units in C.G.S.

TWAIT = 0.0 Arbitrary constant for control of data read in

TRISE = .secs The rise time for laser input

POWER = $ergs/cm^2$ INPUT INTENSITY

ANGLE = 0.0 ANGLE OF INCIDENCE (not used)

Z = 2.EO CHARGE

ZSQ = 5.EO CHARGE SQUARED PLUS ONE

ANCORE = 1.17E23 Arbitrary constant to set the critical density

TEMPIN = 1.E6 ^{0}K Initial temperature input

DTIME = secs Time steps

NPRINT = 4 Number of time step constraints

<u>Constants</u>

DTB	Equal to DTIME the time step
DTC	Half the time step
RANGLE	ANGLE/π/3 in this case = 0
STH2	STH2 = SINE (RANGLE)^2 = 0
CTH	SQRT(1-STH2) = 1
BOLTZ	Boltzmann's constant k
PI	π
CC	Speed of light in vacuum
CHARGE	e
ELMASS	M_e
ALMASS	m_i
AMASS	$(a\ m_e + m_i)$
RT	RT = BOLTZ/AMASS
KRPT	Number of interactions of implicit heat conduction
TRATL	Fraction of total energy allowed to be absorbed
WAVELN	Wavelength of input laser light
FREQL	Frequency of laser light ω
OML	$2\pi\omega$
CKO	2ω/WAVELN

CC12 CC122	Constants used for relaxation time τ
CC17	Used for calculation of electromagnetic energy density
CC18	Used for absorption coefficient
CC19 CC20	Also used for relaxation time
CC21	Used for calculating RDEB
CC25N CC25P	Used for implicit heat transfer calculations
ENCORE RHOCOR ENCR RHOCR RATCOR	Used for initialising density
JM	Number of cells
JMO	Constant equal to JM
JMPI	JM plus one
JMP2	JM plus two
ETOTA	Total energy absorbed
TMASS	Total mass
WTOT	Total input energy
SINC	Phi *POWER
SINX	SINX = ANGLE DEPENDENCE*SINC
SXIN	SXIN=SINX
ESUP	Total power input
ERROR ERRORA	Error check
SXOUT	Power out
TAUE12	Relaxation time τ

TAUE12 Relaxation time τ

ENERGL Pulse energy $/cm^2$

ENERGX incident energy $/cm^2$

Initialise Density Profile

Call subroutine INIDEN returns with initial density and mass for each of the J N cells. There are three separate routines for the formation of density profiles. These are shown schematically below where the initial thickness D of the total plasma is not more than 100 microns, for figures 3, 4, 5.

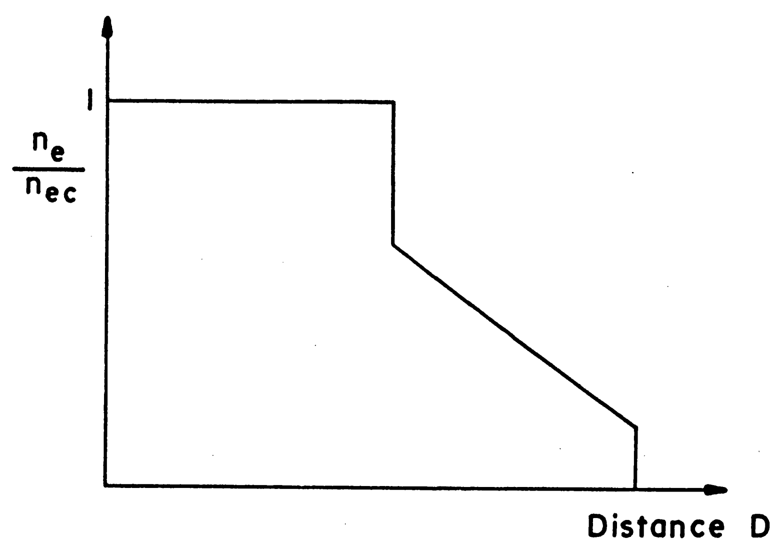

Figure 3 Linear step profile connected to a plateau at constant density equal to the cut off density.

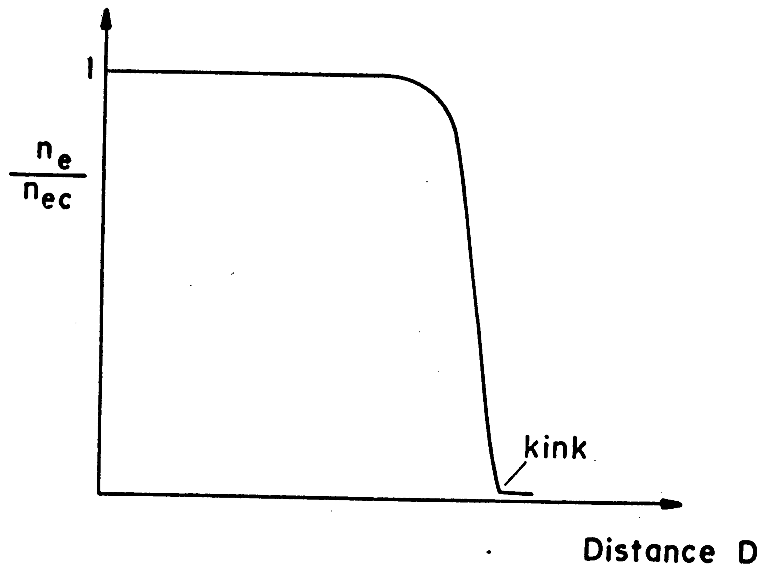

Figure 4 Raleigh profile connected to a plateau at constant density equal to the cut off density with a kink at the vacuum plasma boundary.

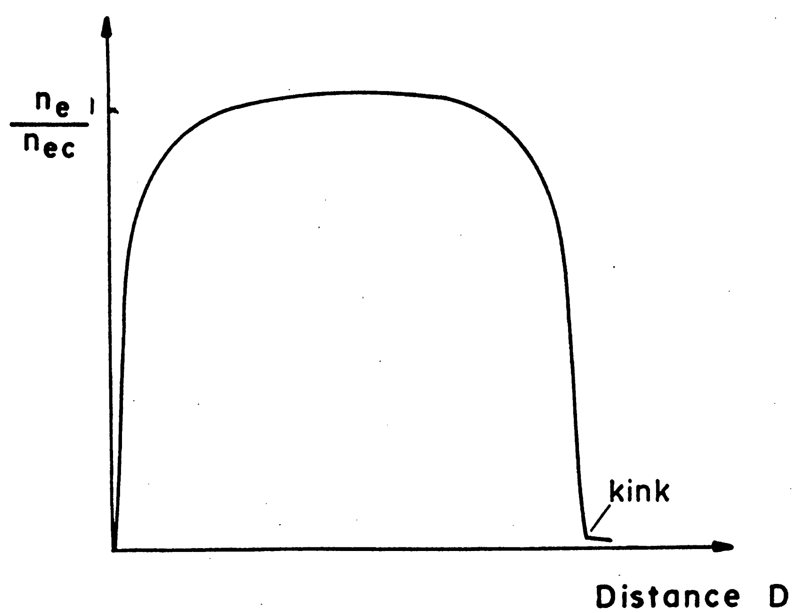

Figure 5 Bi-Rayleigh profile with a kink occurring at both ends of the profile. In all cases the laser light is incident from the right

Initialise Plasma Properties

Calculate

BETA = $1 - n_e/n_{ec} = n^2$

ALNE, ALNI: log terms used for computation of relaxation times

GAMMA The absorption coefficient before laser input

TMASS Calculate the total mass

ETOTA Calculate the total thermal energy and velocities

LASER PULSE PARAMETERS

Calculate the temporal envelope $\phi(t)$ of the laser pulse. For the modified Gaussian assumed here.

$$\phi(t) = \begin{cases} 1.21\,t & t < .455 \\ e^{-2(1-t)^2} & .455 \leq t \leq 1 \\ e^{-(1-t)^2} & t > 1 \end{cases}$$

where T is TIMER

WRITE

Print out the initial conditions and several variations.

Calculations of Interactions

CALL subroutine LASER to ascertain the amount of incoming power at any particular time.

CALL WAEQ routine to calculate the electromagnetic energy density, the power density per unit cell, and other variables for later calculations of the absorption coefficients with a new absorption coefficient to account for power fluxes.

Relaxation Energy - Half time step

Calculate half of the relaxation of the electron ion energy difference - the relaxation time constant τ and the temperature T and the change in temperatures of both species over half a time cycle. DTC denoted by DELT.

Then

TPA(J) = T -Z* ZI* DELT

TPB(J) = TPA(J)

TMA(J) = T + ZI*DELT

TMB(J) = TMA(J)

Implicit intergration of energy equations

Using Richtmyer's[4] iterative implicit finite difference formulation because of the high temperatures involved we then solve for the ion heat conduction then the electron heat conduction.

Second half relaxation energy

Calculate the remaining half of the relaxation electron ion energy difference.

Advance velocity

Including an artificial viscosity we solve for

$$\frac{dv}{dt} = \frac{d}{dx}\left(\frac{E^2 + H^2}{8\pi}\right) - \frac{d}{dx} n\ k\ T + QP \qquad (52)$$

where the n,T contains both electron and ion contributions.

Advance radius and density

xB(J) = xA(J) + UB(J)*DTB (53)

RHOB(J-1) = DM(J-1)/(XB(J)-XB(J-1) (54)

Update

With the new values of the temperatures, velocities, densities, distances and the new electric energy density terms we then update the various plasma properties which existed in the initialised plasma properties.

ENERGY ERROR CHECK

Obtain the total energy before laser input where the thermal energy is

$$ETOTA = m \quad (T_i + z\ T_e) \tag{55}$$

Compute the kinetic energy

$$EKIN = \frac{1}{2}\ m(v_i + v_{i+1})^2 \tag{56}$$

Compute the initial energy

$$EINT = {}^3/_2\ {}^k/_m\ (T_i + z\ T_e) \tag{57}$$

Then the total energy after laser input is

$$ETOTB = EKIN + EINT \tag{58}$$

Then the error at each time step is calculated as

$$ERROR = (ETOTB - ETOTA-WTOT)/(ETOTB-ETOTIN) \tag{59}$$

A further check is made from momentum conservation.

Time and space limitations

To prevent a sound wave from crossing a cell the general Courant-Lewy-Fredericks condition[12] (CLF) for computational stability is imposed on the time step where

$$\Delta t \leq \frac{\Delta}{|v|} \tag{60}$$

where Δ is the mesh size and $|v|$ the velocity of sound. This requires that the time step Δt will be short enough to prevent a sound wave from crossing the cell. The speed of the sound wave as a function of the temperature will vary from cell to cell on the mesh and the limitation on the time step is a local one to be evaluated at each cell. In our case the condition is

$$\Delta t = c \frac{XA(J+1) - XA(J)}{\sqrt{5/3\ k/m\ (TPB(J)+TMB(J))}} \tag{61}$$

where c is a constant and k is Boltzmann's constant.

Allowance is made of a fraction of energy to be transferred from each interface. Energy transfering at higher rates than allowed would lead to instabilities. This condition on time is written as

$$\Delta t_T = \frac{\Delta t\ T_e^{\ n}}{T_e^{\ n+1} - T_e^{\ n}} \tag{62}$$

where Δt is the time step and $T_e^{\ n}$ and $T_e^{\ n+1}$ are the electrons temperatures at times n and n+1. If for any reason $T_e^{\ n} > T_e^{\ n+1}$ then Δt_T will be made smaller by a factor of ten thus allowing more detail and information to be printed.

Restriction is also made to the amount of laser light energy input by imposing the condition that only a fraction TRATL of the total energy, ETOTA, in the plasma divided by WTOT the total laser energy absorbed during the previous time step where Δt_F is the time for that fraction of energy input then

$$\Delta t_F = DTA*\ TRATL*\ ETOTA/WTOT$$

To impose all three constraints above on the time scale the smallest of the three conditions is taken to be the next time step.

CHAPTER 6 Results and Discussions

I Density Profiles

Assuming a collisionless plasma with the collision frequency ν set equal to 0 we obtain the refractive index of a Rayleigh profile as a function of distance x by defining

$$n = \frac{1}{1 + \alpha x} \tag{1}$$

where α is a real constant. The corresponding electron density n_e for the refractive index n above as a function of x is

$$n_e = n_{ec} \left(1 - \frac{1}{(1 + \alpha x)^2}\right) \tag{2}$$

where n_{ec} is the cut off density determined by the frequency of incoming laser radiation ω given by

$$n_{ec} = \frac{m_e \omega^2}{4\pi e^2} \tag{3}$$

where m_e is the electron mass and e is the electronic charge. For a CO_2 laser with wavelength of 10.6 μm, n_{ec} is 9.84×10^{18} cm^{-3}. For a Nd glass laser with wavelength of 1.06 μm, n_{ec} is 9.84×10^{20} cm^{-3}. Figure 1 displays the refractive index n of a Rayleigh profile for various α as a function of distance x. For values of $\alpha \geq \alpha^+$ where $\alpha^+ = \frac{2\omega}{c} = 1.18 \times 10^5 \text{cm}^{-1}$ the plasma exhibits total reflectance for Nd glass laser radiation. The corresponding electron densities as a function of x according to eq.(2) for different α is displayed in Figure 2. The motivation for using this density profile is derived from the results of the chapter on reflectivities. The low reflectivity of light for

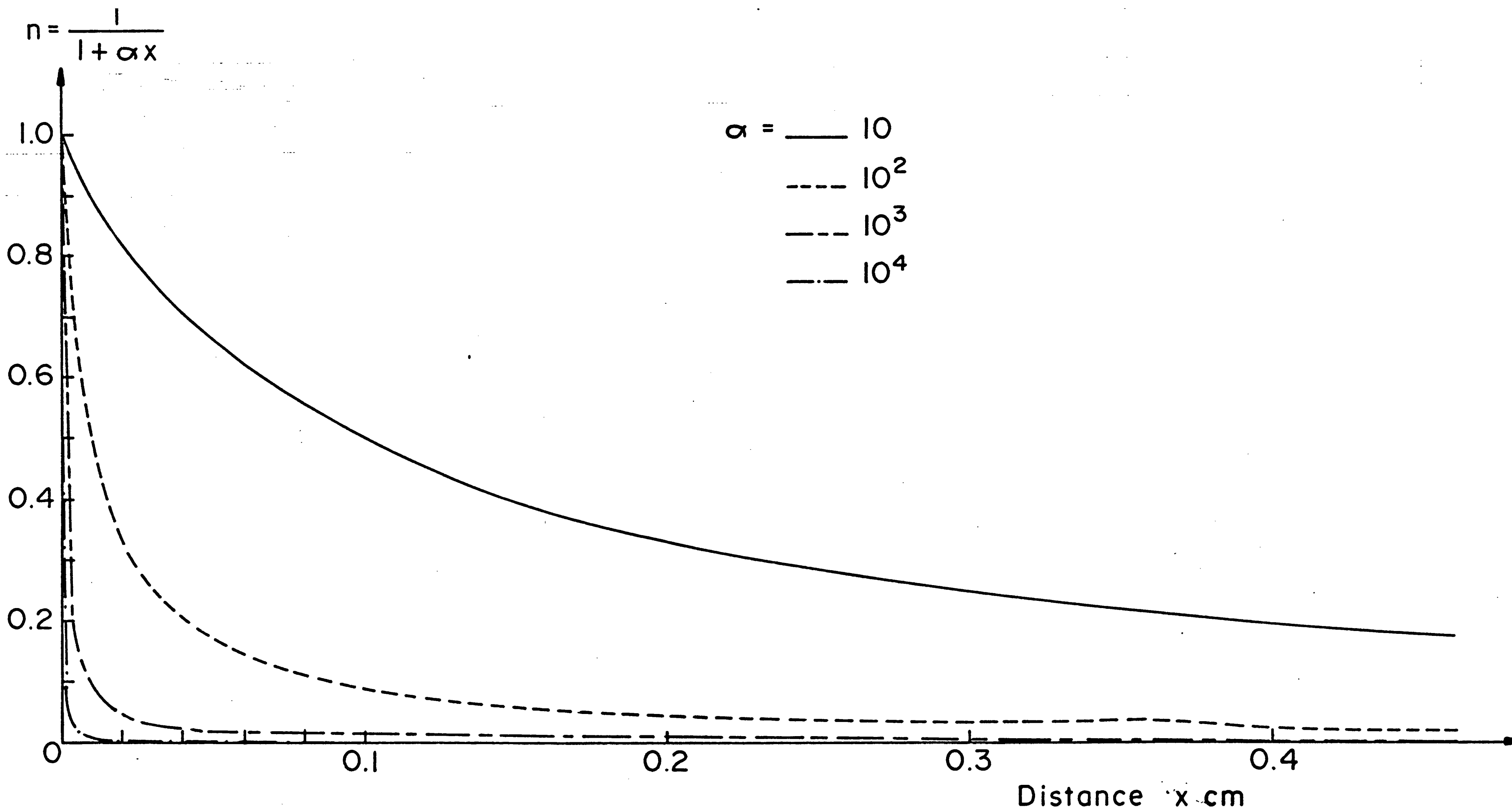

FIGURE 1 Spatial variation of the refractive index of a Rayleigh density profile, where the profile is described by eq. 1 and displayed for different values of α.

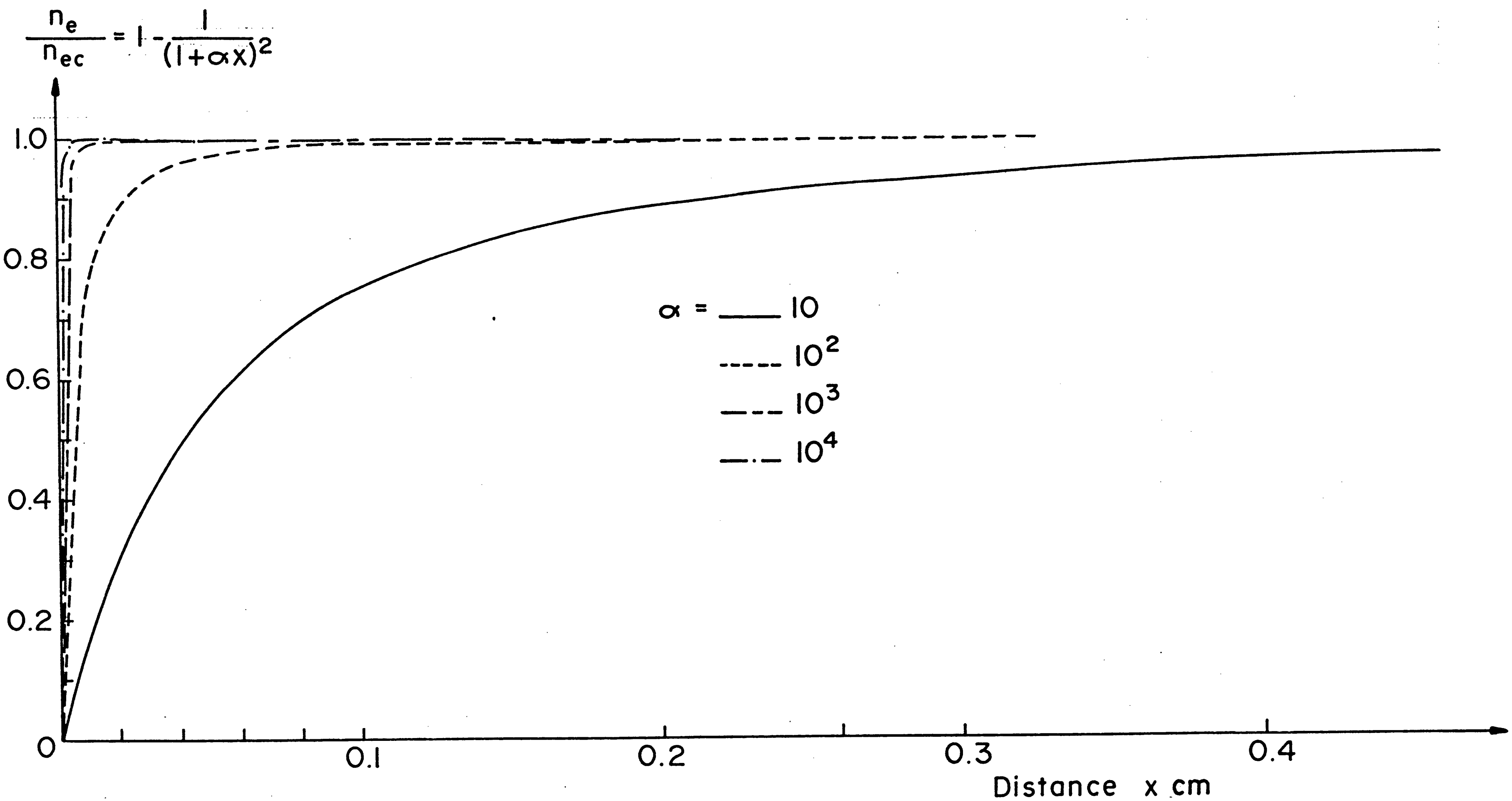

FIGURE 2 The electron density profile of a Rayleigh like profile for different values of α corresponding to eq. (2).

$\alpha < \frac{1}{4}\alpha$ is less than 5%[1]. For the following discussions of the nonlinear force transfer of optical energy into kinetic energy of moving plasma for compression we have selected those cases with a minimum of reflection.

When plasma exists at temperatures where collisional effects are important then the collision frequency ν can no longer be assumed to be 0. If the α in eq. (1) is made of real and imaginary components A and iB where the constants A and B are real variables, the absorption coefficient of the Rayleigh profile will depend on the imaginary part of the refractive index, iK where K is the absorption coefficient given by

$$K = \frac{-Bx}{(Ax + 1)^2 + B^2x^2} \qquad (4)$$

where K is a function of x. In figure 3 are plots of equal and increasing values of A and B. The absorption coefficient peaks in all those cases with the maxima approaching the vertical (x = 0) axis. Plasmas are not always collisionless. Depending on the temperature the collision frequency changes the absorption coefficient in equation 4. Similar to figure 3, figure 4 shows values of increasing B the imaginary part of the refractive index. The variable A remains constant as B increases. The maxima increases with increasing values of B with the maxima approaching the vertical axis with increasing B. When radiation interacts with a Rayleigh profile and it experiences absorption, the absorption of radiation will reach a peak, the value of which is determined by the maxima of the absorption

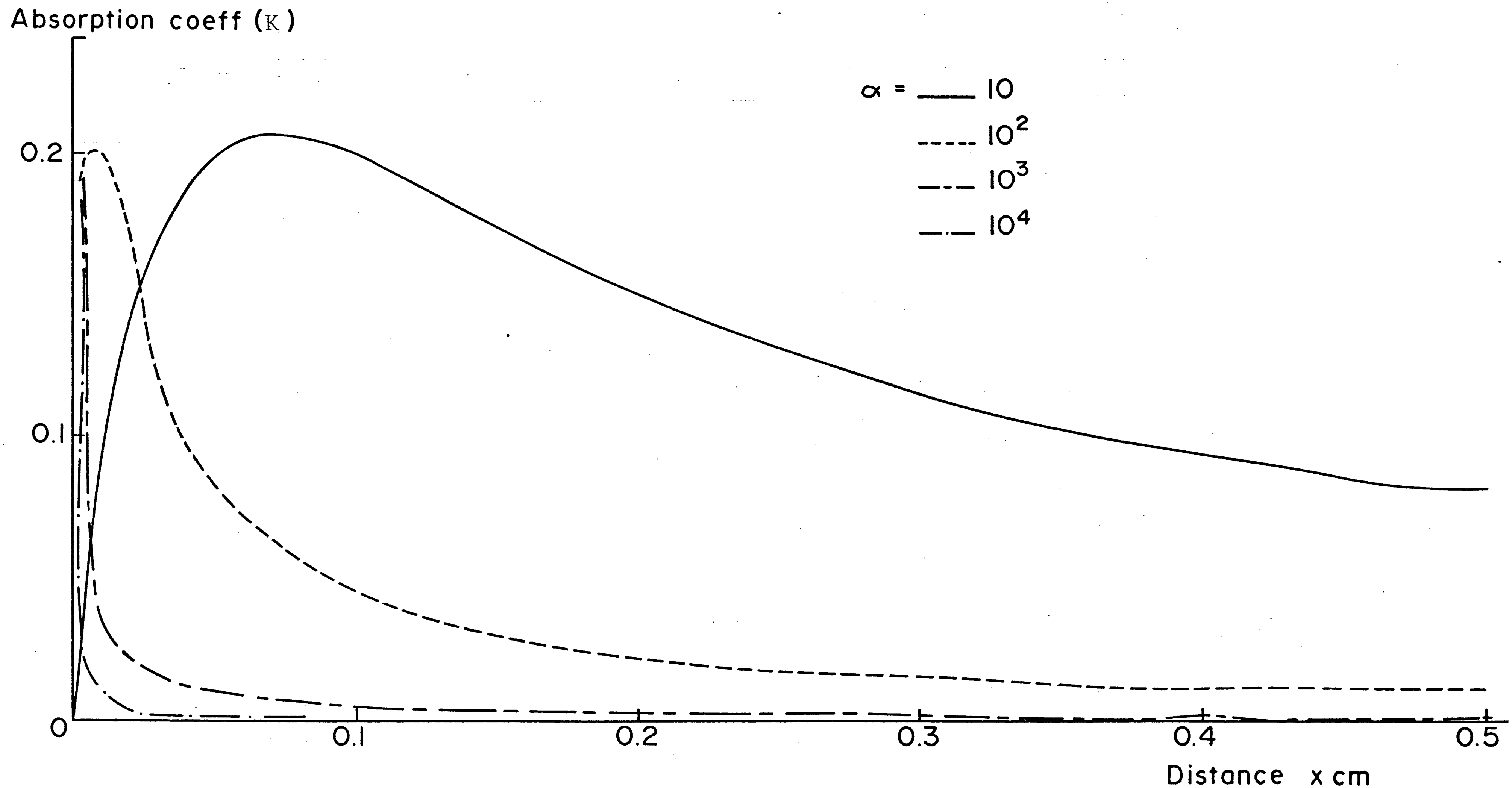

FIGURE 3 The absorption coefficient K of the Rayleigh profile for equal real and imaginary components A and B corresponding to eq. (4).

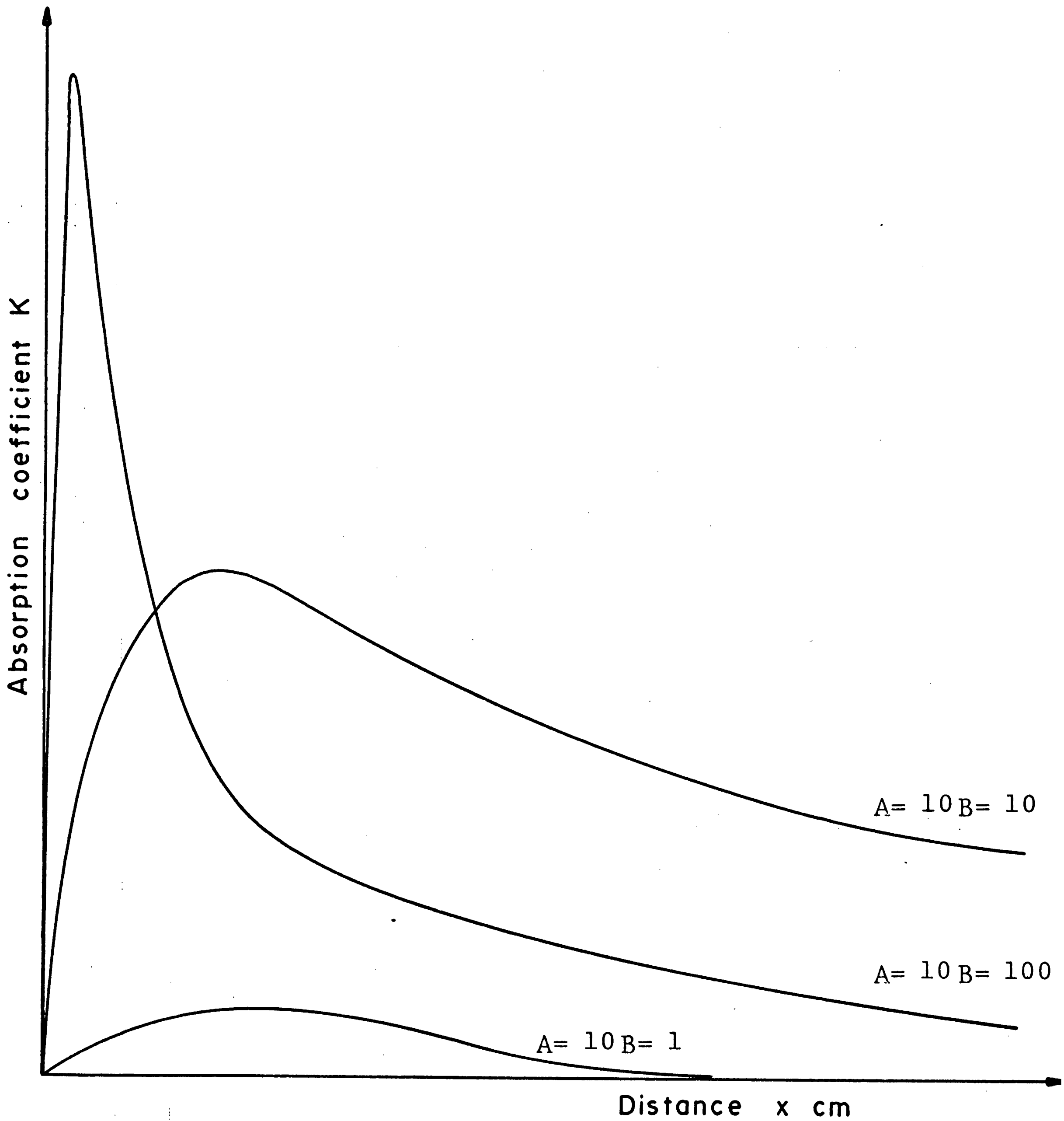

FIGURE 4 Absorption coefficient K of the Rayleigh profile for varying real and imaginary components of A and B corresponding to eq. (4).

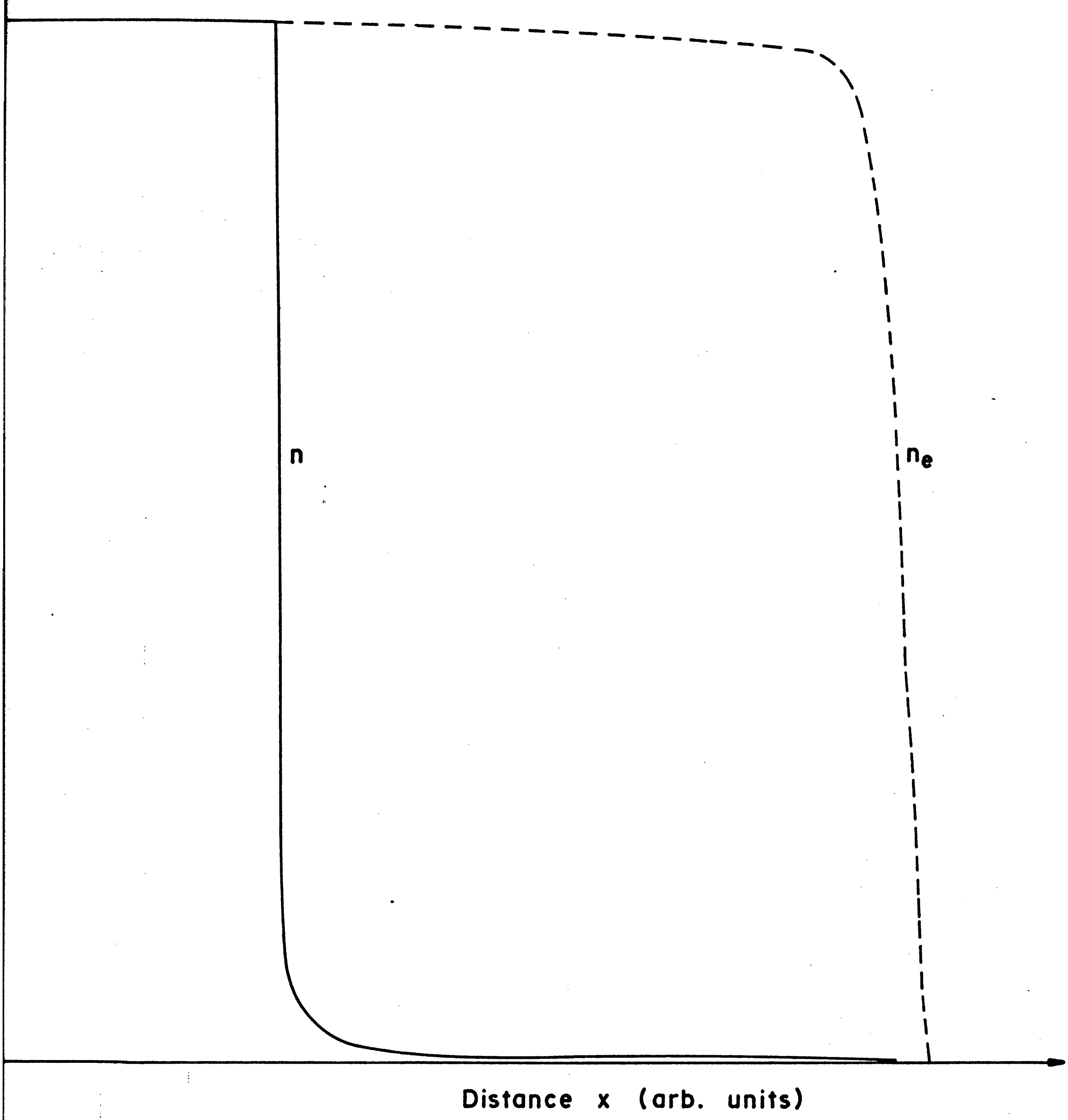

FIGURE 5 The schematic connection of a Rayleigh profile onto a plateau of constant refractive index equal to one corresponding to eq. (5).

coefficient. In figure 5 we connect continuously a Rayleigh profile onto a plateau of constant refractive index equal to one given by

$$n_e = \begin{cases} n_{ec} & x \leq 0 \\ n_{ec}\left(1 - \dfrac{1}{1 + \alpha(x - 50\mathrm{pm})^2}\right) & x \geq 0 \end{cases} \tag{5}$$

The curve on the right corresponds to the electron density. The one on the left the refractive index n. As will be shown later the curve attached onto a constant refractive index of value one exhibits little reflection up to the boundary where the electron density is equal to the cut off density. This will exhibit the same behaviour as that of a linear gradient of electron density whose value monotonically increases to that of the cut off density. This set of profiles, eq. (5) are used as test cases because laser light at non relativistic intensities without self focussing effects will not penetrate plasma equal to or above the cut off density. At the position corresponding to the cut off density, laser light will be reflected. The interaction between reflected and incoming waves forms a standing wave pattern.

An inhomogeneous bi-Rayleigh density profile is seen in figure 6. It consists of constructing two symmetric Rayleigh profiles corresponding to an initial density profile which has the form

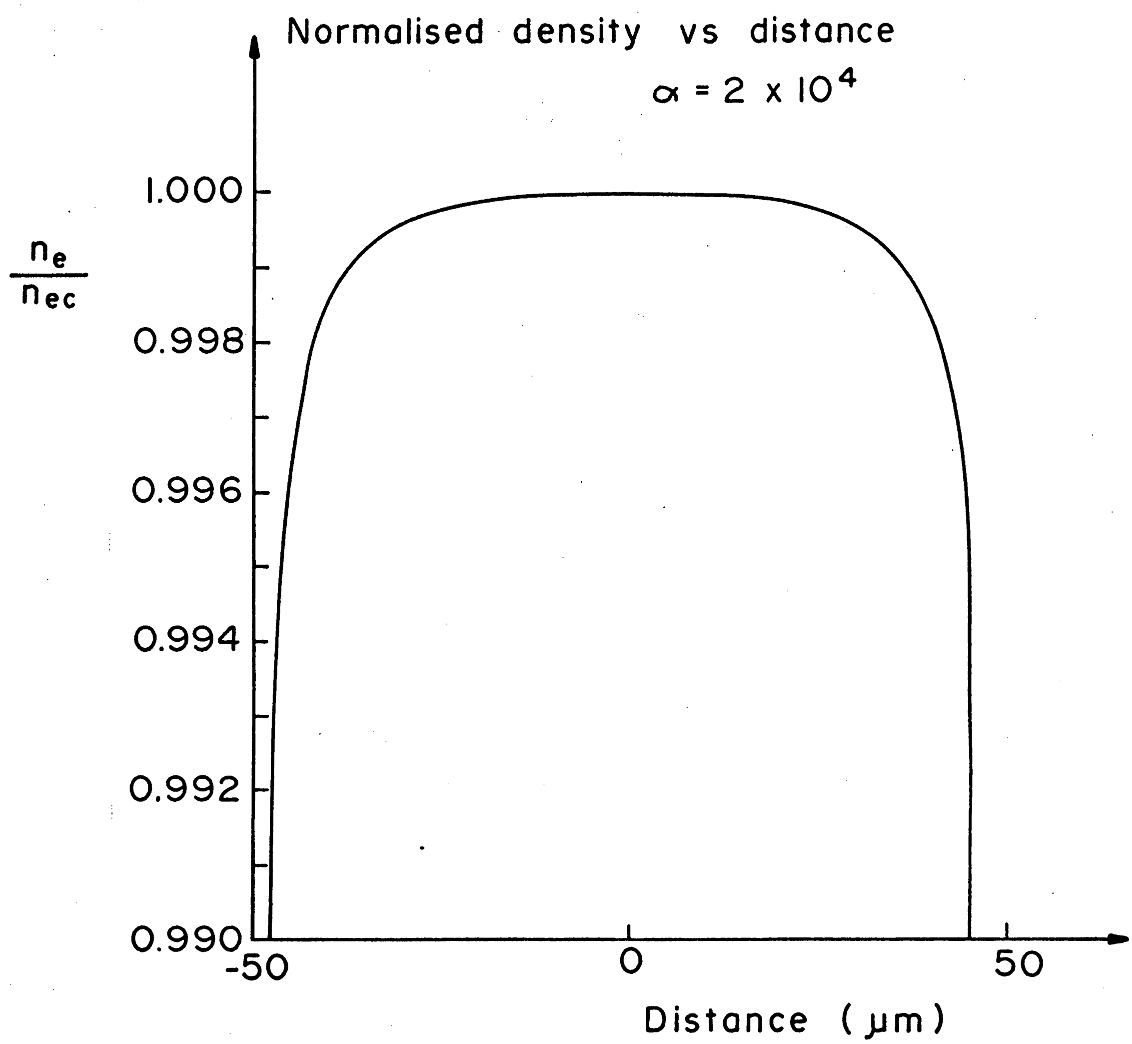

FIGURE 6 An inhomogeneous bi-Rayleigh density profile with an $\alpha = 2 \times 10^4$ cm^{-1} corresponding to eq. (6) In all cases initial temperatures are assumed to be uniform throughout the plasma. The cut-off density n_{ec} varies with the wavelength of laser radiation defined by eq. 3.

$$n_e = \begin{cases} 0 & ;\quad x \geq 50\ \mu m \\ n_{ec}^{+}\left(1 - \dfrac{1}{1 - \alpha(x - 50\mu m)^2}\right)^2 & ;\quad \leq x \leq 50\mu m \\ n_{ec}^{+}\left(1 - \dfrac{1}{1 + \alpha(x + 50\mu m)^2}\right)^2 & ;\quad -50\mu m \leq x \leq 0 \\ n_{ec}/1000 & ;\quad x \leq -50\mu m \end{cases} \tag{6}$$

where n^{+}_{ec} is .01% smaller than n_{ec}.

At lower values of α the plasma exhibits high transmission properties and the laser light penetrates the plasma with rippling effects. The rippling of the electromagnetic energy density will cause bunching of the electron densities driving the electron densities above the critical density. This is undesirable as further transmission of laser light energy into the plasma is terminated. Several other symmetric profiles were tested with similar results.

For higher values of α satisfying equation (6) the electromagnetic wave penetrating into the plasma exhibits a solitary maximum. This corresponds to two blocks of moving plasma. One moving in the direction of propagation of laser light (compression) and the other moving back towards the laser light (expansion). With a bi-Rayleigh profile, a controlled electromagnetic energy wave may be transmitted into the plasma with a high percentage ($\geq$ 45%) of energy deposited into the plasma. Any increase on the energy transfer predicted by Nuckolls [2] (in a gas dynamic scheme) of 5% will increase fusion reaction gains by threefold since G the fusion reaction gain is given by [3]

$$G = \left(\frac{E_o}{E_{be}}\right)^{\frac{1}{3}} \left(\frac{n_o}{n_s}\right)^{\frac{2}{3}} \tag{7}$$

where E_o is the input energy, E_{be} is the breakeven energy, n_o the initial ion density, n_s the solid state density. This shows that a change in E_o for laser input energy increasing in efficiency from 5% to 50% corresponds to an equivalent fusion reaction gain G for 1000 times less laser energy. As a substitute to the Lawson criteria[4], Kidder[5] arrives at an algebraically identical formula as eq. (7). Further corrections to eq. (7) are made by including reheat and bremsstrahlung losses as well as fuel depletion. These processes cannot be expressed in a simple formulation due to the highly nonlinear behaviour of the curves, indicating an ignition process and has been described by P.S. Ray[6].

II Results of Interactions at 10^{-13} secs.

From the numerous cases calculated, we describe the ones where the generation of strong reflection has been generated in the early stage. The formation of the standing wave pushes the plasma towards the nodes and the generated rippling of the density parametrically increases the reflection. The case of figure 7 we find $(E^2 + H^2)/8\pi$ with one local maximum at the time when the laser pulse reaches its maximum intensity. The maximum is not at x = 0 where the initial density maximum is, because the absorption and intensity dependence of the optical constants modify the laser field. The maximum corresponds to an intensity I related to the vacuum intensity I_{vac} by $I = I_{vac}/(\bar{n})$ where $\bar{n}$ represents the refractive index. The swelling of the wave corresponds to $\Theta = (\frac{1}{n}) = 7$. The corresponding plasma velocity at this same time is seen in figure 8, and the electron density in figure 9.

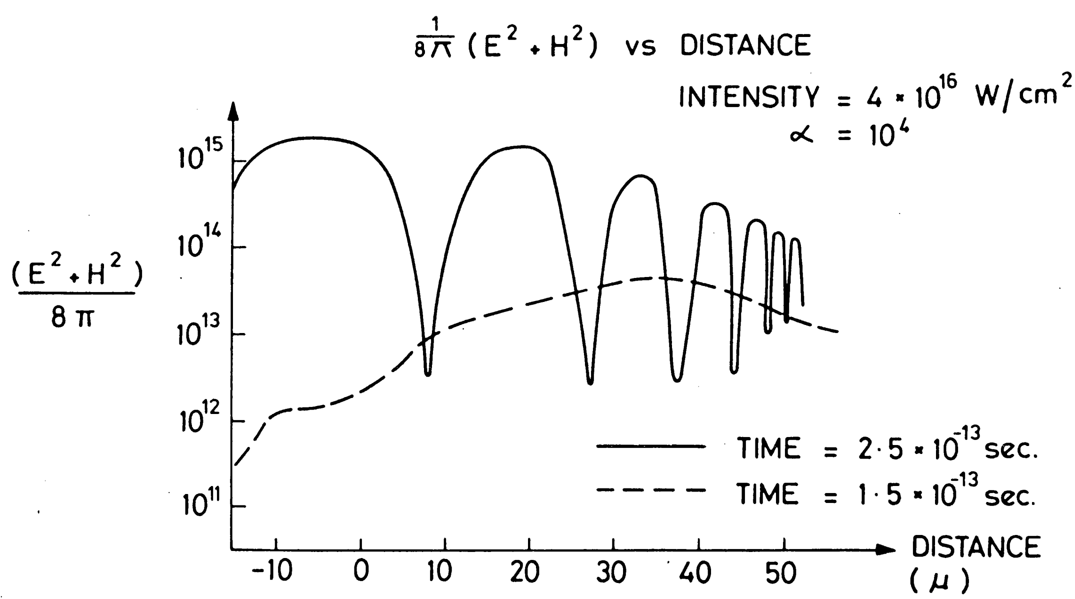

Figure 7

Calculations of $(E^2 + H^2)/8\pi$ for an initial bi-Rayleigh density profile corresponding to eq. (6) with $\alpha = 10^4 cm^{-1}$ at an intensity of $4 \times 10^{16} W/cm^2$ at the times of 1.5×10^{-13} secs and 2.5×10^{-13} secs.

The velocity profile at t = 0.15 psec is positive from x = 35 μm to 50 μm corresponding to an expansion (ablation) of this part of the plasma corona as a 15 μm thick block of plasma with velocities up to 10^7cm/sec. The plasma below 35 μm moves as a whole block to the interior of the plasma (towards negative x). The density at that time, figure 9, shows a similar profile to that of the initial bi-Rayleigh profile eq. (6), especially the Rayleigh like decay at 40 to 50 μm. It shows however, that the initial maximum at $x = 0$ has been moved to 3.8 μm due to the internal compression of the block moving towards $-x$, as the velocity profile is constant. The generation of an instability is seen at $t = .45$ psec where the $(E^2 + H^2)/8\pi$ in figure 7 oscillates, corresponding to a standing wave. The size of the maximum also increases at the later time. The standing wave causes the velocity profile to oscillate in Figure 8.

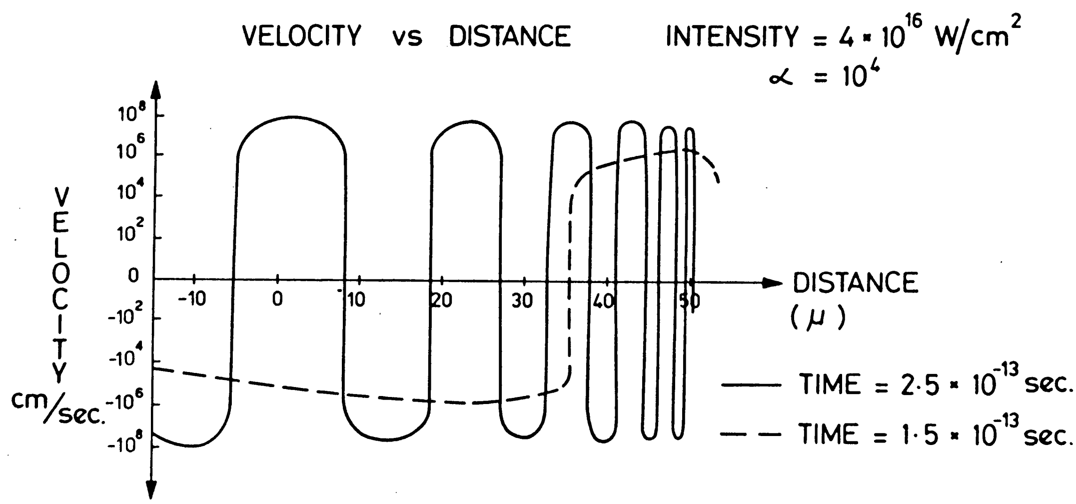

Figure 8

Velocity profiles corresponding to the case of figure 7. Note the initial block like motion of plasma generated by the soliton at 1.5×10^{-13} secs in figure 7.

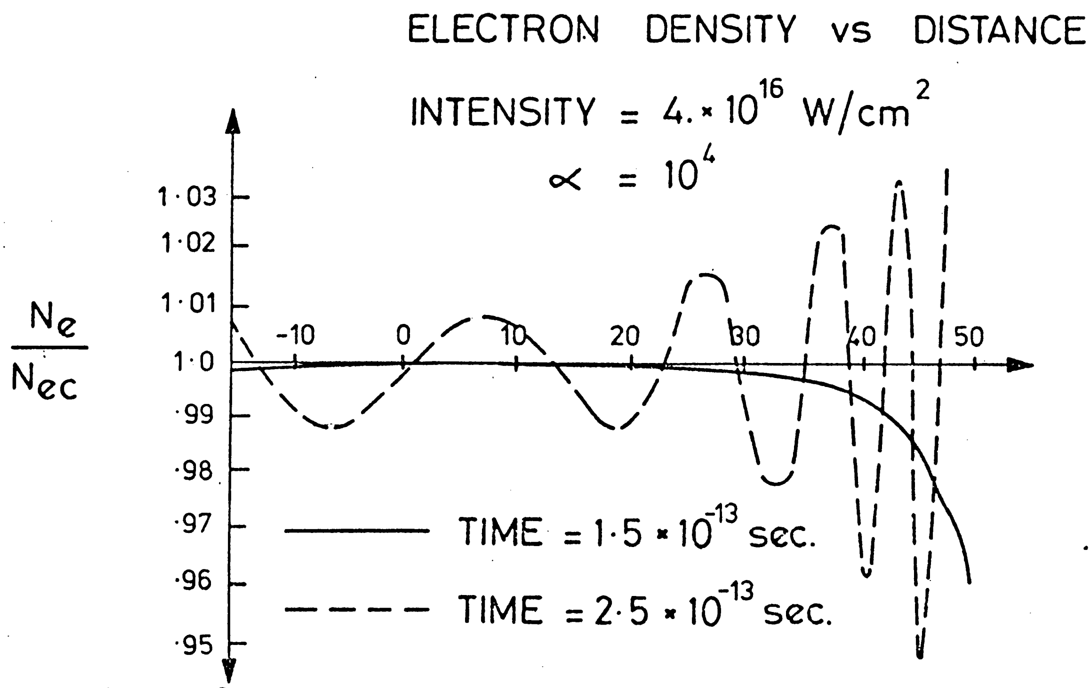

Figure 9
Normalised electron density profile at times corresponding to the cases of figures 7 and 8.

The density, figure (9) shows rippling understood by the motion of the plasma from figure (8). Note that the velocity changes as the gradient of the electromagnetic energy density. The maxima of the density ripples correspond to the gradients of negative velocities, similarly with the minima of the ripples. Later times show a very high relfectivity due to the density increasing above the cut off density, corresponding to a macroscopic Brillouin type [7] dynamic instability.

Compared to the cases of figures 7 to 9, the situation is quite different if $\alpha = 5 \times 10^4 \text{cm}^{-1}$ with a

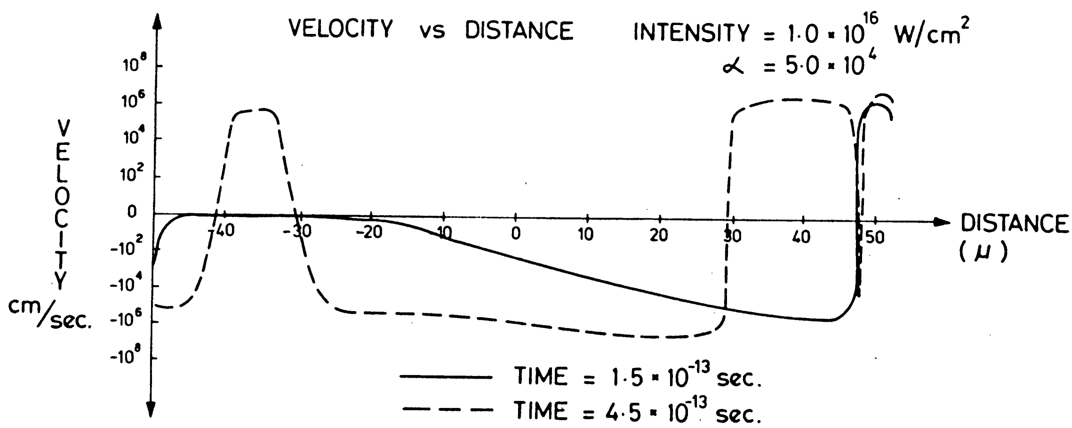

Figure 10

Velocity profiles corresponding to the case of figure 4

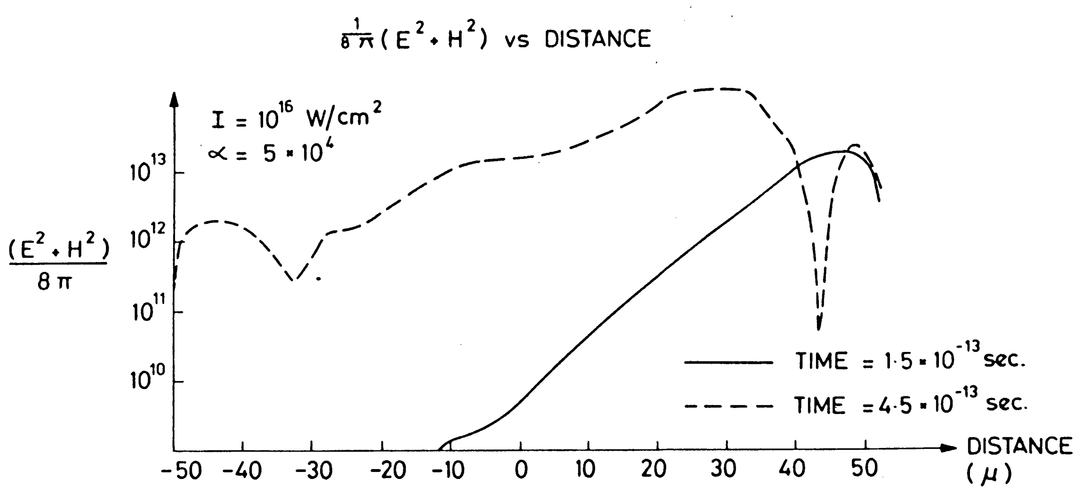

Figure 11

Spatial profiles of $(E^2 + H^2)/8\pi$ for a case with an initial bi-Rayleigh profile with $\alpha = 5 \times 10^4$ cm^{-1} and maximum laser intensity of 10^{16} W/cm^2 at times of 1.5×10^{-13} secs and 4.5×10^{-13} secs.

maximum intensity I of 10^{16} W/cm^2 used (Figure 10 and 11). It shows that at an early time of.15 psec the laser intensity has a maximum near 40μm, with a swelling of 14, and then drops strongly towards negative x. The high value of α generates a density very close to the cut off density, and the smaller intensity than the former case causes a smaller decrease of the collision frequency since the collision frequency has a nonlinear dependence on the intensity described in the nonlinear optical constants section. At the time of .45 psec the swelling of the intensity increases to 120 at x = 30 μm allowing the light to penetrate through the whole plasma without a standing wave pattern. The plasma (figure 11) moves in two blocks from 30 to 50 μm towards positive x (ablation) and far less than 30 μm towards negative x (compression). The change of velocity near -35 μm corresponds to the minimum in $(E^2+ H^2)/8\pi$ near -35 μm.

Computations at short time steps from .15 psec to .45 psec can exist due to the non retardation of potential and that the velocity of light is assumed to be infinite. The scheme from now on is to increase time steps so as to allow realistically several wavelengths of radiation to penetrate and interact with the plasma.

III Reflection at cut off density

Standing wave patterns

Connecting an inhomogeneous Rayleigh density profile onto a constant density at the critical density, upper curve in Figure 12, corresponds to the initial density profile in figure 5, equation (4). When the laser

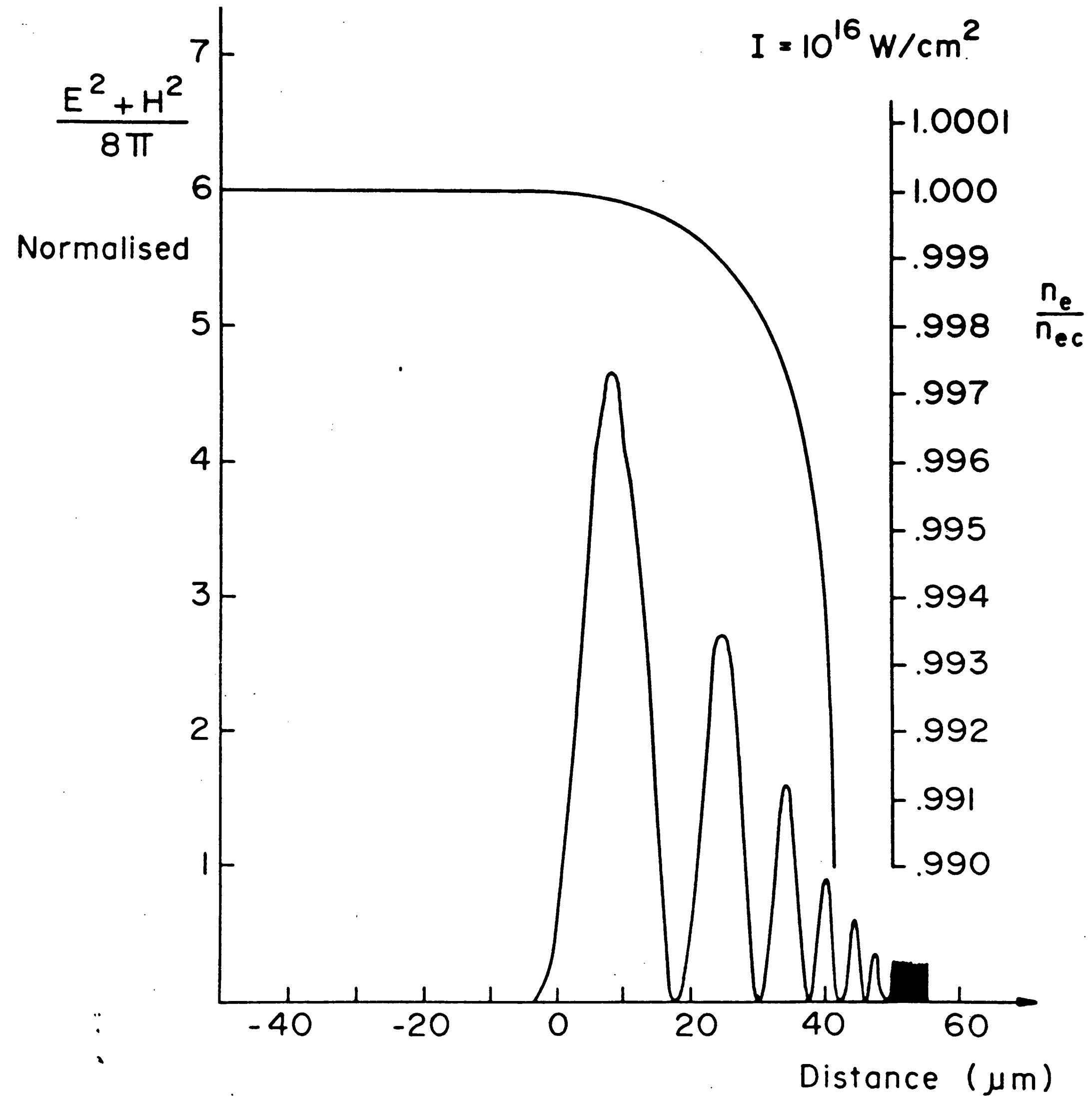

FIGURE 12 The upper curve is an initial inhomogeneous Rayleigh density profile onto a constant density plateau at n_{ec} corresponding to eq. (5) with $\alpha = 10^4$. The standing wave formation at 1.5 psec of the electromagnetic energy

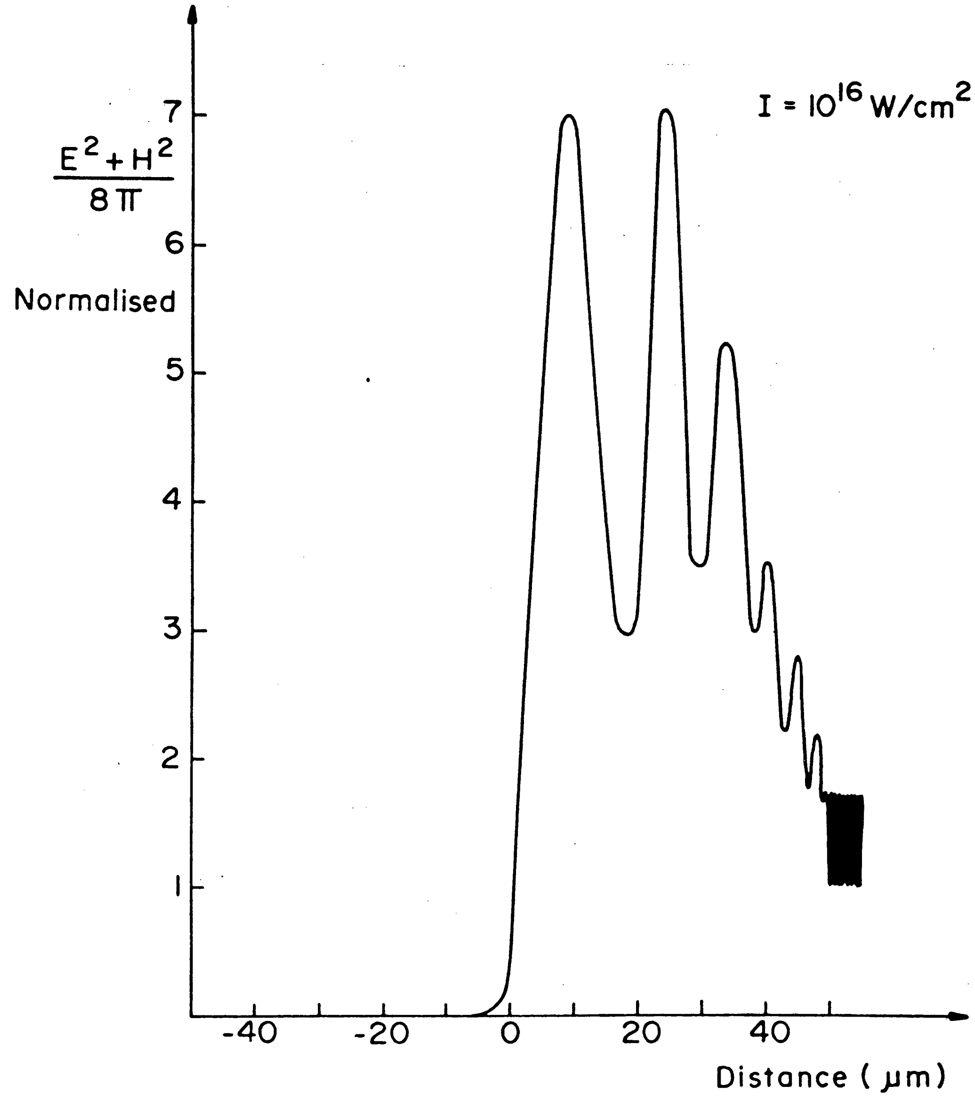

FIGURE 13 For the case of figure 12 with a temperature of 1ev increasing the absorption of the plasma. The formation of a standing wave occurs at the cut off density at times of 1.5 psecs.

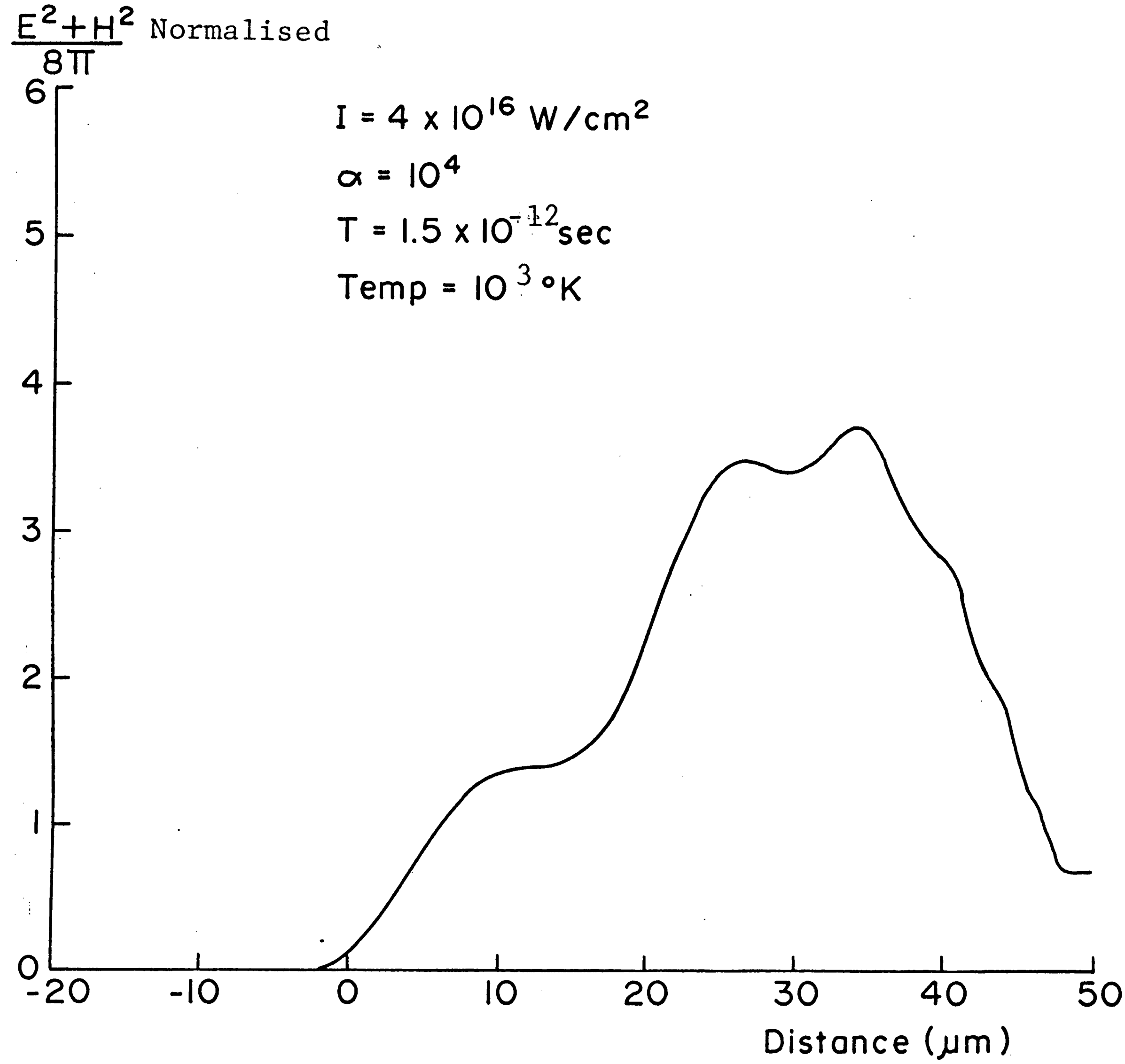

IGURE 14 Same as figure 12 and 13 with a temperature of 10^3 ^{0}K

light of intensity 10^{16} W/cm^2 penetrates into the plasma, it eventually propagates to the electron cut off density where the light will experience total reflection in figure 12. The interaction of the reflected wave at x = 0 and incoming waves causes the formation of a standing wave pattern for the collisionless plasma. The pattern of total reflection is analagous to the cases of a collisionless linear density profile described by Airy functions[8] or by numerical evaluation[9]. The pattern of $(E^2+H^2)/8\pi$ in figure 12, however shows stronger swelling than that of a linear density profile[10].

For the case of a more realistic inhomogeneous absorbing plasma with the temperature reduced to 1 e V we see in figure 13 the electromagnetic energy density irradiated by laser light of intensity 10^{16} W/cm^2 also at the time of 1.5 psec. The oscillations of this field in the plasma corresponds to the cases at times of interaction of 10^{-13} secs where the non linear force causes rapid oscillations of the plasma velocities with a corresponding bunching of plasma density above critical which effectively prohibits further penetration of laser light. Similarly for figure 14, at a lower temperature increasing the amount of absorption of the laser light.

The cases of standing wave patterns, similar to microwave experiments on plasma[11], are not useful for transfer of laser light energy. They are taken as test cases confirming that the phased inhomogeneous Rayleigh profile behaves as a linear density profile confirming the generation of a standing wave pattern and the inefficiency of transfer of laser light energy into random motion of plasma energy.

IV Bi-Rayleigh Profile

The use of a Bi-Rayleigh profile for the initial profile follows a tutorial example in Hora [12], now in detailed numerical description of the whole dynamics of interaction. With the density maximum close to but less than the critical density, eq. (6), the profile will reduce reflectivity and hence generation of standing wave formations. It will exhibit transparency for relatively low laser intensities, the opacity dependent on the temperature of the plasma. Compared with the single phased Rayleigh profile onto a plateau of density at critical, eq. (5) one sees that the Bi-Rayleigh profile allows the electromagnetic field density to transmit across the whole plasma. At the low values of $\alpha = 3 \times 10^3 \mathrm{cm}^{-1}$ in Figure 15 the electromagnetic field transmits sinusoidally which will correspond to bunching of density due to the nonlinear forces, once again causing density to grow above the critical density. Figure 15 represents a generation of instability since further laser light will be reflected back corresponding to a macroscopic Brillouin instability.

Other symmetric density profiles were used. These included

Elliptic density where $n_e = \pm n_{ec} * \sqrt{1 - x^2/.0052}$ (8a)

Exponential density where $n_e = n_{ec} * e^{-ax}$ where a is a constant (8b)

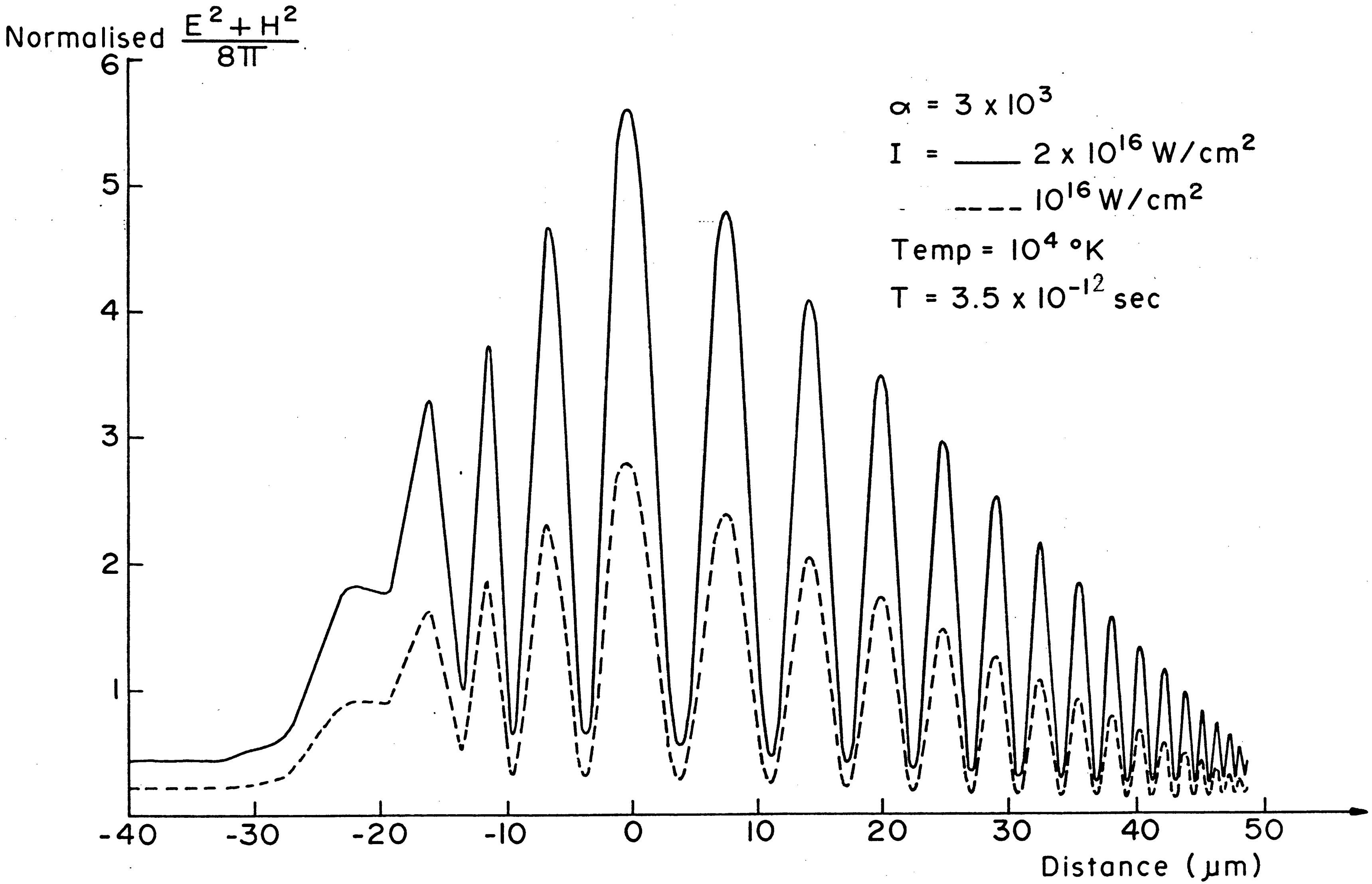

FIGURE 15 Generated electromagnetic energy density for an initial bi-Rayleigh density profile with $\alpha = 3 \times 10^3$ cm^{-1} corresponding to eq. (6) for different intensity fluxes at times of 3.5×10^{-12} sec. Other symmetric profiles, eqs. (8), displayed similar formations.

Witch of Agnesi where $n_e = (n_{ec}*)^3/(x^2 + n_{ec}^2)$ (8c)

The above density profiles with $n_{ec}*$ slightly less than n_{ec} all behaves similar to figure 15, generating standing wave type patterns with velocities oscillating rapidly, the densities bunching above critical density acting as a macroscopic Brillouin instability.

By varying the constant α in eq. (6) the form of the incident electromagnetic field may be controlled to the extent of achieving the desired block like motion, which will drive plasma as a thick block into the interior of the plasma. As a result of conservation of momentum the momentum of the compressed block is matched by the momentum of the ablating mass of plasma.

V Gas Dynamic case

For the pure gas dynamic thermokinetic expansion of plasma the only force appearing in the equation of motion of the plasma is the gradient of the pressure, ∇p. The incident laser radiation will be absorbed by collisions which will heat the plasma and drive it[13]. For a Bi-Rayleigh profile without any interaction with laser pulses, the plasma would react as a symmetric diffusion of the plasma at low velocities away from the maximum of the density profile. In the case of figure 6 the plasma would separate through thermal diffusion at $x = 0$. One block of plasma for $x > 0$ would drift to the right in the direction of the gradient of density from high to low. The other block for $x < 0$ will drift to the left. Assuming that $Te = Ti = T$ is a constant, the gradient of the pressure is equivalent to the gradient of the density and the motion of plasma behaves accordingly moving from values of high to low densities.

At all intensities of laser light interactions the gas dynamic forces acts in unison with the nonlinear forces. As discussed[14] in Chapter 3, Part III, there exists a threshold intensity at which the nonlinear force dominates the gas dynamic force. For Nd glass laser the threshold intensity is near 10^{14}W/cm^2. However the nonlinear force can still exceed the gas dynamic force[14] if the temperature $T_e > 10^4$eV. Even though there may be fluctuations in the electromagnetic energy density with the corresponding change of direction of the velocities, the magnitude of the nonlinear force may be smaller than the gas dynamic force, to the extent that the rippling of $(E^2 + H^2)/8\pi$ will not be evident in the velocities of the plasma. Therefore at intensities below threshold, gas dynamic interactions dominate allowing further transfer of laser light into the plasma without generation of macroscopic instabilities.

At later times, intensities much less than threshold will experience self focussing effects creating higher intensities of laser radiation in the process. The intensity of the light increases till it reaches the instability threshold generating instabilities. A one dimensional plane wave code will not simulate self focussing effects, however, the absolute threshold for instabilities may be simulated.

The gas dynamic force is seen to dominate the nonlinear force in figures 16,17,18. At an intensity of 10^{12} W/cm^2, figure 16 displays initially a solitary wave followed by the formation of a standing wave at later times. The velocities however, do not oscillate in figure 17 as discussed earlier. The electromagnetic energy density increases in time although the maximum value does not increase appreciably. Swelling is only 26. The density of the plasma decreases monotonically in the negative region of the plasma. The magnitude of the density gradient is larger than the nonlinear forces generated by the rippling of the electromagnetic energy density due to the kink at -50 μm. Therefore the velocities (figure 17) at early and later times remain negative without the oscillations which cause bunching of the density profile. The velocities increases at the boundaries of the plasma. The blow off of plasma to regions of lesser densities as more energy is transferred to the plasma is the reason for the increase in velocity. The increasing velocities leads to a constant decrease of the plasma density due to ablation to areas of lower densities in figure 18. This figure describes the vaporisation scheme[15] as a gas dynamic ablation. The laser light at higher intensities will drive the density near the critical density to higher densities. In a purely gas dynamic force scheme there is thermokinetic expansion of plasma driven by collision produced absorption of laser light[13].

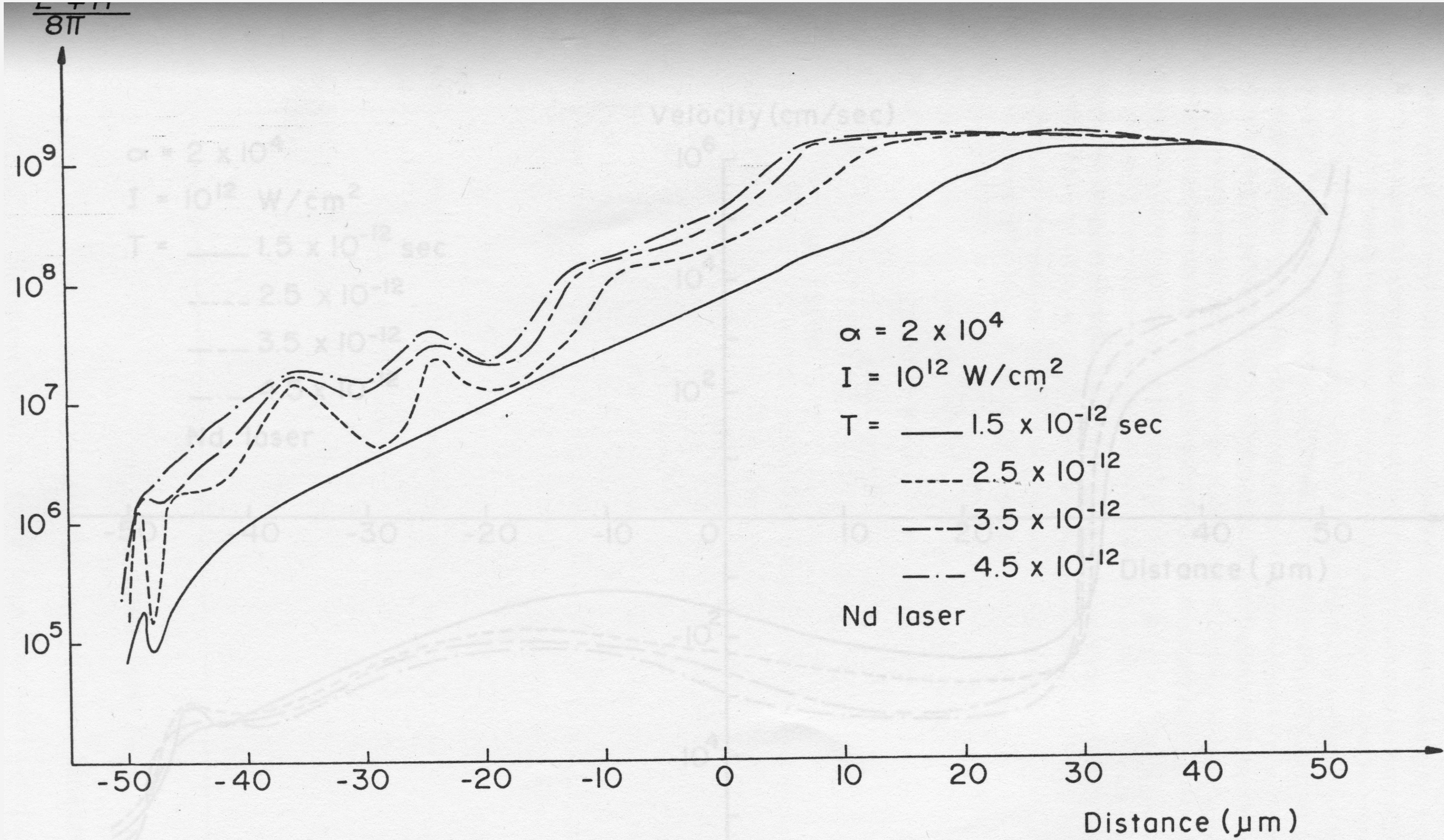

FIGURE 16 For an initial bi-Rayleigh density profile with $\alpha = 2 \times 10^4$ cm^{-1} and incident fluxes of 10^{12} W/cm^2 and temperatures of 10^6 ^0K we observe gas dynamic behaviour of the electromagnetic energy density.

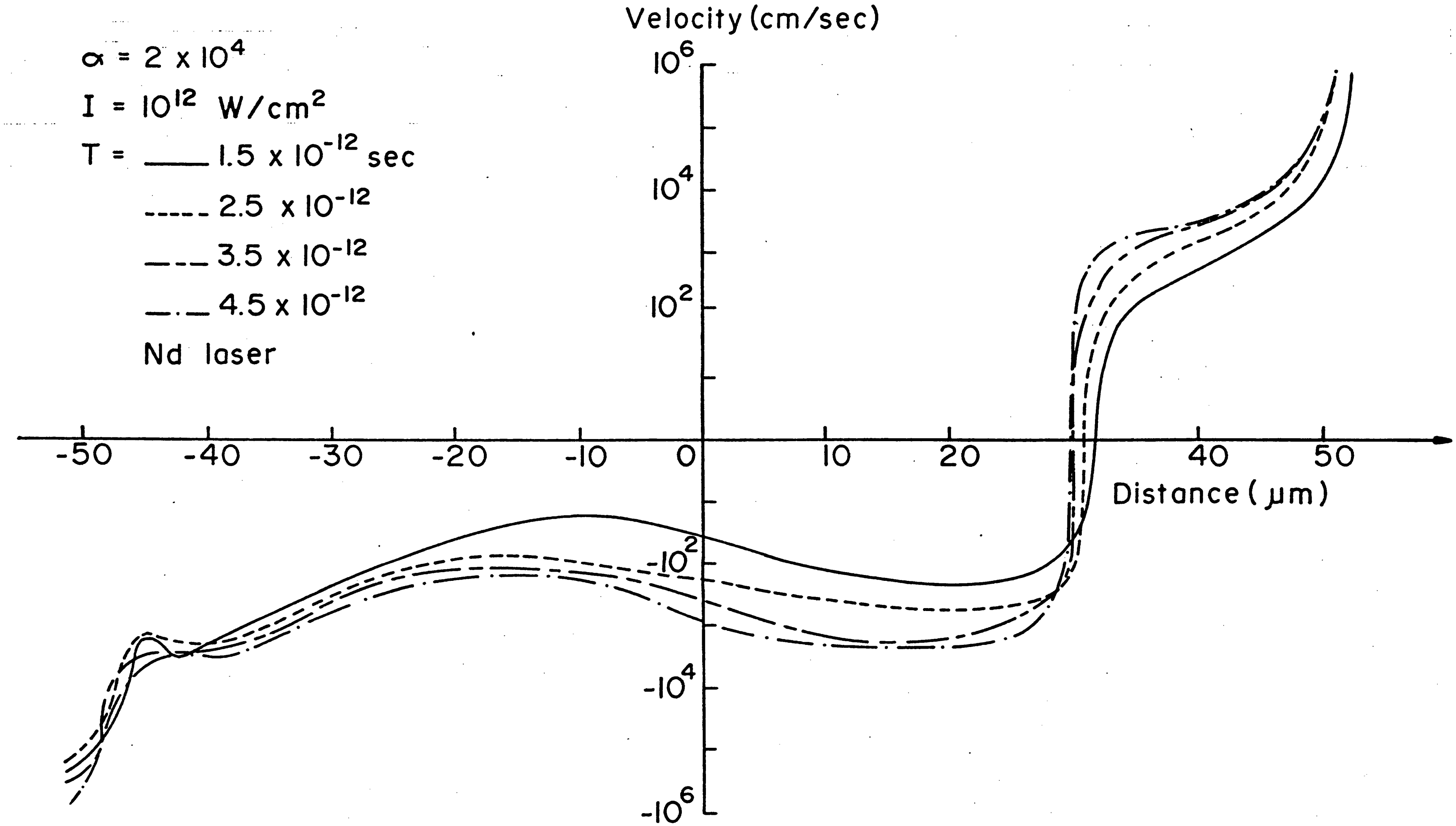

FIGURE 17 The low velocity profiles of the gas dynamic case corresponding to figure 16.

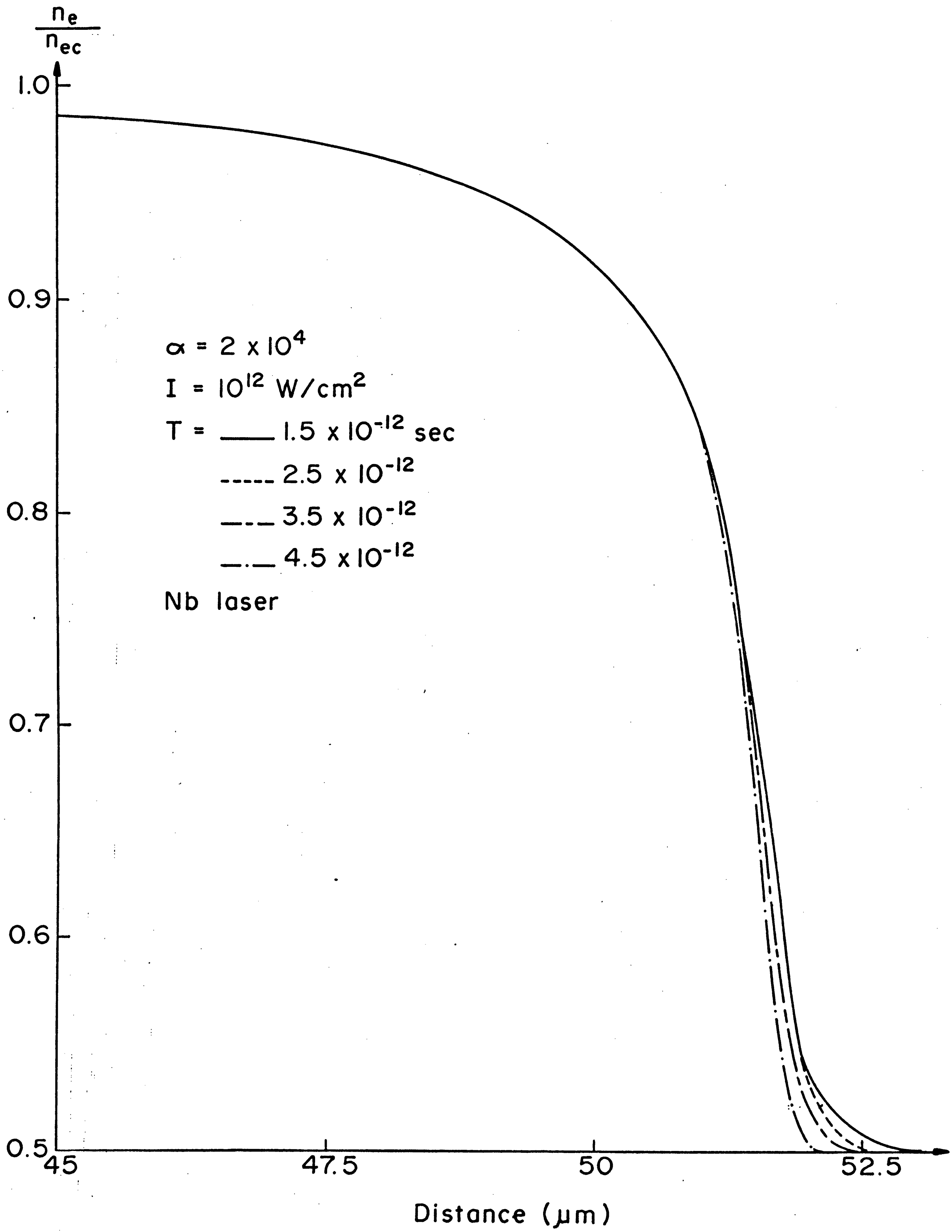

FIGURE 18 The normalised ablating plasma density corresponding to a thermokinetic expansion due to dominating gas dynamic forces observed in figures 16 and 17.

VI Nonlinear Force - caviton

In a gas dynamic vaporisation scheme including collisional absorption of laser radiation, one sees the expansion of plasma as a monotonically decreasing thermokinetic expansion. The motion of plasma due to the gradient of the pressure decreases monotonically. When the nonlinear force is included into the scheme, the ablating plasma is affected by interacting forces and does not necessarily ablate monotonically. Similar to experimental results of Zakharenkov[16], Luther Davies[17] and numerical calculations by Shearer[18] and as discussed in the nonlinear force chapter, we see in figure 19 that for an intensity of 10^{17}W/cm^2 the density of plasma no longer blows off regularly. There is a creation of a caviton, which was first discovered numerically by Shearer, Kidder and Zink[18], and a separate maximum for the density due directly to the nonlinear force. This shock like effect near the critical density causes the plasma to increase above the cut off density prohibiting further transfer of laser light energy. To a lesser extent at an intensity of 10^{16} W/cm^2 there is a smaller caviton created where the density increases to 2% above the cut off density also causing total reflectance. At the higher intensity of 10^{17}W/cm^2 the size of the profile modification occurs earlier than at lesser intensities. The immediate consequence of the profile modification is that the cut off density causes mirroring of any further laser light introducing backscatter of laser light. The ablating mass will appear at later

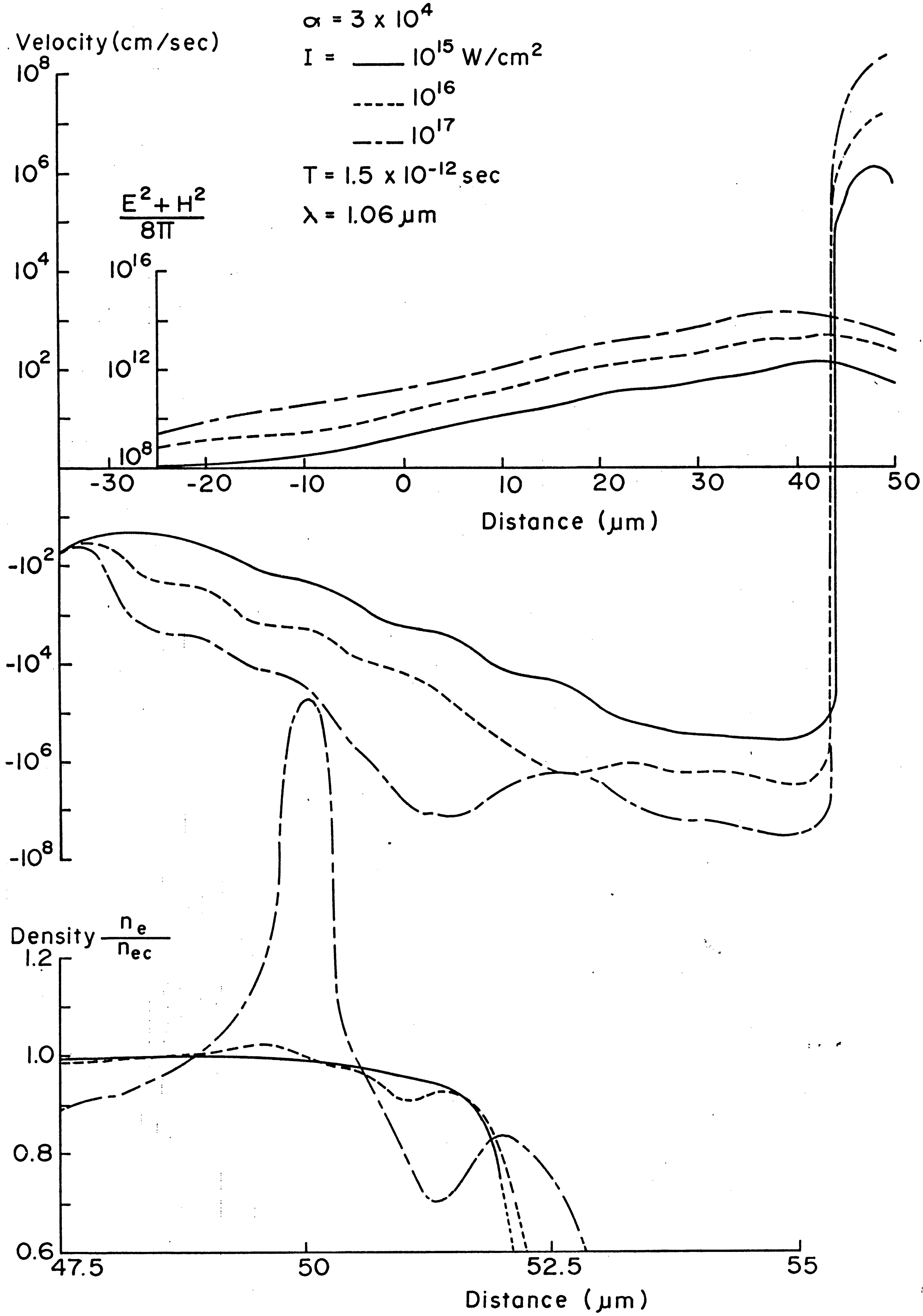

FIGURE 19 Electromagnetic Solitons, with the corresponding velocity profile and density cavitons.

times not dissimilar to the experimental results for high Z materials and longer laser pulses.

At an intensity of 10^{15}W/cm^2 the density profile behaves as in the gas dynamic case and will allow further laser light to transmit into the plasma. It is only at a later stage of interaction that the density of the plasma will form a caviton and a corresponding spiked density profile.

All three intensities display initially a solitary electromagnetic energy density with similar swelling of 24. The velocities of plasma ablating increases with laser intensities and the compressing block increases in velocities with a peak velocity of 10^9 cm/sec for an intensity of 10^{17}W/cm^2.

VII Drilling Effects

In figure 20a, the initial soliton at a time of 1.5 psec generates a velocity profile as seen in figure 20b. There is little change in the density profile at the intensity of 10^{15}W/cm^2. The soliton increases with time till 2.15 psecs. Due to rapid oscillations of the $(E^2 + H^2)/8\pi$ between 30 μm and 50 μm the density increases in this case to just below the critical density thus allowing laser light to continue transmitting into the plasma but at the later stage of 2.55 psecs the $(E^2 + H^2)/8\pi$ is slightly damped and decreases in magnitude. The increase in transparency of the plasma is due to the decrease in the density near the cut off density. At later times of inter-

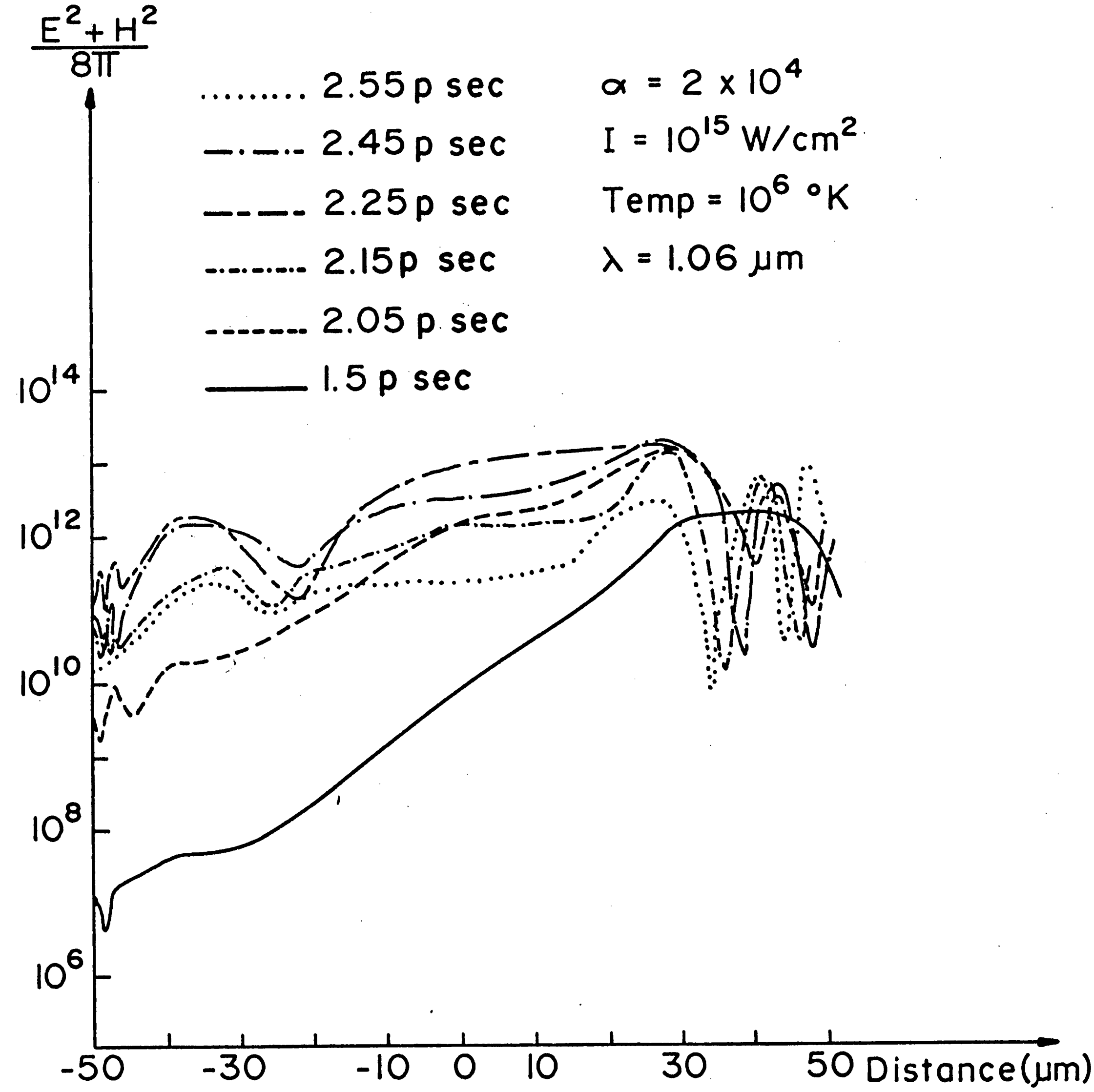

FIGURE 20a

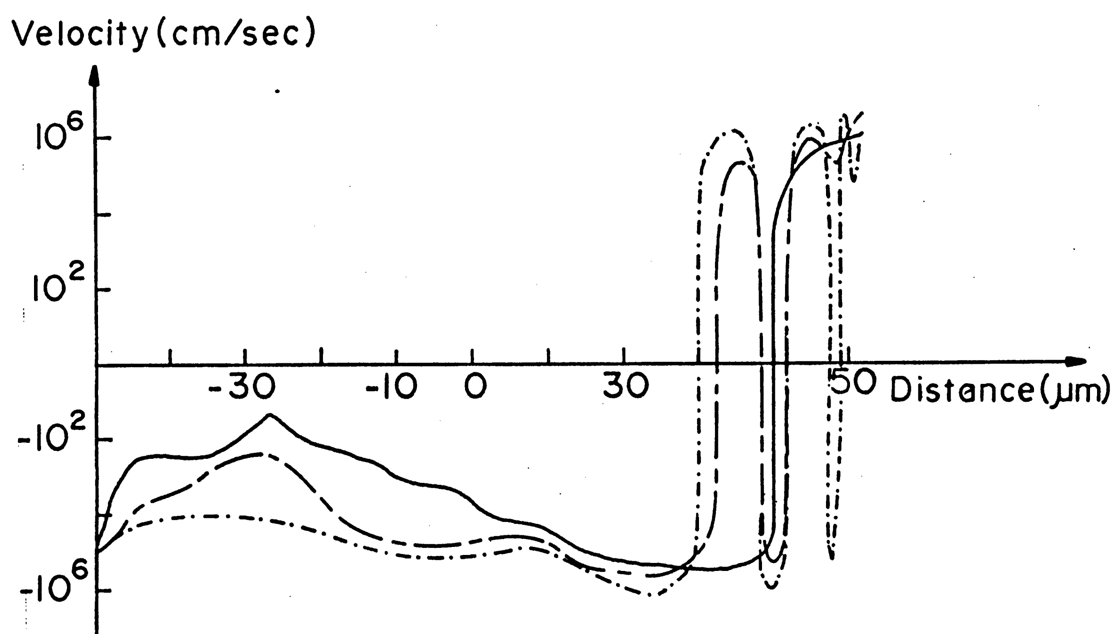

FIGURE 20b Electromagnetic density and corresponding velocity profiles exhibiting drilling effects of section VII.

actions the forces (both thermal and nonlinear) increase the density of the compressed block causing less transparency to the electromagnetic wave.

VIII Temporal Dependence

By adjusting the value of α in the bi-Rayleigh profile case of figure 15 the rippling of electromagnetic energy density is suppressed and will form as a solitary electromagnetic energy wave which we have called a soliton. The importance of the soliton lies in the forces, both gas dynamic and nonlinear force, acting on the plasma. The predominance of the nonlinear force over the gas dynamic forces[14] results in the action on the plasma depending on the gradient of the electromagnetic energy density and to a lesser extent the gas dynamic forces described as the gradient of the pressure or at constant temperature, the gradient of the density.

At the positions of maxima of the electromagnetic energy density the plasma motion reverse. Where the gradient of the $(E^2 + H^2)/8\pi$ is negative the plasma velocity is negative and vice versa. Due to collisional damping at lower temperatures near the critical density the electromagnetic energy is collisionally damped as seen in figure 21 at a temperature of 2×10^5 ^{0}K. The higher the temperature of the plasma the lower the collision frequency and hence the lower the absorption of the plasma. At a temperature of 10^7 ^{0}K the plasma is approximately collisionless and the formation of a wave

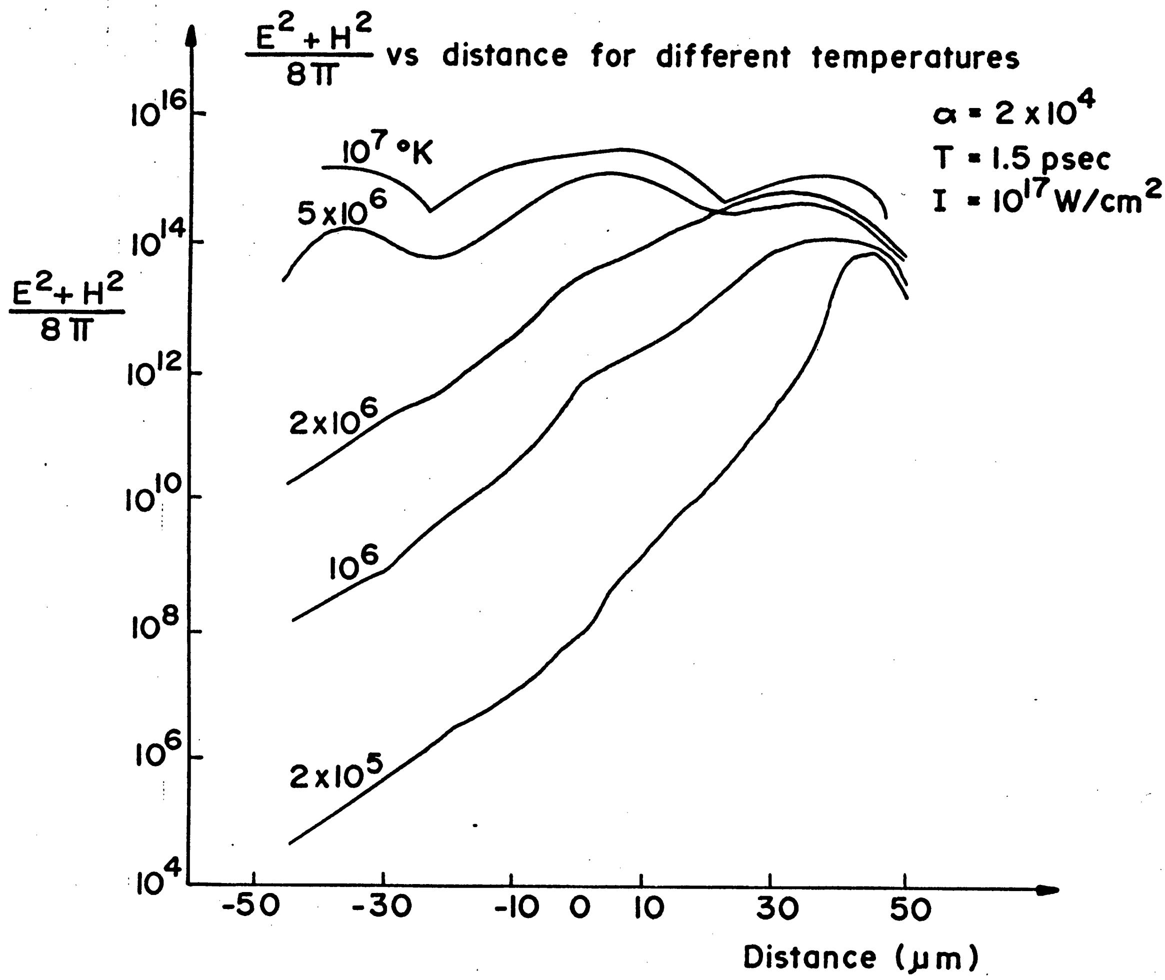

FIGURE 21 Dynamically developed electromagnetic energy density $(E^2+H^2)/8\pi$ for the initial density profile of figure 6 at varying initial temperatures. For intensities of 10^{17} W/cm^2 and times of 1.5 psec we see the formation of solitons with stronger decrease due to larger collisional absorption.

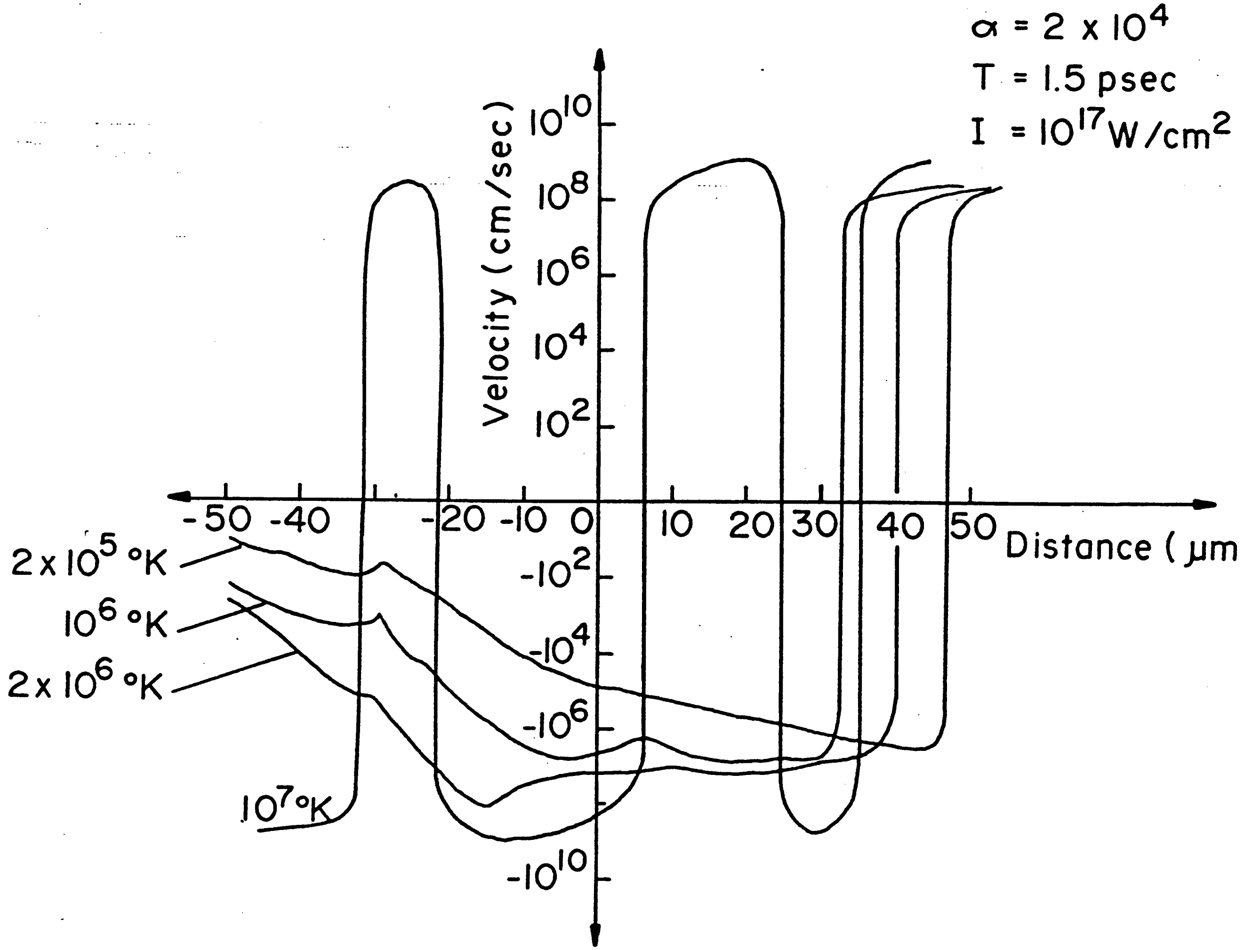

FIGURE 22 The velocities of plasma for the initial density profiles of figure 6 for varying initial temperatures at an intensity flux of 10^{17} W/cm^2 corresponding to figure 21.

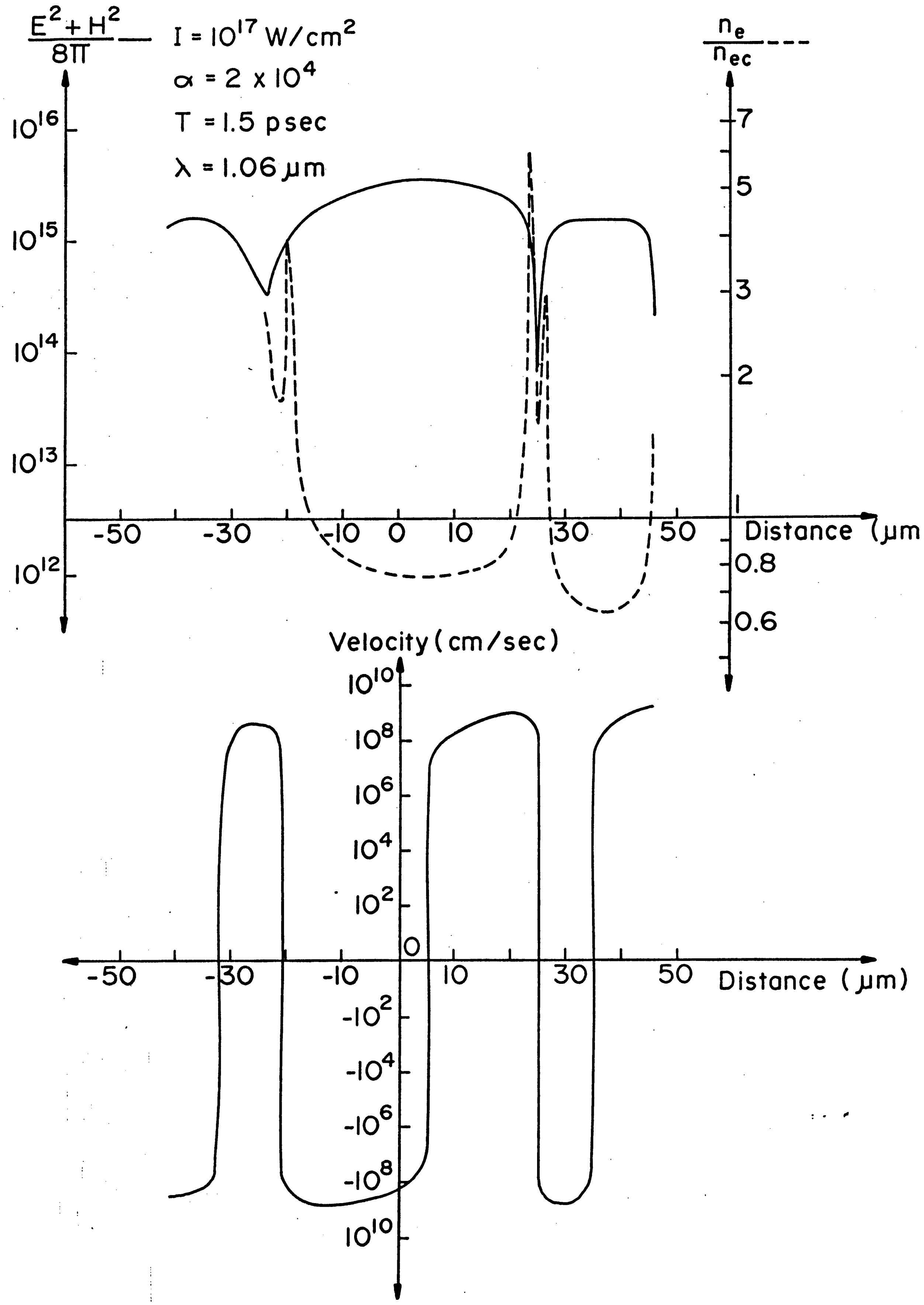

FIGURE 23 Electromagnetic energy density $(E^2+H^2)/8\pi$ normalised density and corresponding velocities for a uniform temperature of 10^7 ^{0}K

inside the plasma absorbs energy via adiabatic dynamic collisionless absorption. Since no energy is transferred at 10^7 ^{0}K to the plasma via collisions the absorption of the optical energy is due to the nonlinear force driving the plasma to velocities up to 10^9 cm/sec in figure 22. The position of the maxima of the solitons vary with the temperatures and at higher temperatures the position of change of velocities approach $x = 0$ which is the split point of plasma velocities for a purely gas dynamical case.

We look more closely at the case of 10^7 ^{0}K in figure 23. The electromagnetic energy density generates a velocity profile with velocities oscillating in the direction of the gradient of $(E^2 + H^2)/8\pi$. The velocities bunch up the density profile which cause spikes in the density to six times the cut off density. It was hoped to try to collapse the densities into each other since the spikes corresponds to plasma moving in opposite directions. Simulation of such a situation would lead to high compressions of plasma at both -20 μm + 25 μm. Due to necessary restrictions for computational stability conditions which were not satisfied it was not possible to simulate the situation any further.

IX Generation of Instabilities

The initial formation of a soliton at a time of 1.5 psec is evident in figure 24. corresponding to the electromagnetic energy soliton is the well behaved ablation and compression of blocks of plasma , the

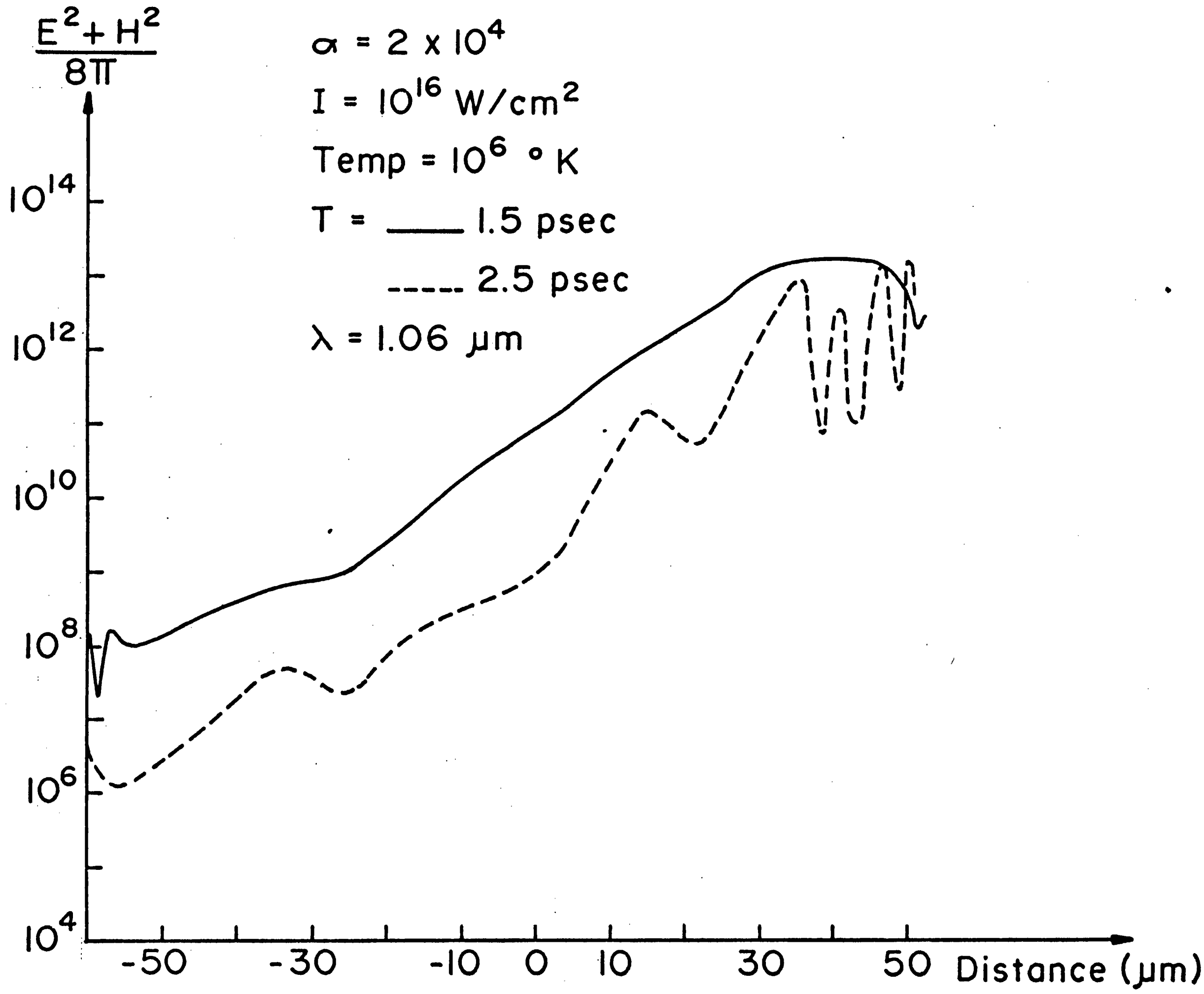

FIGURE 24 Electromagnetic energy density $(E^2 + H^2)/8\pi$

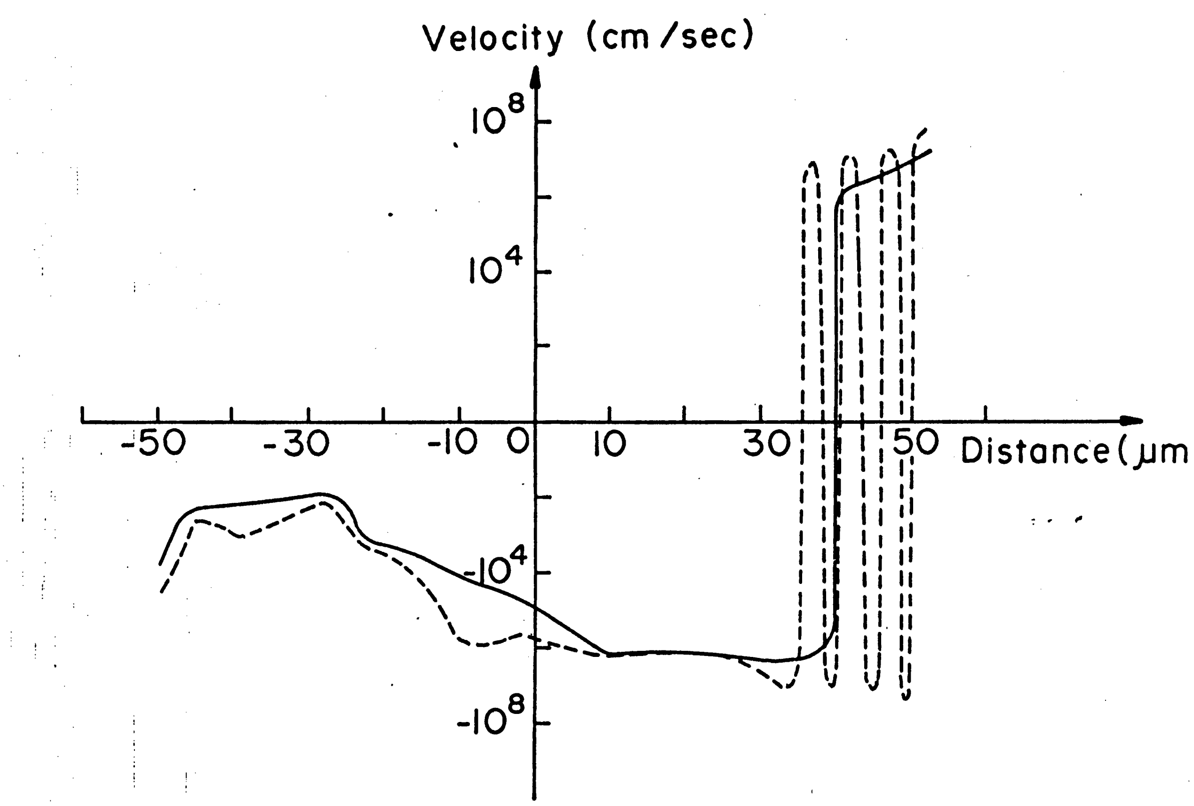

FIGURE 25 The velocity formation of a macroscopic Brilloin instability at a time of 2.5 psec for the corresponding $(E^2+H^2)/8\pi$ values of figure 24.

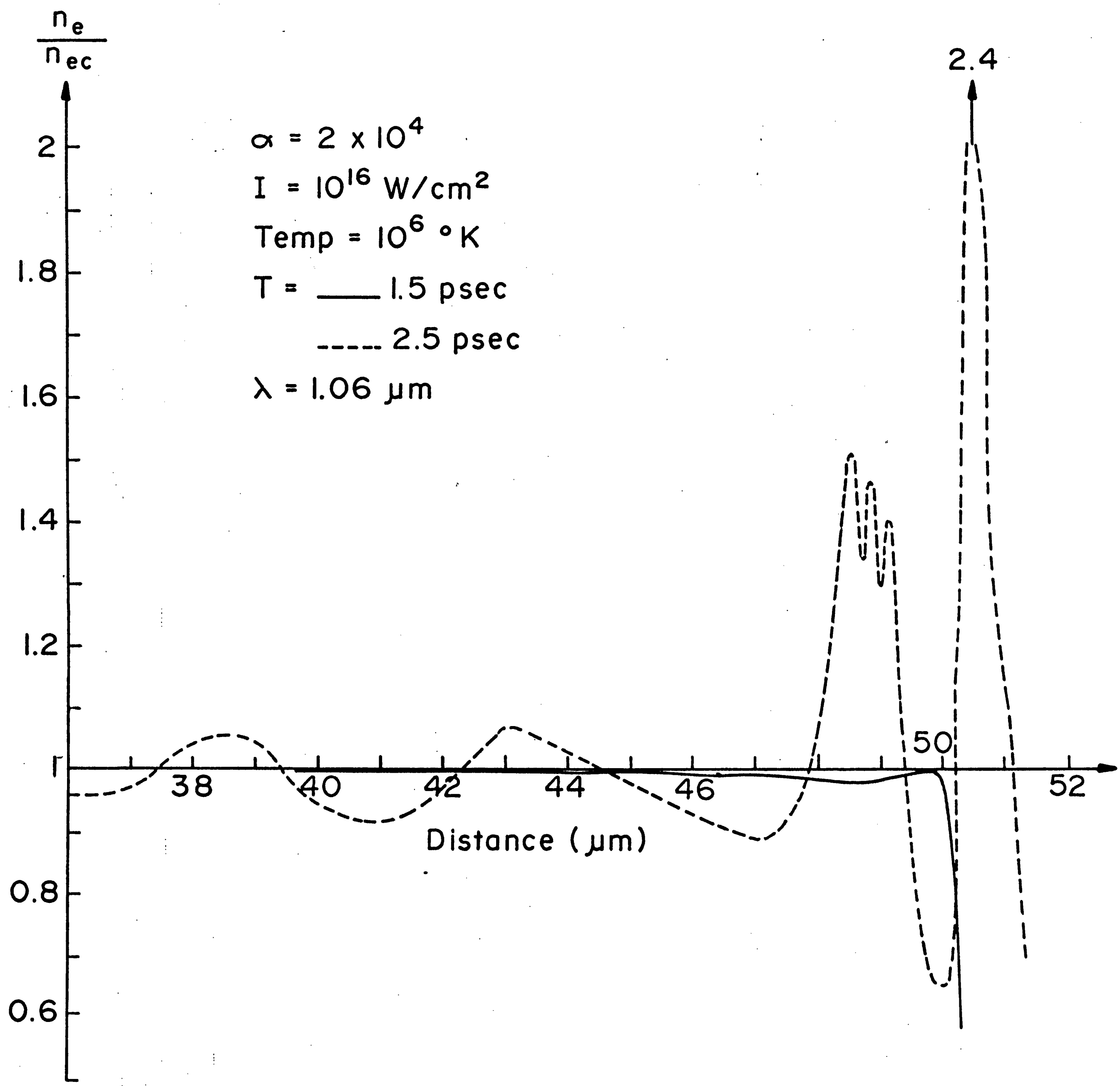

FIGURE 26 The density formation due to macroscopic Brillouin instability at a time of 2.5 psec corresponding to figures 24 and 25.

boundary between the two existing at the maximum of the soliton at 40 μm, figure 25. The initial bi-Rayleigh profile with $\alpha = 2 \times 10^4$ in figure 25 is perturbed slightly at the early stage of interaction. The slightly perturbed density profile will allow further laser light transfer into the plasma since the density does not rise above the critical density. Further transfer of laser light energy at an intensity of 10^{16}W/cm^2 produces a macroscopic Brillouin instability similar to the interactions at 10^{-13}secs. These fluctuations drive the plasma according to the gradient of fluctuations of $(E^2 + H^2)/8\pi$ and one sees the bunching of the density profile. The maxima of the $(E^2 + H^2)/8\pi$ corresponds to the minima of the density and vice versa.[19] The velocities directed towards each other cause the density to rise. Velocities directed away from each other means a dip in the density profile. The density of plasma via this mechanism is increased to 2.4 times the critical density at the corona of the plasma at 5 μm This is of no benefit to fusion effects requiring that high densities be at the center of the plasma or the interior rather than the corona which will diffuse out into the regions of lower densities. Efforts are to be made in keeping the coronal densities low and the "core" densities high which will allow further transfer of energy either thermally or dynamically into the core of the plasma. The generation of Brillouin type instability will drive laser energy back towards its source rather than allow transfer of energy into the plasma

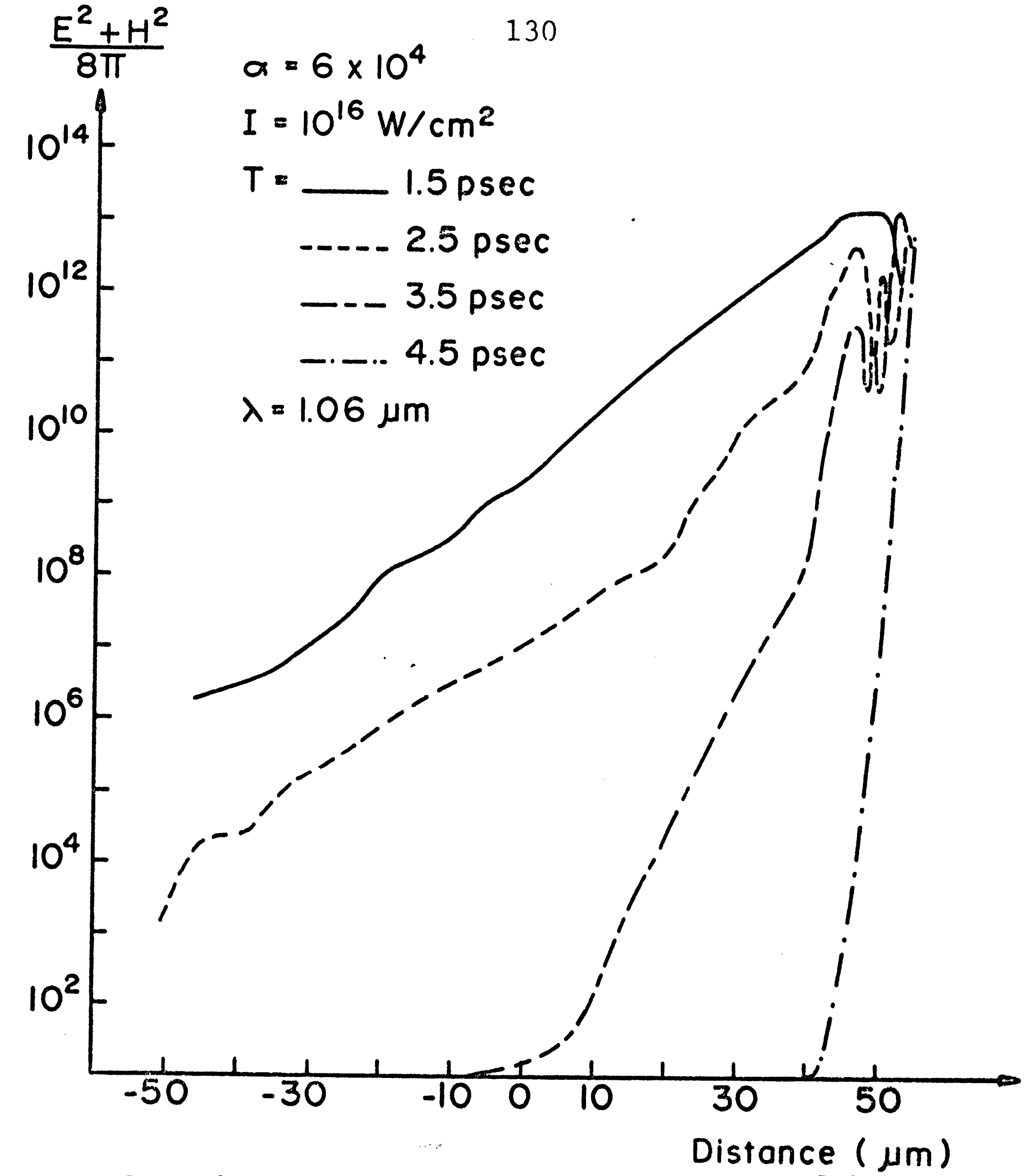

FIGURE 27 Electromagnetic energy density profile at different times.

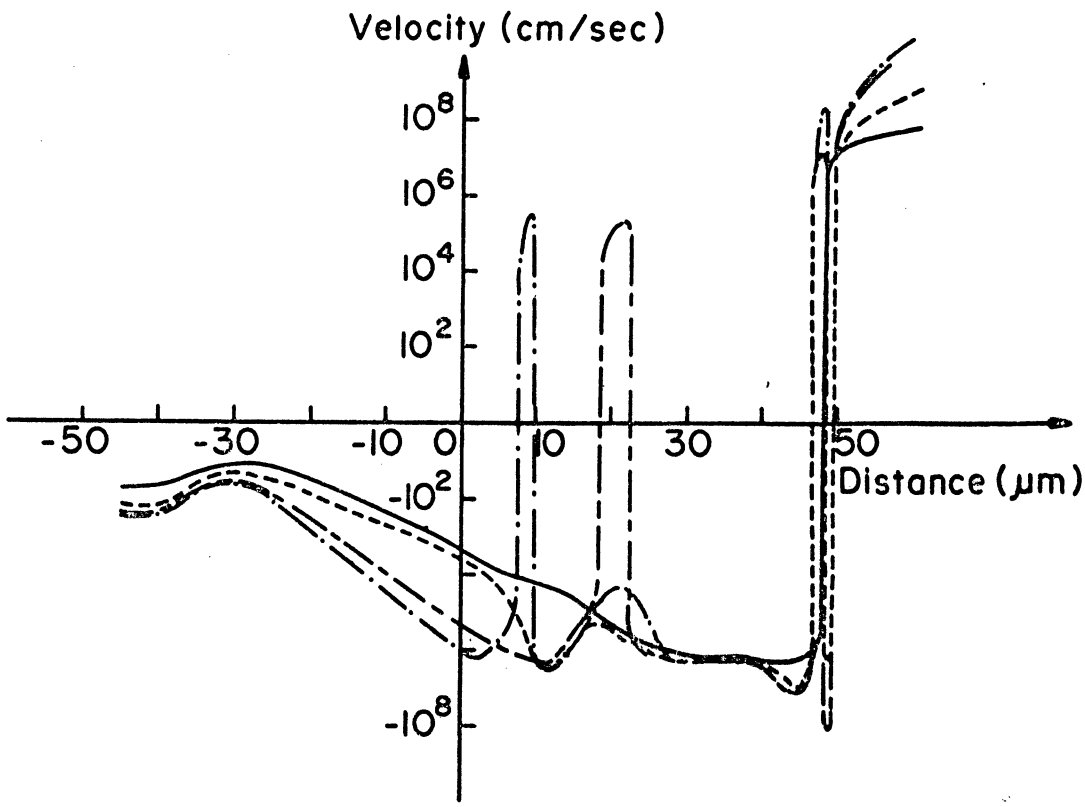

FIGURE 28 Velocities corresponding to figure 27.

X Damping of the electromagnetic energy density

The results from figures 24,25,26, showed that the density of the plasma is raised much above critical. Similarly for $\alpha = 6 \times 10^4$ cm^{-1} the density is raised much above critical and the behaviour of the laser light in the plasma is displayed in figure 27 with the corresponding velocities in figure 28. The electromagnetic wave is critically damped at the later stage of 4.5 psec which verifies previous discriptions of the densities above critical density causing reflection of laser light. The decay of laser light is due to collisional damping.

XI Development of Solitons

The soliton is seen in figure 29 to move inwards indicating further ablation of plasma due to the nonlinear force and hence higher compression of velocity of plasma towards the interior, together with higher velocities. At the later time of 4.5 psec a macroscopic Brillouin type instability occurs with the formation of standing waves. Further computations show that the sizes of solitions are directly proportional to the intensity of laser light. At longer wavelengths, the shock hammering type effect of longer wavelengths since there exists less penetration of laser light causes an increase in density above critical with a corresponding caviton. The relatively low laser intensities of 10^{13}W/cm^2 causes a nonlinear force compression in figure 29 due to the gradient of the electromagnetic energy density. The density gradient of the Rayliegh

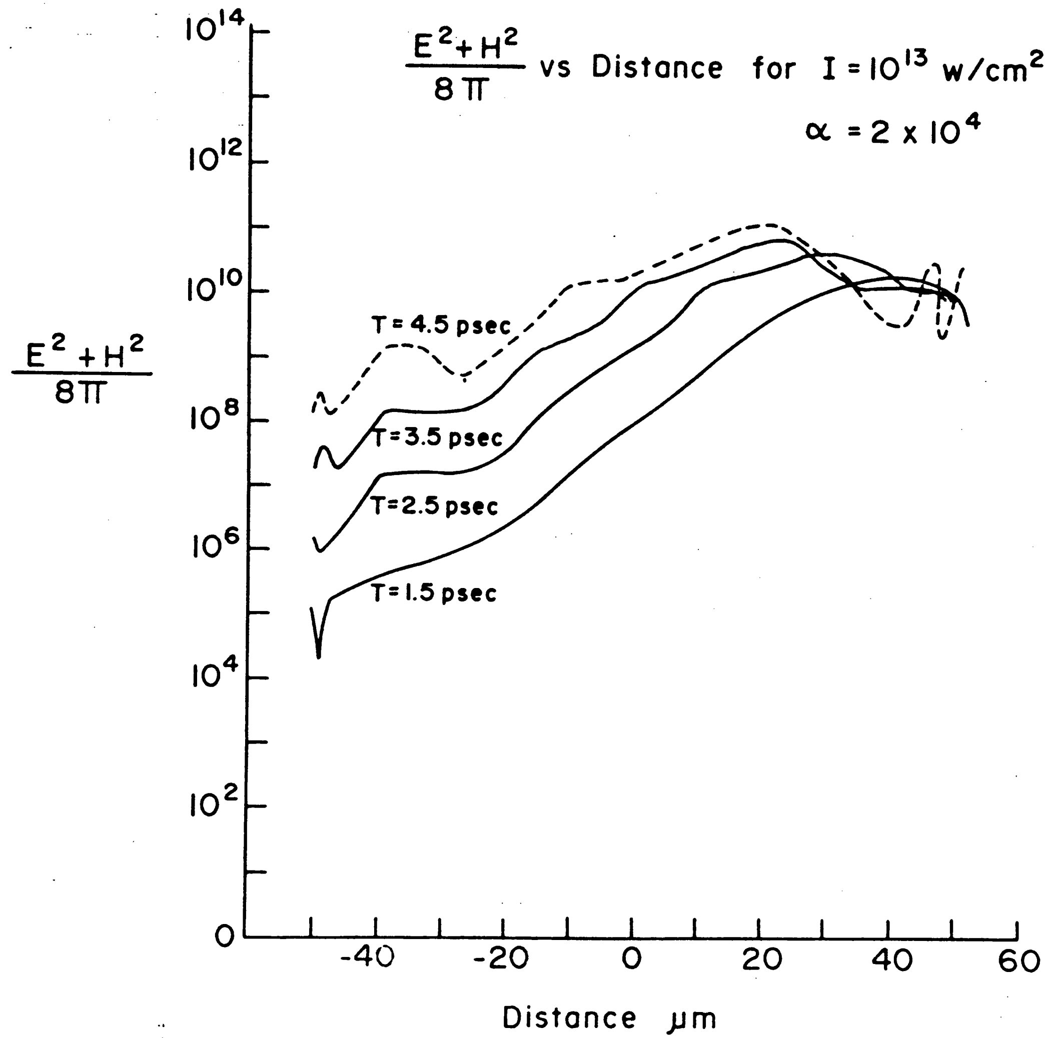

FIGURE 29 Time dependent solutions of $(E^2+H^2)/8\pi$ at initial temperatures of 100ev and initial profiles as figure 6. The generated soliton at 1.5 psec moves towards the interior of the plasma till a dynamic Brillouin instability occurs.

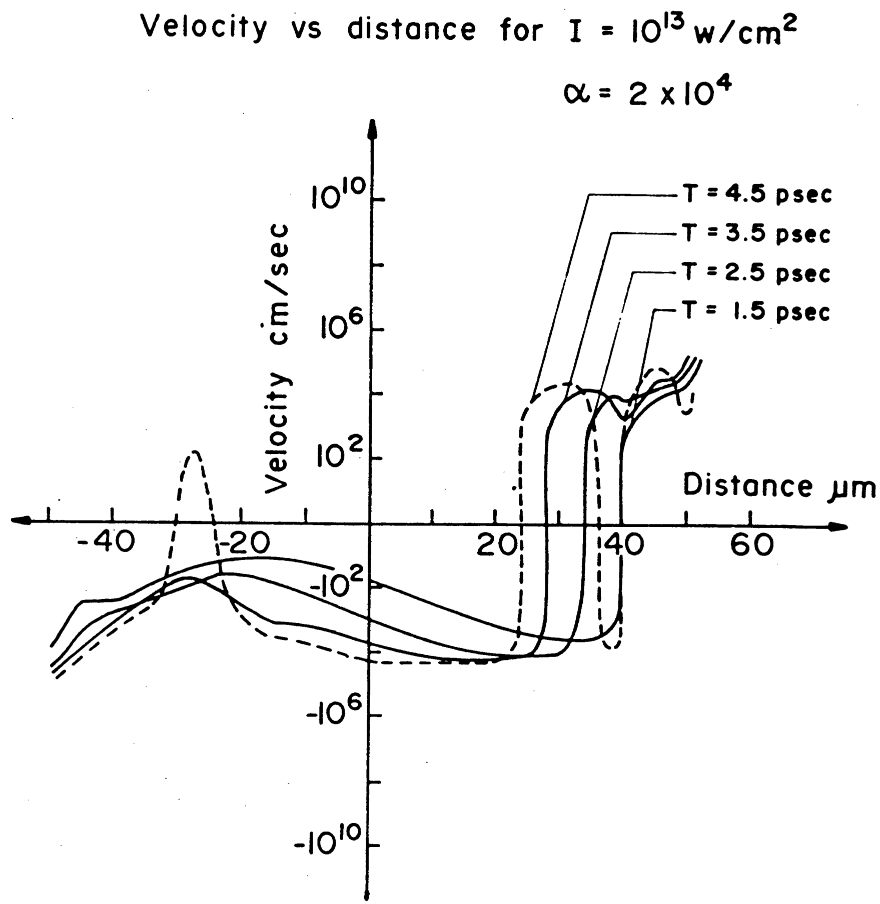

FIGURE 30 The velocity profile of plasma corresponding to figure 29. Note the increase in velocity as the soliton increases in size and the change in direction for velocity corresponding to the change of gradient of the electromagnetic energy density. The dynamic Brillouin instability occurring at 4.5 psec causes rapid fluctuations in plasma velocities.

profile allow variation of the force dependent only on the plasma frequency for a collisionless plasma[20] where the nonlinear force can be described as

$$F_{nl} = \frac{E_{v^2}}{16\pi} \frac{\omega_p^2}{\omega^2} \quad \alpha \qquad (9)$$

This is evident from figure 29 at a time of 1.5 psec when the ablating force corresponds to the radiation in the initial plasma density. Future development of the soliton depends directly on the variation of the density and the increase of the temperature in time allowing the soliton to increase in size with corresponding increases in the compression velocities. Higher temperatures allow fluctuation of the electromagnetic energy density. Lower temperatures leads to collisional effects causing the damping of the laser light. Either way efficiency of transfer of light into the plasma is low. This suggests that a stable variation in density and a constant rate of temperature allow the soliton to increase in size and to progress unhindered into the core of the plasma where high compression velocities may occur.

XII Interactions at different intensities

Schematically the sizes of solitons vary directly with the intensity of laser light for constant initial conditions, figure 31. The higher growth rate at higher intensities for development of instabilities by both thermal and dynamic processes exhibits further evolution of solitons. Due to the action of the non-

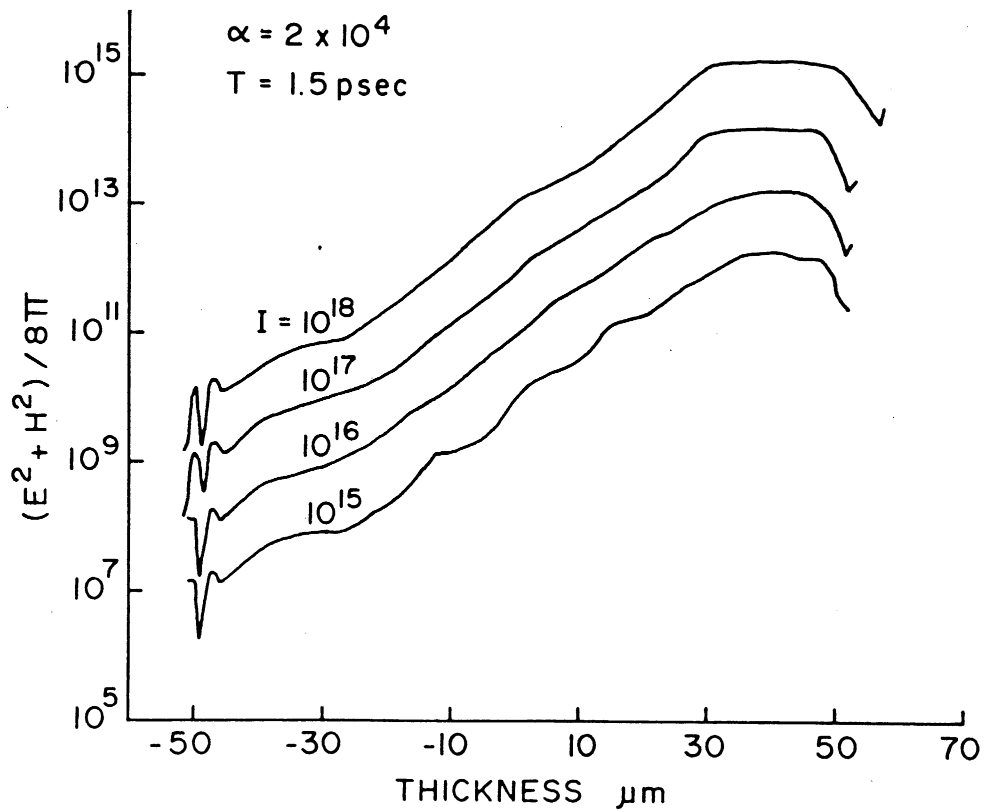

FIGURE 31 For initial density profiles of figure 6 and initial temperatures of 100ev we see that the sizes of the electromagnetic solitons generated at 1.5 psec vary directly with the incident intensity of laser light.

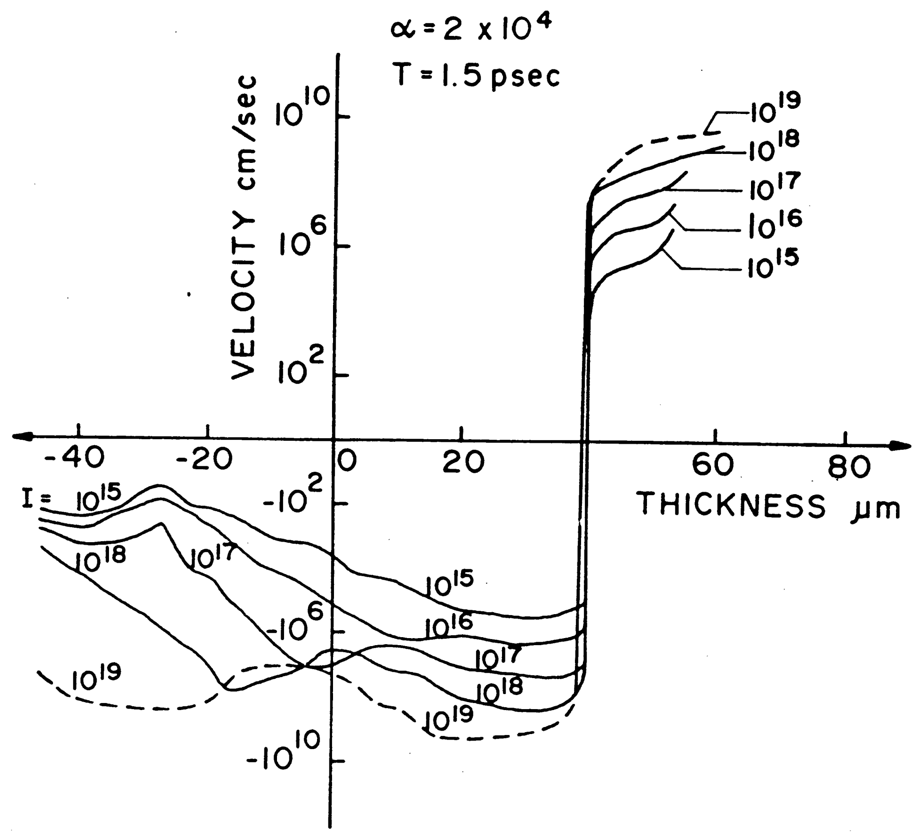

FIGURE 32 The velocity of plasma corresponding to the electromagnetic energy density of figure 31. Thick blocks of plasma move towards the interior of the plasma due to the nonlinear force generated by the solitons.

linear force thick blocks of plasma with low entropy compressions are generated with the magnitudes of the ablations and compressions, determined by the maximum values of the solitons. The swelling of the solitons are not very high, agreeing with the prediction of relatively low momentum transfer[21]. The plasma velocities generated move in thick blocks and for intensities of 10^{17} W/cm^2 reach velocities exceeding 2×10^8 cm/sec, figure 32.

XIII Energy transfer dependence on intensity

As a consequence of computation of various cases of figures 31 and 32, kinetic energy dependence on the intensity of laser light was discovered, figure 33. Evaluation was made of the amount of kinetic energy E_k that had been transferred by the nonlinear force which both the gas dynamic expansion and the thermokenetic acceleration had neglected. Evaluation was made of

$$E_k\ (I) = \frac{1}{x_2 - x_1} \int_{x_1}^{x_2} \frac{m_i\ n_i\ v_i^2}{2} dx \tag{10}$$

for dependence on the laser intensity, figure 33. The result is that the transferred kinetic energy is increasing nearly quadratically against the neodymium glass laser intensity such that

$$E_k \quad \alpha \quad I^{1.8} \tag{11}$$

for the range of intensities $5 \times 10^{15} < I < 10^{18}$ W/cm^2 which expresses the nonlinear nature of the interaction. The energy transfer is a nonlinear, macroscopic,

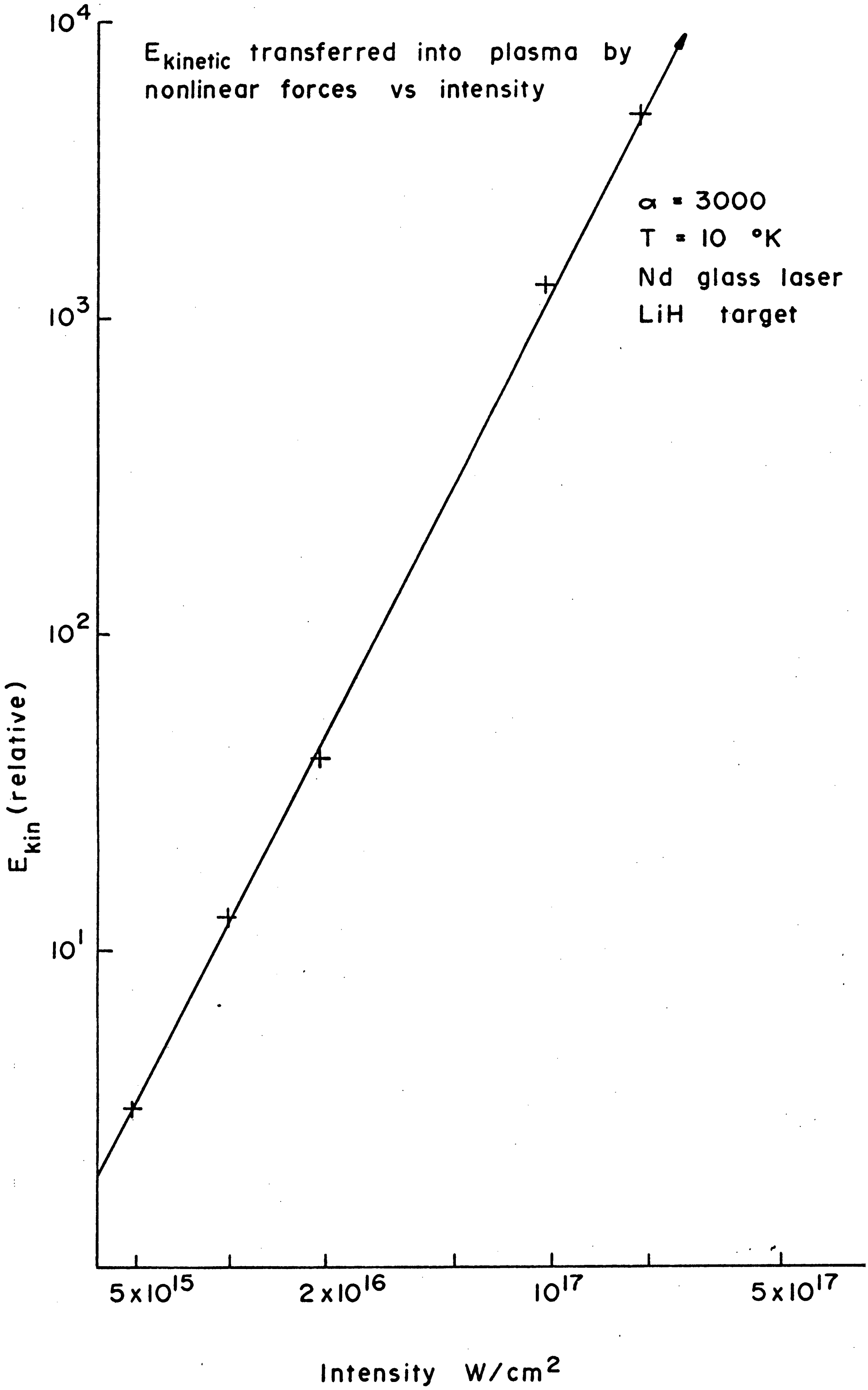

FIGURE 33 Kinetic energy transferred to the plasma dependent on laser intensity justifying the non-linear nature of the interaction. Results of exponents from eq. (11) varied from 1.6 to 1.9 for different α.

electrodynamic absorption process.

Isenor[22] had observed such nonlinear results experimentally as far back as 1964. Metz[23] had shown a threshold intensity at which results of impulse showed that above this threshold the momentum transferred to the target rises rapidly with increase in incident light energy.

Other experiments found the relationship to have an exponential value ranging from .38 to .8. Engelhardt et al[24] found the exponential to be .38. Gregg and Thomas[25] found the exponent to be .8 for aluminium and .53 for Lithuim Hydride, Opower et al[26] found the exponent to be .39. These results can be shown to be consistent with equation (10).

The acceleration $\alpha \quad |E|^{\theta} \quad \alpha \quad P^{\theta/2}$

The final maximum velocity v_{max} is given by acceleration multiplied by τ, the pulse duration of the laser

then
$$V_{max} = \text{acceleration x } \tau \ \alpha \ P^{\theta/2}\tau$$
$$E_{max} = V^2_{max} \quad \alpha \ P^{\theta}\ \tau^2$$

that is $E^*_{max} = \dfrac{E_{max}}{\tau^2} \quad \alpha \ P^{\theta}$ (12)

So that all the experiments can be seen to have a superlinear relationship when one normalises the result i.e. using equation 12 then the exponent of the experimental results lie between 1.6 and 1.9. All these earlier experiments need an interpretation by including self-focussing.

XIV Temperature vs. Intensity

There appears in Yamanaka et al[27] a threshold

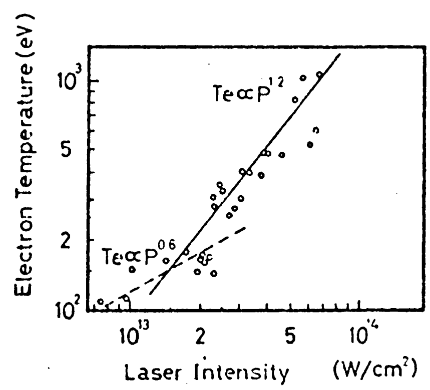

Figure 3 4 Experimental observation of electron temperature dependence on laser light intensity by Yamanaka et al.[27]

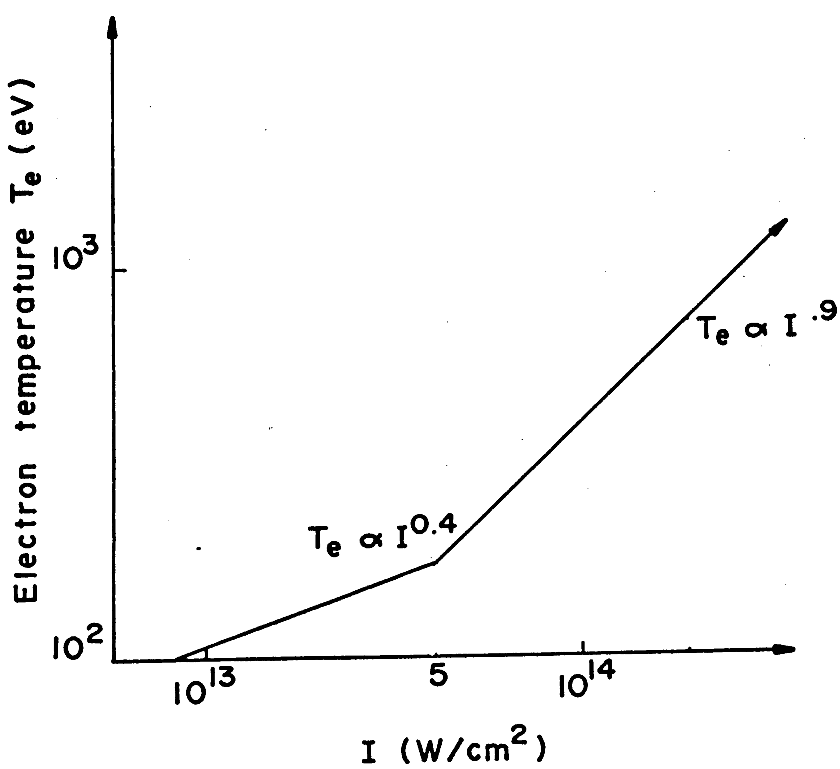

Figure 35 Results of maximum electron temperatures generated by the dynamic nonlinear force scheme.

intensity at which the temperature dependence of electrons on laser intensity rises from

$$T_e \; \alpha I^{.6} \quad \text{to} \quad T_\alpha \; \alpha I^{1.2} \tag{13}$$

at above 10^{13} W/cm^2.. See figure 34. Similar to Donaldson[28] here $T_e \; \alpha I^{.66}$ for $I < 10^{13}$ W/cm^2.

Similarly using the nonlinear force model, simulations were made of shorter pulses of radiation of 1.5 psec and a plot was made, figure 35, of the maximum of electron temperatures against the intensity and there appears the existence of the threshold intensity changing temperature gradients at 3 x 10^{13} W/cm^2.

The gradients of the temperatures differ than those of Yamanaka et al. but allowing for errors due to calibration errors in the laser intensities the simulated curve fits into Yamanaka's experimental results. These results also express the nonlinear nature of the interactions. The difference can be due to the self-focussing diameter which may vary with the power of Yamanaka's case.

XV CO_2 Laser Results

Using an initial bi- Rayleigh density profile with a cut off density determined by the frequency of the laser light, simulations were made of interactions of CO_2 laser at 10^{16}W/cm^2 and Nd glass laser at 10^{16}W/cm^2 and 10^{18}W/cm^2. Figure 36 represents the electromagnetic energy density $(E^2 + H^2)/8\pi$ at 1.5 psec, figure 37 are the profiles for the corresponding velocities and figure 38 the density profiles showing the corresponding minima (cavitons) due to the nonlinear force acceleration.

The similarity of results for both wavelengths at 10^{16} W/cm^2 lies in the maximum values of the electro-

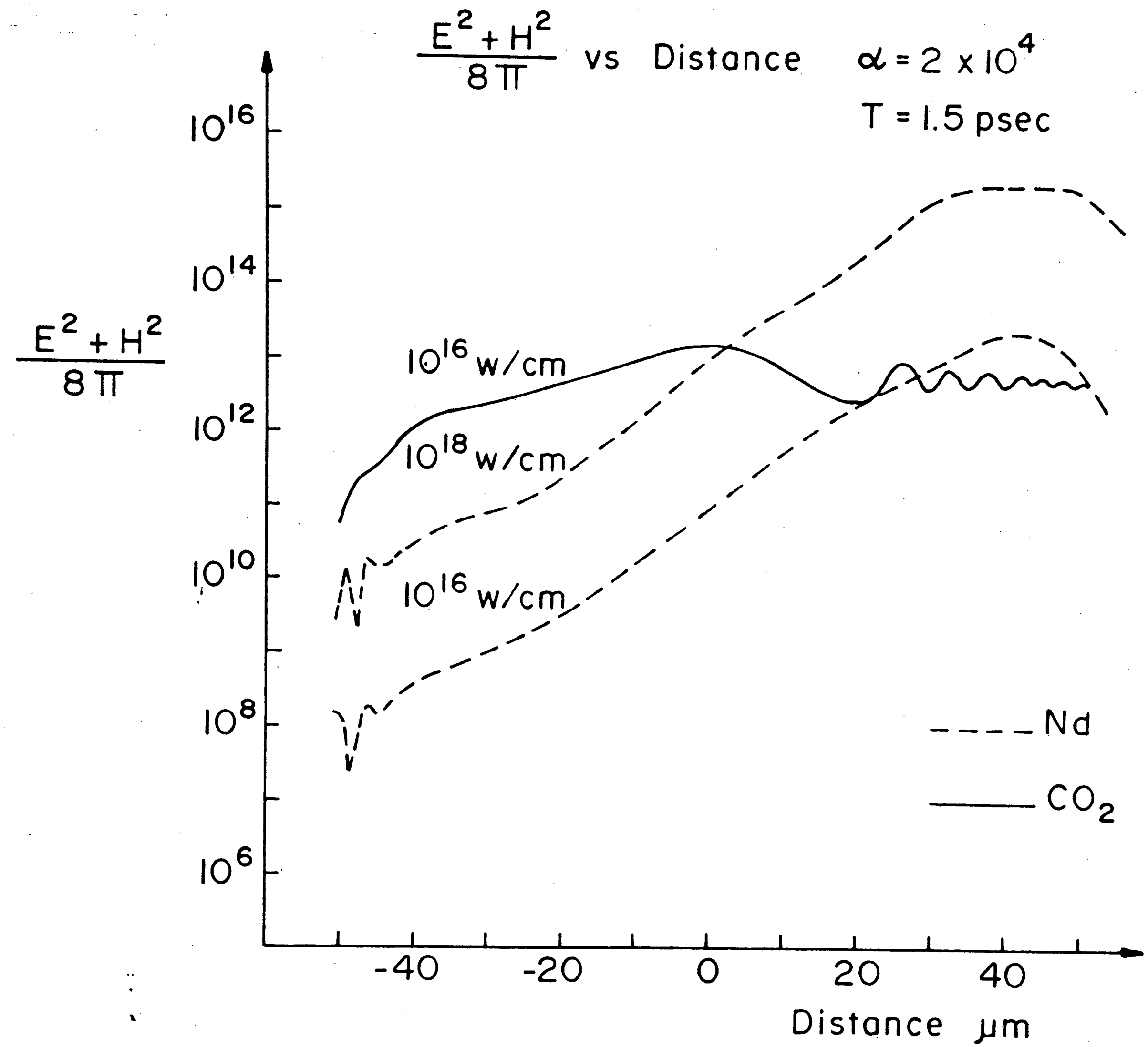

FIGURE 36 With an initial bi-Rayleigh profile corresponding to figure 6, the electromagnetic energy densities are plotted for intensities of 10^{16} W/cm² for CO_2 and 10^{16} W/cm² and 10^{18}W/cm² for Nd glass lasers.

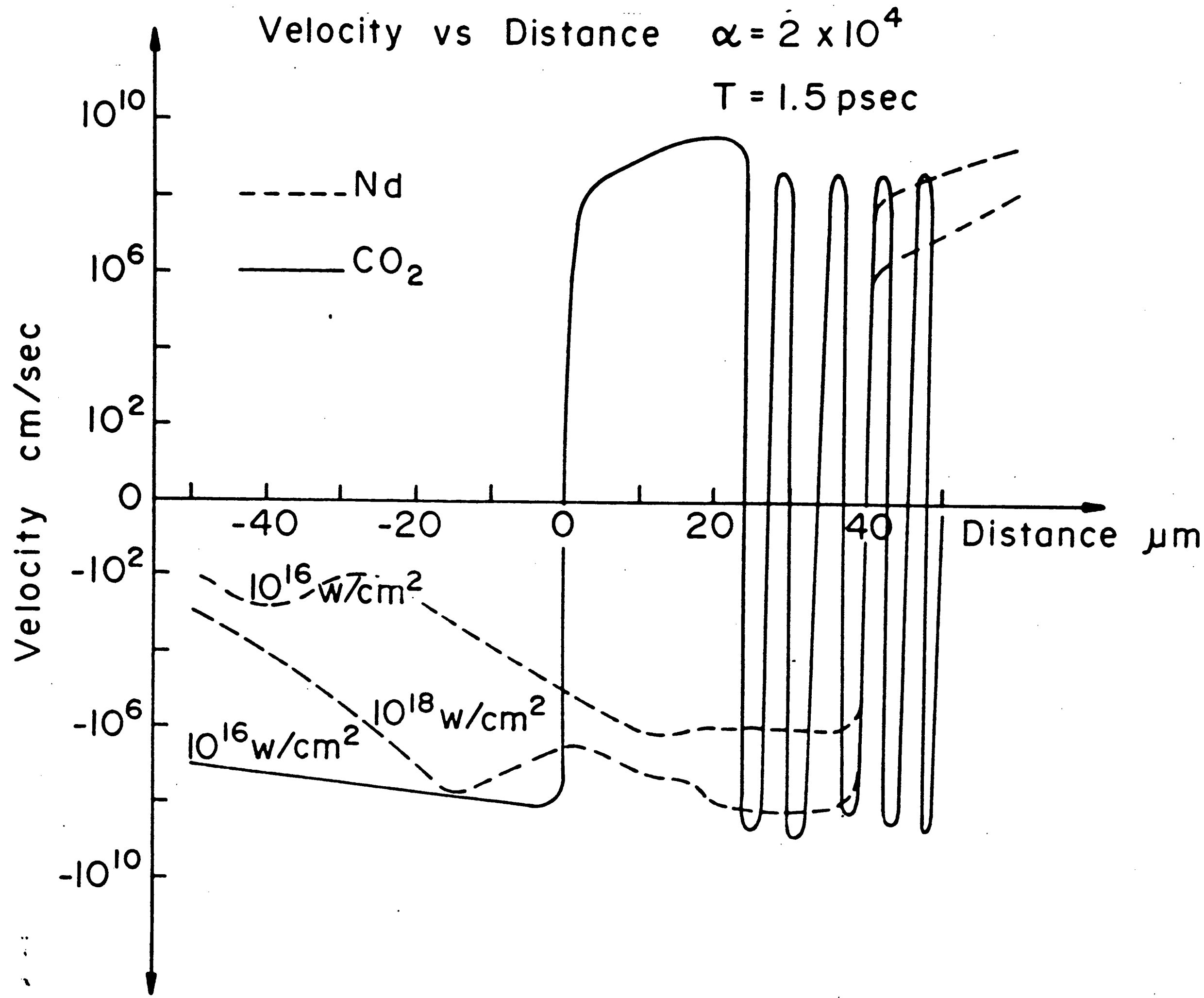

FIGURE 37 The resulting profiles at times of 1.5 psec for the cases of figure 36.

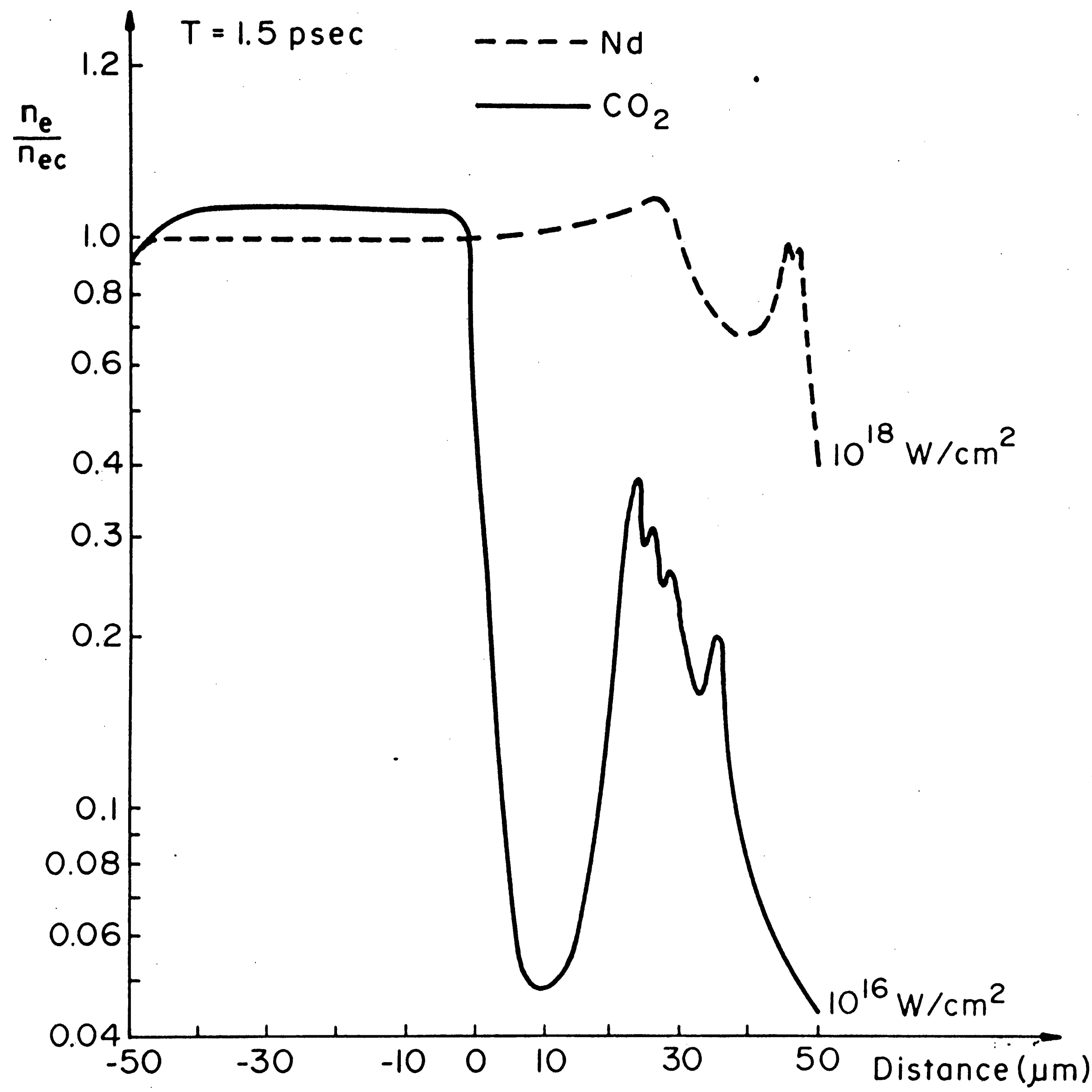

FIGURE 38 Density profiles of the cases for Nd glass lasers at 10^{18} W/cm^2 and CO_2 laser at 10^{16} W/cm^2 at 1.5 psec. Both density formations show the existence of a caviton occuring in the vicinity of a change in the gradient of the electromagnetic field soliton.

magnetic energy density which are nearly equal. Both cases show moderate swelling of the intensity above the vacuum value. In the CO_2 case, a relatively strong reflection occurs due to the oscillation of the field at the peripheral part of the plasma. The case of neodymium glass at 10^{18} W/cm^2 results in a pronounced soliton with a swelling of 31.

Looking at the velocity profiles (fig.37) we see that in all cases there is a compressing block like motion of plasma in the direction of the laser beam acting as highly efficient compression. However the maximum velocities attained between 10^8 and 10^9 cm/sec corresponds only to the different wavelengths of CO_2 and Nd glass if the intensities differ by a factor of 10^2.

This example shows that for different wavelengths of laser light with equal intensity, similar electromagnetic energy density maxima are observed while block like velocities are comparable in magnitude only when intensities differ by a factor of 100. This is well known from the electron energy due to the quivering motion in the laser fields. Similar results are known from the high energy ions in the order of Mev produced from solid targets after relativistic self focussing at the same laser power with different wavelengths[29]. The important conclusion we arrive at is that equal plasma velocities occur due to the nonlinear forces if the product

$$I\lambda^2 \tag{14}$$

are equal. The difference of 10^2 for I the intensity occurs if λ is the wavelength of CO_2 laser at 10.6 μm and the wavelength of Nd glass laser is 1.06 μm. This is precisely the $I \lambda^2$ that was measured with high accuracy in the range of intensities of 10^{13} W/cm^2 to 10^{17} W/cm^2 from the Los Alamos Group[30].

CHAPTER 7 CONCLUSIONS

With the aim of treating larger transfer of laser energy into the plasma for improved fusion energy gain, the properties of very low reflectivity was discussed on the basis of the Rayleigh profile. The exhibitance of low relflectivities allows a high percentage transfer of laser light into the plasma. The formulation of a collisionless dielectrically induced nonlinear force was derived to be proportional to the constant α for the Rayleigh density profile. By suitable arrangement of the Rayleigh profile, the action of the laser in the plasma allows for separate blocks of compressed and expanded plasmas. The desired effect meant more efficient transfer of laser energy as a macroscopic collisionless process. The problem of "internal reflections" studied by step wise approximations was found to be a numerical paradox as the high order approximation did not converge to the exact value.

Simulations of the laser plasma interactions were made. The use of the general gas dynamic scheme included macroscopic absorption. The governing equations of motion and conservation equations were used including the nonlinear force and corrections to the optical constants at higher intensities. The fully dynamic solutions of the laser plasma interactions at times of 0.1 psec verified the block like motions of the plasma due to the nonlinear force The block motions were due to electromagnetic solitons formed by the suppression of reflectivities at the junction of the plasma and vacuum by judicious choice of the constant α. At the short times of picoseconds, thermalisation does not occur so that the compression of plasma is adiabatic and one can assume that the electron fluid remains below the Fermi energy level. The special part of the code for solving the Maxwellian equations neglected retardation of the electromagnetic field. Realistically at a time of .1 psec, this assumption is questionable as the electromagnetic wave travels approximately 30 μm (approximating vacuum conditions) and interacts only with the corona of the plasma. In the plasma the group velocity of laser light is c $|\bar{n}|$ which is effectively less than c. Therefore the very general and complicated code had to be extended to times of picoseconds which will allow the laser light pulse to interact dynamically with the whole plasma. After numerous simulations with initial bi-Rayleigh density profiles, special solutions for discussions and observations were singled out for physical interpretations. We succeeded with this temporal extension at least up to such times where the retardation problem was overcome and the interaction time was still short enough to allow predominance of the nonlinear force effects. Cases of reflection at the cut off density were observed with the formation of standing waves. Reflections at the density cut off occurred at temperatures corresponding to both collisions and collision free plasmas. (Lindl and Kaw). The standing wave behaviour generated by interaction of reflected and incoming waves for the Rayleigh case corresponds to both theoretical and experimental results using a linear density profile. The use of bi-Rayleigh profiles with the maximum density slightly less than the cut off density allowed transmission of the laser light across the whole plasma. However standing wave patterns occurred as it did with other symmetric type density profiles. Supression of the standing wave pattern is observed by varying the values of α in the bi-Rayleigh profile, with a subsequent formation of a soliton. At short times the soliton does not automatically generate a density caviton. At the high intensity of 10^{17} W/cm^2 the caviton is observed at 1.5 psecs as a direct consequence of the action of the nonlinear force. At the lower intensity of 10^{16} W/cm^2 the size of the soliton at 1.5 psec generates a smaller caviton. At 10^{15} W/cm^2 the caviton is not evident till later times.

The behaviour of the soliton is to increase in time till a macroscopic instability occurs. The growth of the soliton occurs as the maximum of the soliton moves towards the interior of the plasma. Associated with the increasing maximum of the soliton is the velocities of the plasma, moving as two separating blocks. The increase in magnitude of the soliton maximum and the velocities suggests that there is an increasing efficiency of transfer of light energy into the plasma until a macroscopic instability occurs. An efficient transfer of energy is observed and high adiabatic compression velocities are experienced. In a spherical case, if the growth and lifetime of the soliton can be extended then the compression velocities attained drives the plasma to high compression densities and at later times when electron-ion thermal equilibration occurs together with high compression densities then conditions for highly efficient fusion gains are satisfied.

It was the basic need for the very general code to include the macroscopic absorption in the general form of nonlinear response to increasing laser intensity. The behaviour of the absorption of laser light is demonstrated. The higher the initial temperature of the plasma the lower the collision produced absorption of laser light. This is evident for temperatures of 10^7 ^{0}K where the plasma is effectively collisionless and allows the laser light to penetrate into the whole plasma. It is also observed that the higher the temperature of the plasma the larger is the maximum value of the soliton. This behaviour acting in conjunction with the controlled growth of the soliton further enhances the efficiency of energy transfer.

The dynamics of the soliton confirms the block like motion of plasma at high intensities. This demonstrates the high efficiency of transfer of the optical energy into compression of plasma. As in the cases of .1 psecs, the extended times of psecs confirms that for the short interaction times, which effectively negates collisional thermalisation, the collapse of the plasma remains adiabatic, similar to a Fermi degenerate plasma. The nonlinear force scheme makes possible compression by non thermal dynamically collisionless absorption of radiation.

Despite initially low reflectivities of the selected bi-Rayleigh density profiles there is a generation of density rippling occurring at later times which is described as a macroscopic Brillouin instability. Depending on the characteristic length L of the plasma defined by L.M.Goldman as 3×10^{-3}cm, the instability threshold occurs at 3×10^{14}W/cm^2. Raman scattering threshold is larger by a factor by c/v_e where v_e is the velocity of the electron. Therefore for non relativistic intensities we disregard Raman instability as an instability mechanism in this model. The onslaught of the instability generates rippling of the velocities which causes, even at low velocities near the cut off density, increase in the plasma density to above the critical density. The high reflectivities of the plasma at later times is due to that mechanism.

Evaluation of the momentum transfer of laser radiation into the plasma was made. The evaluations made showed that the momentum transferred was low compared to the gas dynamic case, however in agreement with Krokhin, this is still of sufficient magnitude for laser fusion. The energy transfer of radiation into the plasma for different intensity expressed a nonlinear relationship where the macroscopic dynamical non thermalising nonlinear absorption law is

$$E_{kin} \propto I^{1.8}$$

Confirmation was made of the wavelength intensity dependency of laser radiation, where $I^2\lambda$ should be a constant. The generated electromagnetic densities of radiation from CO_2 and Nd glass lasers of equal intensities were the same in agreement with electric field-intensity dependences. Velocities attained from CO_2 and Nd glass lasers were comparable in magnitude only when intensities differ by a factor of 100. The gas dynamical model is inadequate to explain the experimentally observed phenomena. The inclusion of the nonlinear force does explain the phenomena and the result verifies the very general property of the developed numerical code.

For further development, we can use the confirmation of the nonlinear force compression scheme. Further work has to be followed by varying initial and boundary conditions for optimising the condition of collapsing under adiabatic conditions. For this work however, the influence of reaction reheat has to be known, where work is still under discussion.

The Osterberg problem has been digested and the issue settled on the basis of a plane wave re-radiation condition. This should be developed in the future on the basis of analytical predictions as done by Osterberg.

REFERENCES

CHAPTER 1 INTRODUCTION

1. M.L.E. Oliphant, Lord Rutherford, Proc. Roy. Soc. A141, 259 (1933).
2. M.L.E. Oliphant, P. Harteck and Lord Rutherford, Proc. Roy. Soc. A144, 692 (1934).
3. N.G. Bavov, O.N. Krokhin, Soviet Physics JETP, 19 123 (1964).
4. J.M. Dawson, Physics of Fluids, 7, 981 (1964); H. Hora, Inst. Plasma Phys., Garching, Rept. 6/23 (1964).
5. Yu. V. Afanasyev, O.N. Krokhin, G.V. Sklizkov, IEEE J. Quantum Electronics, QE2, 483 (1966).
6. J. Nuckolls, L. Wood, A. Thiessen, G. Zimmerman, Nature (London), 239,139 (1972); J. Nuckolls, Laser Interaction and Related Plasma Phenomena, H. Schwarz and H. Hora, Eds. (Plenum Press, N.Y.) Vol. 3B, (1974).
7. R.A. Haas et al., Phys. Fluids, 20,322 (1977); K.R. Manes et al. J. Opt. Soc. Am., 67, 717 (1977); I.R.Gekker, O.V. Sizukhin, JETP Lett., 9,243 (1969).
8. S. Rand, Phys. Rev. B, 136,231 (1964).
9. H. Hora, Opto-Electronics, 2, 201 (1970).
10. F.F. Chen, Laser Int. and Related P.P., Vol.3A, 297(1974)
11. T.P. Hughes, M.B. Nicholson Florence, J. Phys. A2, 588 (1968); H. Hora ref. 9; S. Rand, ref. 8.
12. R.E. Kidder, UCRL-Preprint 71775 (1969).
13. A. Carusso et al. Il Nuovo Cemento, 45B, 176 (1966).
14. H. Hora, Australian Journal Physics 29, 375 (1976).
15. H. Hora, J. Opt, Soc. Am., 65, 882 (1975).

16. P. Kaw and J. Dawson, Phys. Fluids, 13,472 (1970)

17. W.L. Kruer, J.M. Dawson, Phys. Rev. Letts. 24, 1174 (1970).

18. J.W. Shearer, S.W. Mead, J. Petruzzi, F. Rainer, J.E. Swain, C.E. Violet, Physical Review A6, 764 (1972),

19. H. Hora, E.L. Kane, J.L. Hughes, J. Appl. Physics, 49,923(1978)

20. J.W. Shearer, R.E. Kidder, J.W. Zink, Bull. Am. Phys. Soc., 15, 1483 (1970).

21. A.Y. Wong, R.L. Stenzel, Phys. Rev. Letts., 34, 727, (1975).

22. J.W. Shearer, R.E. Kidder, J.W. Zink, Bull. Am. Phys. Soc., 15, 1483 (1970).

23. H. Azechi et al., Phys. Rev. Letts., 39, 1144 (1977).

24. R. Fedosyevs et al. Phys. Rev. Letts., 39, 932 (1977)

25. H. Hora, Nuclear Fusion, 10, 111 (1970).

CHAPTER 2 REFLECTIVITIES

References

1. H. Hora, Laser Plasmas and Nuclear Energy, (Plenum Press, New York, 1975).
2. H. Hora, Z. Phys, 226, 156 (1969); A.J. Palmer, Phys. Fluids 14, 2714 (1971); J.W. Shearer and J.L. Eddleman, Phys. Fluids 16, 1753 (1974); F.F. Chen, Laser Interaction and Related Plasma Phenomena, H. Schwarz and H. Hora, Eds, (Plenum, New York, 197 4) Vol. 3A, p.291; M.S. Sodha, A.K. Ghatak and V.K. Tripathi, Progress in Optics, E. Wolf Ed., (Acad, Press, New York, 1976) Vol. 13, p.171; M.S. Sodha, D.P. Teware, A. Kumar and V.K. Tripathi, Appl. Phys. 3, 141 (1974); 6,119 (1975); M.R. Siegrist, Opt. Comm. 16, 402 (1976); K.R. Manes, H.G. Ahlstrom, R.A. Haas, and T.F. Hotzrichter, J. Opt. Soc. Am. 67, 717 (1977); H. Hora and E.L. Kane, Appl. Phys. 13, 165-170 (1977).
3. P. Mulser, Phys. Letters Vol. 28A. 151, 1968.
4. H. Osterberg, J. Opt, Soc. Am. 48 (1958) 513.
5. H. Hora, Henaer Jahrbuch (1957), p.131.
6. H. Hora, Phys. Fluids, 17, 939, (1974).
7. J. Lindl and P. Kaw, Phys, Fluids, 14, 371-377 (1971).
8. J.R. Wait, E.M. Wave in Stratified Media, Pergamon (1962)

CHAPTER 3 NONLINEAR FORCE

1. L.D. Landau and E.M. Lifshitz, Electrodynamics of Continuous Media (Pergamon, Oxford, 1966).

2. C. Schaefer, Einfuhrung in Die Theoretische Physik, Berlin, Gruyter, Third edition, Vol. 3, Part 1.

3. L.C. Steinhauer, H.G. Ahlstrom, Physics of Fluids, 13, 1103 (1970).

4. H. Hora, Opto-Electronics 2, 201 (1970).

5. P. Mulser, Z. Naturforsch, 25A, 282 (1970); R.G. Rehm, Phys. Fluids 13, 921 (1970);.

6. J.W. Shearer, R.E. Kidder, J.W. Zink, Bull.Am. Phys. Soc., 15, 1483 (1970).

7. E.J. Valeo, W.L. Kruer, Phys, Rev. Letters,33,750 (1974).

8. K.A. Brueckner,R.J.Janda,Nuclear Fusion,17,451(1975); K.A. Brueckner, Laser Interaction and Related Plasma Phenomena, H Schwarz and H. Hora Eds. (Plenum Press, New York, 1977) Vol. 4B, p.891.

9. A.Y. Wong, R.L. Stenzel. Phys. Rev.Letts., 34, 727 (1975).

10. H.C. Kim, R.L. Stenzel, A.Y. Wong, Phys. Rev. Letts., 33, 886 (1974).

11. Yu.A.Zakharenkov et al., Soviet Physics JETP, 43, 283 (1976).

12. H. Azechi et al.,Phys. Rev. Letts., 39, 1144 (1977).

13. R. Fedosejevs et al., Phys. Rev. Letts. 39, 932 (1977)

14. T.P. Donaldson, I.J. Spalding, Phys. Rev. Letts, 36, 467 (1976).

15. H. Hora, Phys. Fluids 12, 182 (1969).

16. A. Schülter, Z. Naturforsch, 5A, 72 (1950).

CHAPTER 4 ABSORPTION OF LASER LIGHT

1. A. Schülter, Z. Naturforsch., 5A, 72 (1950).
2. L. Spitzer Jnr., R. Harm, Phys. Rev. 89, 977 (1953)
3. L. Oster, Reviews of Modern Physics, 33, 525 (1961)
4. P.A.G. Schuer, Monthly Notices Royal Astronomical Society, 120,231 (1960).
5. J.M. Dawson, C. Oberman, Physics of Fluids, 5, 517, (1962).
6. J.M. Dawson, "Advances in Plasma Physics", Volume 1, Interscience, New York (1968).
7. R.A. Haas et al., Phys. Fluids, 20, 322 (1977); K.R. Manes et al., J. Opt Soc. Am ., Vol. 67 717 (1977)
8. S. Rand, Phys. Rev. B, 136, 231 (1964).
9. H.S. Green, Nuclear Fusion 1, 69 (1961).
10. R.E.Kidder, UCRL-PREPRINT 71775 (1969); H. Hora, J. Opt. Soc. Am., 65, 882 (1975).
11. W.L. Kruer, Comments Plasma Physics, 2, 139 (1976).
12. D. Dubois, Laser Interaction and Related Plasma Phenomena, H.Schwarz and H. Hora eds. (Plenum Press, New York) 1974, Vol. 3A, p.267, M. Lubin, IBID, Vol. 3B, p.607.
13. J.W. Shearer, Lawrence Livermore Lab. Report, UCID - 15745 (1970).
14. K.H. Spatschek, Fortschritte der Physik, 24, 687 (1976).
15. A.Y. Wong, Laser Interaction and Related Plasma Phenomena. (Plenum Press, New York) (1977).Vol.4B.
16. L. Spitzer Jnr., Physics of Fully Ionized Gases (Interscience Pub. N.Y.) Second Edition, (1962).

CHAPTER 5 LASER PLASMA MODEL

1. H.S. Green, Nuclear Fusion, 1, 69 (1961).
2. L. Spitzer Jnr., Physics of Fully Ionized Gases (Interscience Publishers, New York) Second Edition, (1962).
3. R.E.Kidder,S. Barnes, UCRL Report 50583 (1969).
4. R.D. Richtmyer, K.W. Morton, Finite Difference Methods for Initial Value Problems (Intersicence Publishers, New York) (1968).
5. J. Von Neumann, R.D. Richtmyer, J. Appl. Phys, 21, 232 (1950).
6. M.W. Jaffrin, R.F. Probstein, Physics of Fluids,7, 1658 (1964).
7. S. Chapman, T.G. Cowling, Einführung in Die Theoretische Physik (Gruyter, Berlin) Third Edition, Volume 3, 1, 1950.
8. S.I. Braginskii, Reviews of Plasma Physics, 205,(1968)
9. A. Masani, Y. Borla, A. Ferrari, A. Martini, Nuovo Cimento, 48, 326 (1967).
10. M.S. Maxon, E.G. Cormon, Phys. Rev., 163,156 (1967).
11. L.D. Landau, E.M. Lifshitz, Electrodynamics of Continuous Media (Pergamon, Oxford) p.203-207,(1966).
12. R. Courant, K. Friedrichs, H. Lewy, Über Die Partiellen Differenzengleichurgen Der Mathematischen Physik, Math. Ann. 100, 32-74 (1928).
13. R.E.Kidder,UCRL Preprint 71775 (1969);
H. Hora, J. Opt. Soc. Am., 65, p.882 , (1975)

CHAPTER 6 RESULTS

1. H. Hora, Jenaer Jahrbuch, 131, (1957).

2. J. Nuckolls, L. Wood, A. Theissen, G. Zimmerman, Nature (London), 239, 139 (1972); J. Nuckolls, Laser Interaction and Related Plasma Phenomena, H. Schwarz and H. Hora, Eds. (Plenum Press, New York) Vol. 3B, (1974).

3. H. Hora, Nuclear Fusion, 10, 111 (1970).

4. J.D. Lawson, Proc. Phys. Soc. London. B70,6, (1957).

5. R.E. Kidder, Nuclear Fusion, 4, 797 (1974).

6. H. Hora, P.S. Ray, Bulletin American Physical Society, 21, 73 (1976); P.S. Ray, ph.D Theses.

7. F.F. Chen, IBID, (Plenum Press), Vol.3A, 297, (1974); L.M. Goldman et al., Phys. Rev. Lett., 31,1184(1973)

8. J. Lindl, P. Kaw, Phys. Fluids, 14,2714 (1971).

9. R.J. Faehl, N.F. Roderick, Phys. Fluids, 20,279(1977).

10. H. Hora, IBID,(Plenum Press, New York) Vol. 1,383, (1971).

11. R.L. Stenzel, A.Y. Wong, H.C. Kim, Phys. Rev. Letters, 32, 654 (1974).

12. H. Hora, Soviet Journal of Quantum Electronics, 6, 51 4, (1976).

13. P. Mulser, Z. Naturforsch 25A, 282 (1970); R.G. Rehm, Phys, Fluids 13, 921 (1970); E. Panarella, P. Savic, Canadian Journal of Physics, 46, 183 (1968) A.F. Haught, D.H. Polk, Phys. Fluids, 13, 2825 (1970).

14. L.C. Steinhauer, A.G. Ahlstrom, Phys. Fluids, 13, 1103 (1970).

15. Yu. V. Afanasyev, O.N. Krokhin, G.V. Sklizkov, IEEF J. Quantum Electronics, QE2, 483 (1966).

16. Yu. A. Zakharenkov, N.N. Zorev, O.N. Krokhin, Yu. A. Mikhailov, A.A. Rupasov, G.V. Sklizkov, A.S. Shikanov, Soviet Physics - JETP, 43, 283(1976).

17. M.R. Siegrist, B. Luther-Davies, J.L. Hughes, Opt. Comm. 18, 603 (1976); B. Luther-Davies, J.L.Hughes, Phys. Letts, 58A, 399 (1976).

18. J.W. Shearer, R.E. Kidder, J.W. Zink, Bull. Am. Phys. Soc. 15, 1483 (1970); J.W. Shearer, LLB Report, UCID15745 (1970).

19. Similar to the Microwave Observations by H.C.Kim, R.L. Stenzel, A.Y. Wong,Phys.Rev. Letts.33,886(1974)

20. H. Hora., D. Pfirsch and A. Schlüter, Z. Naturforsch, 22A, 278 (1967).

21. P.N. Krokhin, Nuclear Fusion, 16, 1203 (1976).

22. N.R. Isenor, Appl. Phys, Letts, 4, 152 (1964); W.I. Linlor, Appl. Phys. Letts, 3, 210 (1963).

23. S.A. Metz, Appl. Phys. Lett, 22; 212 (1973); H. Hora, Appl. Phys. Lett., 23, 39 (1973).

24. T.V. Engelhardt Westinghouse SCI Paper 68-1E5-PLASL-p4, (1968).

25. D.W. Gregg, S.J. Thomas, J. Appl. Physics, 37, 2787 (1966)

26. H. Opower, W. Kaiser, H. Puell, W.Heinicke, Z. Naturforsch, 22A, 1392 (1967).

27. C. Yamanaka et al., Phys. Rev. A6, 2335 (1975).

28. T.P. Donaldson, I.J. Spalding, Phys. Rev. Letts., 36,467(1976)

29. H. Hora, J.L. Hughes, E. Kane, J. Appl. Phys., 49,923(1978)

30. D. Giovanelli, D. Henderson, G. McCall, R. Perkins, See G.B. Lubkin, Physics Today, 19 Sept. 1977.

NUCLEAR INSTRUMENTS AND METHODS 144 (1977) 27-32 ; © NORTH-HOLLAND PUBLISHING CO.

ADVANCED FUEL NUCLEAR REACTION FEASIBILITY USING LASER COMPRESSION II

R. CASTILLO, H. HORA, E. L. KANE, V. F. LAWRENCE, M. B. NICHOLSON-FLORENCE, M. M.. NOVAK, P. S. RAY, J. R. SHEPANSKI, R. I. SUTHERLAND, A. I. TSIVINSKY and H. A. WARD

Department of Theoretical Physics, University of New South Wales, Kensington, Sydney, Australia

Several problems are considered in order to study the properties of the nonlinear-force compression of plasmas by lasers used to reach conditions for advanced clean fuel nuclear reactions as well as to distinguish from gas-dynamic compression. The propagation of light in inhomogeneous media is based on a simpler, computationally economic programme. The Goos–Haenchen effect is used for discussions of wave propagation and a laser amplifier without superradiance designed. Corrections for α-reheat are derived and a very short-range relativistic self-focusing discovered with relatively low thresholds. Entropy production and electron-radiation interaction are treated relativistically.

1. Introduction

Following the preceding article[1]), there exists the possibility of generating clean nuclear energy from laser compressed plasmas, if for example the reaction $H + {}^{11}B = 3\alpha$ is used. One necessary condition is the use of the nearly isentropic transfer of the laser energy into kinetic energy of plasma[2]), which is of such high efficiency that the advanced clean fuel reaction becomes feasible at laser pulse energies of less than 1 MJ. Compression based on the gas-dynamic ablation[3]) results in efficiencies much lower than necessary to get feasible conditions. Though the MIGMA[4]) project, an alternative for clean fusion, has reached an advanced level, there are some reasons still to proceed with the nonlinear force compression method for laser fusion by clean reactions.

There are some experimental barriers against gasdynamic compression which have not been included in the present extensive numerical simulation for forecasting energy generation[5]). One of these phenomena is the simple rule that the laser intensity has to be less than 10^{14} W/cm^2 for neodymium glass lasers and 10^{12} W/cm^2 for CO_2 lasers for which, however, symmetric compression[3,6]) and reasonable fusion yields have been established. At higher intensities, the phenomenon of fast ions has been observed[7,8]) which can be considered as an experimental proof of the action of nonlinear forces[9]) similar to analogous cases with microwaves[10]).

One general theoretical aspect puts a further limitation to the intensity of the laser radiation for gas-dynamic ablation. While the main energy of the highly sophisticated laser pulse is to be concentrated within the last 100 ps, its intensity must not exceed such values which result in collision times longer than the interaction times. These absolute limits restrict the neodymium glass laser intensities to[11]) less than 10^{16} w/cm^2 also if instabilities generate an anomalous effective collision frequency higher than the nonlinear Coulomb collision frequencies[12]). On the other hand, a power density of 10^{19} W/cm^2 is necessary to compress the plasma for nuclear reactions[13]). One way out may be the gasdynamic compression scheme of Afanasyev et al.[14]) in addition to the compression with the nonlinear force scheme[1]).

This paper discusses a series of several theoretical results which were performed to test the various aspects of the gas-dynamic and nonlinear force compression scheme, where connections with the problem of clean reaction of, for example, $H + {}^{11}B$ etc. are included; in addition radiation problems are considered which themselves are similar to those related to the laser produced pair-production[2,15]).

2. Propagation and reflection of waves

For the action of the nonlinear force for compression it is of importance that the laser radiation penetrates an inhomogeneous plasma with a minimum of reflection. It has been found for the case of linearly increasing electron densities that the generation of reflection is very strong and the resulting standing wave pushes electrons (plasma) towards the nodes and causes dynamic absorption[2]) instead of thick fast moving blocks of plasma. Though the example (see pp. 64–72 in ref. 2) still results in 23% transfer of laser energy into

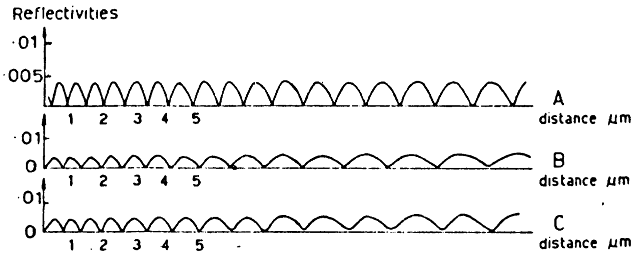

Fig. 1. Reflectivity R of a set of vacuum – Rayleigh plasma ($\alpha = 10^4$ cm^1; $\lambda = 1.06\ \mu$m) – homogeneous plasma with continuous refractive index without collisions at various thicknesses d of the Rayleigh plasma. Case (a) is the exact solution, case (b) is the approximation with 1000 steps of equidistant homogeneous plasma and case (c) with 1000 steps.

net kinetic energy of a thick block of plasma, further suppression of reflection is necessary.

One example for low reflectivity is the use of a density profile which results in an optical refractive index depending on the depth x

$$\tilde{n} = \frac{1}{1+\alpha x}, \qquad (\alpha > 0), \tag{1}$$

corresponding to an electron density n_e for a collisionless plasma of

$$n_e = n_{ec}[1 - 1/(1+\alpha x)^2], \tag{2}$$

where n_{ec} is the critical density (cut-off) at which the plasma frequency ω_p is equal to the optical frequency ω. The case of eq. (1) has been first discussed by Rayleigh (Rayleigh profile) and has elementary solutions of the wave equation of the type[16])

$$E_y(x) = (1+\alpha x)^{\frac{1}{2}} \exp\left[\pm i \ln(1+\alpha x)\left(\frac{\omega^2}{c^2\alpha^2} - \frac{1}{4}\right)^{\frac{1}{2}}\right], \tag{3}$$

$$H_z(x) = \left[\pm\left(\frac{\varepsilon_0}{\mu_0} - \frac{\alpha^2}{4\omega^2\mu_0^2}\right)^{\frac{1}{2}} - \frac{i\alpha}{2\omega\mu_0}\right](1+\alpha x)^{-\frac{1}{2}} \times$$
$$\times \exp\left[\pm i \ln(1+\alpha x)\left(\frac{\omega^2}{c^2\alpha^2} - \frac{1}{4}\right)^{\frac{1}{2}}\right]. \tag{4}$$

Reflection occurs at the interface between a Rayleigh medium and a homogeneous medium only, and *not* within the Rayleigh medium. The more general result of Osterberg[17]) on vanishing "internal reflection" gave rise to several controversies. The solution to the problem can be seen from the calculation of a Rayleigh-like plasma of various thickness between homogeneous plasma (fig. 1). The exact solution of the reflectivity agrees in magnitude with the approximation of steps of plasma with constant refractive index if enough steps (100 or 1000) are used. What is then called "internal reflection" is nothing else than the WKB-like increase of the amplitude of the reflected mode which is singly produced at the interface of the Rayleigh-plasma to the homogeneous plasma only[18]). The simplification of the described numerical treatment leads to a more precise solution of the wave equation in inhomogeneous media for general computer programmes.

One open question is the result that the dielectrically explained spreads of the minima of the curves in fig. 1 are different for the exact case (curve a) and for the stepwise approximation (curves b and c). It has to be noted that cases with a small number of steps can differ from the results in fig. 1 drastically.

One further question of the propagation of radiation in plasma is the momentum of the photons. In agreement with the recoil in inhomogeneous surfaces[9,19]) and with the transport of a wave-packet[20]), the photon momentum is

$$p = \frac{h\omega}{c}\frac{1}{\tilde{n}}(1 - \omega_p^2/2\omega^2). \tag{5}$$

Peierls[21]) found a similar expression for transparent solids first, modified, however, such that a basic difference exists compared with plasma. The basic problem of the Abraham or Minkowski description has been discussed by Dewar[22]) and some aspects of the problem of the brief arresting of energy with electrons during its exchange with the plasma electrons in connection with the Fizeau effect have been considered by Shepanski[23]).

The switching-on and switching-off process of the light when penetrating a plasma gives a vanishing net transversal motion[20,24]) also under relativistic conditions in difference to other authors[25]).

The Goos–Haenchen effect (side shift of a wave at total reflection)[26]) is not only of fundamental interest with respect to the correct use of quantities of phase or intensity, but also e.g., for the codes in laser produced plasmas. An important application is in the penetration of radiation around a spherical target within the skin depth, as has been pointed out for laser produced plasmas[27]) to explain some early experiments[28]). The inclusion into numerical codes needs a clear analysis of the use of phases or intensity, which has been discussed, for example, by Renard[29]).

One consequence of these calculations is immediately connected with laser fusion, namely for la-

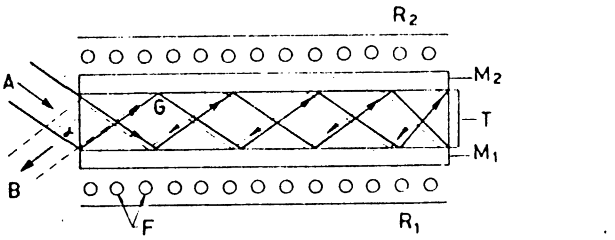

Fig. 2. Laser amplifier without superradiance. The laser beam is incident at an angle x on a medium G adjacent to an optically inverted medium M so that $\alpha > \alpha_c$ (α_c critical angle of total reflection). The reflectivity is larger than one[34]) and has specific maxima[33]).

ser technology. Lasers always emit superradiation in addition to the desired giant pulses. This superradiance had to be suppressed by 10^{-6} of the main laser power, before the first convincing fusion neutrons were generated with neodymium glass lasers[30]). The same happened with CO_2 lasers[31]). Only the sufficient suppression of the superradiance led to neutrons. For iodine lasers it is a much more difficult problem if large cross sections of the beam are used[32]). One way to reach laser amplification without superradiance is described in fig. 2.

3. Correction of the α-reheat

In laser compressed nuclear reactions, the heating of the plasma by the reaction products, protons or alphas, is of importance and has been used in several detailed numerical codes[35]). One problem is then, what mean free path or what penetration depth R has to be used for the nuclei? The slowing down (equilibration) of fast ions in plasma is an old problem in plasma[36]) and nuclear[37]) physics. One application for relativistically fast electrons was made possible by Bagge's modification of the Bethe–Bloch formula of solids for plasma and the derivation of measured penetration depth of relativistic electrons in plasma[38]).

The application of the similar methods for alphas led to the penetration depth[39]) in plasma of electron density n_e and temperature T

$$R = 2\frac{e^2}{kT}\frac{m_p}{m_e}\,\mathrm{Ei}[\ln(\chi E_0^2)], \tag{6}$$

where the function Ei(x) is the integral-logarithm. As a result, the length R can differ by more than a factor of ten from the measured lengths for solids of the same density. Fig. 3 shows the result for solid state density of HB. The general values of density are used in the computer codes; further theoretical work is undertaken to compare the differing plasma theories. The correlation with the depths in tokamaks, as determined by Düchs and Pfirsch[40]), is close though different models have been used.

For the calculation of the α-reheat in the codes the reaction gain G is given by:

$$G = \frac{\varepsilon_F}{E_0}\int_0^\infty \mathrm{d}t \int_0^{R(t)} \mathrm{d}x\,\mathrm{d}y\,\mathrm{d}z\, \frac{n_i[R(t)]^2}{A}\langle\sigma v\rangle, \tag{7}$$

where ε_F is the energy released per reaction, n_i is the ion density, A is 2 or 4 and $\langle\sigma v\rangle$ is the temperature averaged cross section where the adiabatic decrease of the temperature is included. We have used the following condition to take into account the appropriate adiabatic cooling of the plasma and the transfer of the reaction energy into kinetic energy of expansion. If T_g is the energy generated by nuclear reactions during one time step of integration, the temperature is calculated by

$$T = \left[T_0 + \sum_{\nu=1}^{N} \Delta_\nu T_g\left(\frac{R_\nu}{R_0}\right)^2\right](R_0/R)^2, \tag{8}$$

where R_ν are the radii at each time step of numerical integration during which an increase of the temperature $\Delta_\nu T_g$ by reheat occurs.

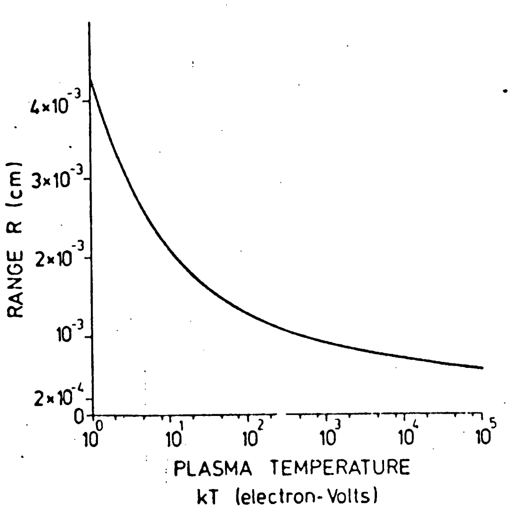

Fig. 3. Penetration depth R of α-particles from the $H^{11}B$ reaction in plasma of solid state density of HB as function of the temperature[39]).

4. Relativistic self-focusing

The self-focusing resulting from relativistic particle mass and energy influences becomes important for pre-focused laser beams of power greater than 10^{10} W [41,42]). Previous non-temperature dependent calculations given in ref. 41 show the self-focusing length as a function of beam intensity for n_e/n_{co}^{NR} ratios of 10^{-3}, 10^{-2}, and 10^{-1}, where n_e is the electron number density and n_{co}^{NR} is the non-relativistic cut-off density of the Nd glass laser (10^{21} cm^{-3}). The magnitude of l_{SF} is inversely proportional to the square root of this ratio for $n_e/n_{co}^{NR} \equiv N$ with $N \leq 0.7$; furthermore, the distributions are roughly symmetric and convex downward with minimums near I_{REL}, a characteristic relativistic intensity (relativistic threshold) of value 3.66×10^{18} W/cm^2 for Nd glass.

Further new calculations for N values around unity and above exhibit extremely small l_{SF} values, as well as limiting minimum intensity levels for non-singular l_{SF} results. Employment of the complex refractive index, the nonlinear Lorentz gas – Coulombic expression for the collision frequency, and a relation between the local laser beam wavelength within the plasma to the beam radius[41]) gives

$$\frac{l_{SF}}{d_0} = \frac{1}{2}\left(\frac{|\tilde{n}(I)| + |\tilde{n}(I/2)|}{|\tilde{n}(I)| - |\tilde{n}(I/2)|}\right)^{\frac{1}{2}}, \tag{9}$$

where $\tilde{n}$ is the exact complex refractive index resulting in

$$|\tilde{n}(I)| = \left|\left[1 - \frac{N}{(1+I/I_{REL})^{\frac{1}{2}}}\right]^2 + \left(\frac{\nu}{\omega}\right)^2 \frac{N^2}{(1+I/I_{REL})}\right|^{\frac{1}{4}}, \tag{10}$$

with d_0 the beam width between the half-irradiance maximum points of the radial laser intensity distribution and ν/ω the normalized collision frequency. It is readily seen from eq. (9) that for $|\tilde{n}(I/2)| > |\tilde{n}(I)|$ the solution becomes singular and then imaginary at this "threshold" intensity I_S; this occurence was not found in the calculations of ref. 41 but is crucial in the conditions illustrated in fig. 4. In particular, the collision frequency (ν) magnitude is of maximum importance near this cut-off; temperature, ion charge number, and qualitative allowance of field-induced collective effects on the total energy can all be influential in this region. Included in fig. 4 are the l_{SF}/d_0 vs I distributions for $T = 0$ eV and $Z = 1$: $N = 0.1$, 0.9, 1.0, 1.5, and 10.0; for $T = 100$ eV: $N = 1.0$ and 1.5 with $Z = 1, 2, 5$, and 10 as well as a 0.01 energy multiplying factor for $N = 1.0$ and $Z = 1$; and for $T = 1000$ eV: $N = 1.0$ and $N = 10.0$, both for $Z = 1.0$.

N values > unity produce the cusp-like distributions with the extremely small minimum self-focusing lengths, the minimum allowable intensities deeply found in the relativistic regime with $N \gg 1$. For $N = 1$ the influence of temperature is minimal up to 100 eV; however, an increase of plasma temperature to 1000 eV yields a two order of magnitude decrease in minimum intensity. It is seen that for N values around unity a small change in N produces a large change in both magnitude and shape of the $l_{SF}(I)$ distribution for $I < I_{REL}$; the distributions are mutually closer with $I > I_{REL}$. The influence of temperature, for a fixed N, is negligible for $N \gg 1$.

It is of interest to qualitatively estimate the influence of non-collisional electromagnetic field induced charged particle collective motions by introducing a multiplying factor F ($F \leq 1.0$) times ($kT + \varepsilon_{KIN}$) terms in the collision frequency expression. This factor describes eventually occurring instabilities by an "effective absorption" given by

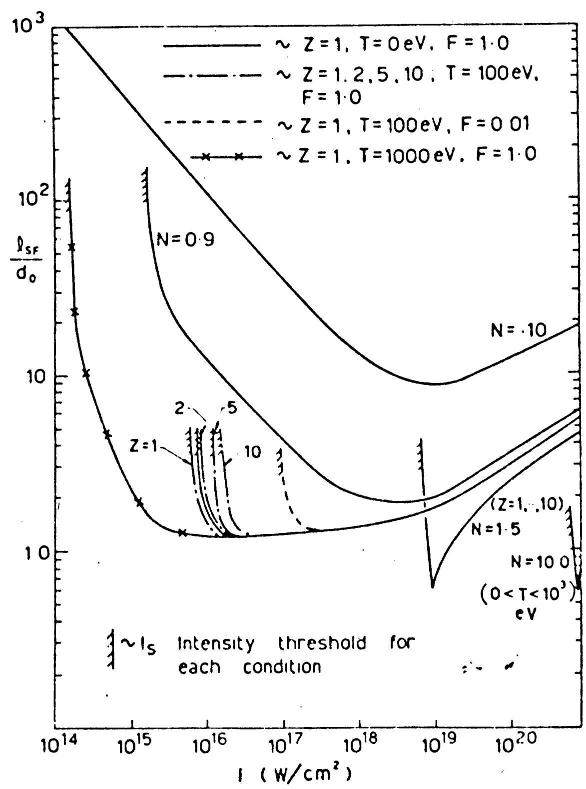

Fig. 4. Relativistic self-focusing length as a function of Nd glass laser intensity. Unlabeled curves are for $N = 1$.

an "effective collision frequency" $\nu_{eff} = \nu / F^{3/2}$. The results for $N = 1.0$, $T = 100$ eV, and $F = 0.01$ are shown in fig. 4. The minimum allowable intensity is increased by about an order of magnitude but the curve does merge with the other $N = 1.0$ distributions.

Finally, for $N = 1.0$ and 1.5, and $T = 100$ eV, fig. 4 shows the dependence on ion charge number for $Z = 1, 2, 5$, and 10. The Z-influence does not seem to be as great as for temperature; differences are negligible in the $N = 1.5$ situation. For the most part, the minimum value of l_{SF}/d_0 for a particular N is adequately determined in a $T = 10$ eV, $Z = 1$ calculation; the threshold intensity I_s for a physically correct relativistic self-focusing solution is nevertheless strongly dependent on T and Z.

Physically, the above results indicate the relativistic self-focusing is suddenly initiated as I_s is achieved, perhaps explaining the fast ion production[7,8]) resulting from self-focusing induced electron oscillation energies ε_{osc} of a few 10^5 eV. This leads to a nonlinear force expansion[9]) with translational ion energies ε_i given by exact integration[11]) of

$$\varepsilon_i = Z\varepsilon_{osc}, \tag{11}$$

with Z the ionic charge. The observed ion energies for Al^{11+} of 2 MeV [7]), or for W^{20+} of 2 MeV [8]) are then of the right order of magnitude. The energy deposited by the laser into the volume of the self-focused light cone corresponds reasonably well to the total energy of the accelerated plasma with MeV ions.

5. Entropy generation and radiation problems

For the calculations of the entropy generation in the numerical codes, the basic derivation of the equation of motion, of energy conservation and entropy generation has been studied. It was shown that a term proportional to the acceleration of plasma in the generalized thermodynamical force found in the relativistic theory[43]), can be obtained for a stationary system using the hypothesis of cellular equilibrium and introducing "constant conditions", in the energy current.

We can then write in general, the relation

$$\chi^q = \mathrm{grad}\, T + A\, \mathrm{d}v/\mathrm{d}t, \tag{12}$$

for the thermodynamical force χ^q causing the heat current, where T is the temperature, v is the barycentric velocity, and A is a constant depending on the density, and the following relation for the thermodynamical force of diffusion

$$\chi^d = \mathrm{grad}\, \eta + B\, \mathrm{d}v/\mathrm{d}t, \tag{13}$$

where η is the chemical potential and B is proportional to the density.

On the other hand considering the particular case of a set of particles, confined in a box, it was shown that it is possible to get the conservation laws for the number of particles and for the entropy from the conservation of the energy–momentum tensor. These expressions are similar to the formulae given by Landau and Lifshitz[44]) for the case of a fluid. They also agree with remarks by Tolman[45]) about the role of the mass and energy, in a relativistic theory.

These two results were obtained in connection with the formulation of thermodynamics of moving systems. The case of a body in motion in presence of an external field dependent on time still remains to be studied.

The case of a stationary field has been already solved for dielectrics, and also for a conductor using the Onsager theory[46]). Schmutzer gave a solution using the Onsager theory and taking into account the gravitational field[47]).

The way in which the conditions of thermodynamical equilibrium are changed by the presence of a variable field must be studied more closely. This is of particular importance since these conditions are basic to the application of the hypothesis of cellular equilibrium, the concept underlying the whole Onsager theory. For one special case, the problem of variable fields has been solved, namely for the generation of mechanical forces in the medium. The generated recoil due to the variation of the intensity of radiation in a homogeneous plasma[20]) is the same as the recoil of a constant radiation to an inhomogeneous plasma[9,19]).

Further problems of electrons in high intensity laser radiation were studied with respect to radiation losses in pair-production, the energy exchange, showing a defect compared to the case of Einstein[48]) for nonrelativistically moving molecules. Novak has used for these calculations the anharmonicity of the oscillators in the black-body radiation.

6. Conclusions

For the propagation of laser radiation in inhomogeneous plasmas, a more computationally economic code has been developed for exact solutions of the wave equation. The Osterberg problem of vanishing generation of local reflection has been explained by the WKB-like change of the wave amplitudes. The phase or intensity description of waves was studied within the problem of the Goos–Haenchen effect for application to the propagation of radiation in the surface of laser irradiated pellets. One consequence of the Goos–Haenchen application is the design of a laser amplifier with complete suppression of superradiance, which is highly necessary for laser compression of plasmas.

The corrections due to alpha penetration in high density plasmas has been calculated on the basis of the Bethe–Bloch formula. The generation of α-reheat was included into the codes for the calculation of gains by using a formula exactly covering the adiabatic cooling during expansion.

The relativistic self-focusing has been extended to critical densities and shows an unexpected result of short focusing lengths within the nonrelativistic region with a remarkable threshold at relatively low intensities. The thresholds correspond to the thresholds measurement of fast ions which destroy the ideal gasdynamic condition. The generation of oscillation energies of 100 keV and more for electrons is reproduced quantitatively as well as multi-MeV ion kinetic energies and their linear Z-dependence as exact solution of the nonlinear-force equation.

For the entropy generation a relativistic derivation is used including diffusion(chemical potentials) and the radiation interaction of electrons at very high intensities has been studied.

It is gratefully acknowledged that this work was realized only by the decissions of the University of New South Wales in favour of these activities, and by the support of Prof. E. P. George, Head of School of Physics. Some parts were funded by the Australian Research Grand Commission, Grant No. B75/15538.

References

1) H. Hora, Nucl. Instr. and Meth. 000 (1977).
2) H. Hora, *Laser Plasmas and nuclear reactions* (Plenum, New York, 1975).
3) J. H. Nuckolls, *Laser interaction and related plasma phenomena* (eds. H. Schwarz and H. Hora; eds. Plenum, New York, 1974) vol. 3B, p. 399.
4) C. Maglich, Nucl. Instr. and Meth. 119 (1974) 275.
5) R. C. Seamans and L. R. Hofstad, Nuclear News (May, 1975) p. 79.
6) H. G. Ahlstrom et al., Laser Focus (Sept. 1975); R. Hofstadter, J. Opt. Soc. Am. 65 (1975) 1204.
7) A. W. Ehler, J. Appl. Phys. 46 (1975) 2464.
8) M. R. Siegrist, B. Luther-Davies, and J. L. Hughes, Opt. Comm. 18 (1976) 603.
9) H. Hora, Phys. Fluids 12 (1969) 182.
10) A. Y. Wong and R. L. Stenzel, Phys. Rev. Lett. 34 (1975) 727.
11) H. Hora, Austr. J. Phys. 29 (1976) 375.
12) S. Rand, Phys. Rev. 136 (1964) 13231; T. P. Hughes and M. B. Nicholson-Florence, J. Phys. A(2) 1 (1968) 588; H. Hora, Opto-Electronics 2 (1970) 201.
13) J. Emmett, J. Nuckolls and L. Wood, Sci. Am. (June 1974), p. 24.
14) Yu. V. Afanasyev, N. G. Basov, P. O. Volosevich, E. G. Gamalii, O. N. Krokhin, S. P. Kurdyumov, E. I. Levanov, V. B. Rozanov, A. A. Samarskii and A. N. Tikhonov, JETP Lett. 21 (1975) 68.
15) J. W. Shearer and J. L. Eddleman, Phys. Fluids 16 (1973) 1522; H. Hora, Opto-Electronics 5 (1973) 491.
16) H. Hora, Jenaer Jb. (1957) p. 131.
17) H. Osterberg, J. Opt. Soc. Am. 48 (1958) 513.
18) V. Lawrence and H. Hora (to be published).
19) J. Lindl, P. Kaw, Phys. Fluids 14 (1971) 371.
20) R. Klima and V. A. Petrzilka, Czech. J. Phys. 1318 (1968) 1292.
21) Sir R. Peierls, Proc. Roy. Soc. (to be published).
22) R. L. Dewar, Energy–Momentum tensor, ANU Report (1976).
23) J. R. Shepanski, Am. J. Phys. A347 (1976) 475.
24) M. B. Nicholson-Florence, Thesis (Essex, 1973).
25) T. W. Kibble, Phys. Rev. 138B (1965) 740.
26) F. Goos and H. Haenchen, Ann. Physik 1 (1947) 333; J. L. Carter and H. Hora, J. Opt. Soc. Am C1 (1971) 1640.
27) H. Hora, Ann. Physik. 22 (1969) 402.
28) A. G. Engelhardt, T. V. George, H. Hora and J. L. Pack, Phys. Fluids 13 (1970) 212.
29) R. Renard, J. Opt. Soc. Am. 84 (1964) 1193.
30) F. Floux, D. Cognard, L. C. Denoeud, G. Piar, D. Parisot, J. L. Bobin, F. Dolebeau and C. Fauquignan, Phys. Rev. A1 (1970) 821.
31) D. Baboneau, G. di Bona, P. Chelle, M. Decroissette and J. Martineau, Phys. Letters 57A (1976) 247.
32) K. Hohla, ibid.
33) H. Hora and H. A. Ward, Letter-Patent Australia (1976).
34) C. J. Koester and E. Snitzer, Appl. Optics 3 (1964) 1182; A. A. Koloko, JETP Lett. 21 (1975) 324.
35) E. Goldman, Plasma Phys. 15 (1973) 289.
36) M. N. Rosenbluth, W. M. MacDonald and D. L. Judd, Phys. Rev. 107 (1957) 1.
37) E. Fermi and E. Teller, Phys. Rev. 72 (1947) 399.
38) E. Bagge and H. Hora, Atomkernenergie 24 (1974) 143.
39) P. S. Ray and H. Hora, Nucl. Fusion 16 (1976) 535.
40) R. Düchs and D. Pfirsch, in Proc. Int. Conf. on *Plasma and nuclear fusion*, Tokyo (Nov. 1974) (IAEA, Vienna, 1974) vol. 1.
41) H. Hora, J. Opt. Soc. Am. 65 (1975) 882.
42) M. R. Siegrist, Opt. Comm. 16, no. 3 (1976) 402, J. Appl. Phys. 47 (July, 1976).
43) G. A. Kluitenberg, S. R. DeGroot and P. Mozer, Physica 19 (1953) 690.
44) L. D. Landau and E. M. Lifshitz, *Fluid mechanics* (Pergamon, London, 1959) pp. 499–506.
45) R. C. Tolman, *Relativistic thermondynamics and cosmology* (Clarendon, Oxford, 1958) p. 121.
46) L. D. Landau and E. M. Lifshitz, *Electrodynamics of continuous media* (Pergamon, London, 1956) pp. 47, 92–126.
47) E. Schmutzer, Exp. Tech. Phys. 22 (1975) 393.
48) A. Einstein, Z. Physik 18 (1917) 121.

NUMERICAL CALCULATIONS OF LASER INTERACTION WITH PLASMAS INCLUDING MOMENTUM TRANSFER OF THE NONLINEAR FORCES*)**)

V.F. Lawrence and H. Hora

Dept. of Theoretical Physics, The University of New South Wales, Kensington, NSW Australia

Abstract

In order to study the action of the nonlinear force of electrodynamic laser-plasma interaction without thermalization, numerical calculations with a very general two-fluid numerical code were performed including nonlinear variation of the optical constants (dependence of the collision frequency on the laser intensity) and detailed description of the reflection of laser radiation based on Maxwell's equations. For laser pulses of less than 1 psec, the dynamics are characterized by the nonlinear force mainly. Using Rayleigh-like density profiles, the generation of instabilities as well as their suppression has been demonstrated. The energy transferred to two thick blocks of plasma (one moving against the laser light, the other with it under compensation of momentum) increases nearly quadratically on the laser intensity.

---

*) Presented at the Fourth International Workshop Conference on "Laser Interaction and Related Plasma Phenomena" at Rensselaer Polytechnic Institute, Troy, New York, 8-12 November, 1976.

**) Supported by the ARGC grant No. B75/15538.

I. INTRODUCTION

Plasma dynamics for the interaction of high intensity laser radiation with solid targets and the instantaneously generated plasma, can be determined by the nonlinear force which is the immediate electrodynamic interaction, and by the gasdynamic pressure occuring after thermalization of the radiation and heating of the ions. The basic properties of these nonlinear forces have been developed over the last ten years[1-7] and the expansion of plasma and the subsequent compression has been demonstrated numerically[7-9] and experimentally[10,11], as well as indirectly by self focussing and generation of fast ions or fast plasma groups and ion separation by the charge number Z.[7]

The importance of the action of the nonlinear force, especially for short laser pulses (for neodymium glass lasers around 1 to 10 psec and for CO_2 lasers around .1 to 1 nsec) consists of the possibility of a non thermalizing transfer of optical energy into kinetic energy of plasma for compression, which has a minimum of entropy production and is therefore highly efficient. Followed by an isentropic compression, the same fusion reaction yields can be reached with about 1000 times less laser energy[12] than in the case of the gasdynamic laser compression scheme of Nucholls[13]. As the laser pulses have to be about 20 times less than in the Nucholls case the total advantage is that the required laser system could be smaller by a factor of 50, when using non linear force compression, based on a rough calculation. The advantage of less complications (instabilities) at short interaction times and the use of, experimentally verified[4], fast blocks of ions (fast ions[7]) as well as avoidance of the necessary delay due to thermalization[14] (all disadvantages in the Nucholls scheme) may be reasons enough to orient efforts towards the nonlinear force compressions. The use of high intensity CO_2 lasers[15] will necessarily require such a scheme, as the thermalization delay has been neglected unawares in numerical calculation of gasdynamic compression models, otherwise it would require[14] laser pulses of 10 nsecs or more.

The non linear force compression has not been studied numerically to the same extent as the gasdynamic compression. As the necessary laser intensities have only become available over the last two years a very intensive study is necessary now. This paper presents results of a very general one-dimensional code, where we used initial electron densities $n_e(x)$ of the Rayleigh type

$$n_e(x) = n_{ec}\left(1 - \frac{1}{(1+\alpha x)^2}\right) \qquad (1)$$

where $x>0$ and α is a constant. Equation (1) corresponds to a refractive index $\tilde{n}$ of

$$\tilde{n} = \frac{1}{1+\alpha x} \qquad (2)$$

for which the laser penetrates with a minimum of reflectivity[16].

II. THE ONE-DIMENSIONAL CODE

The calculations were based on a modified numerical code of which the very general gasdynamic part had been developed by E. Goldman[17] and the nonlinear forces have been included in the following way. All quantities depend on the one spatial coordinate α only and laser light is incident from +x. Electrons and ions are separately treated (index i and e) where fully ionised preferably DT-plasma or LiD plasma is presumed. The equations of continuity for the densities $n_{e,i}$ or velocity $v_{e,i}$ is

$$\frac{\partial n_{e,i}}{\partial t} + \underline{\nabla}\cdot(n_{e,i}\,\underline{v}_{e,i}) = 0 \qquad (3)$$

and the equation of motion (force density) contains the temperatures $T_{e,i}$ (k∿Boltzmann constant) and the electric and magnetic field strengths $\underline{E}$ and $\underline{H}$ for linearly polarized laser radiation describing the terms of the nonlinear force

$$m_i\left(\frac{d}{dt}v_i + v_i\frac{d}{dx}v_i\right) = -\frac{d}{dx}n_i kT_i \qquad (4)$$

$$m_e\left(\frac{d}{dt}v_e + v_e\frac{d}{dt}v_e\right) = -\frac{d}{dx}n_e kT_e + \frac{d}{dx}(E^2+H^2)(8\pi) \qquad (5)$$

The equation of energy conservation

$$\tfrac{1}{2}\frac{\partial}{\partial}\, n_{e,i}m_{e,i}v_{e,i}^2 = -kT_{e,i}\frac{d}{dt}n_{e,i} - n_{e,i}k\frac{d}{dt}T_{e,i} + W_{e,i} \qquad (6)$$

$T_{e,i}$ contains the change of the temperature both by the gasdynamic (adiabatic) motion as well as by thermal conductivity, using the collision frequency

$$\nu = \frac{\omega_p{}^2 \pi^{3/2} m_e{}^{1/2} e^2 \ln\Lambda}{8\pi(2kT_e)^{3/2}} \tag{7}$$

with the plasma frequency ω_p, coulomb logarithm $\ln\Lambda$, mass m_e and charge of electron e. The power density of thermal energy input from the laser field at each x is given by W_i, where the exact nonlinear optical constant was used

$$\tilde{n}^2 = 1 - \frac{\omega_p{}^2}{\omega^2+\nu^2}\left(1 + i\frac{\nu^x}{\omega}\right) \tag{8}$$

where ν^x was identical with ν of Eq. (7), however including the energy ε_{osc} of the electrons from the quivering oscillation in the laser field[7] by substituting T_e by $T = T_e + \varepsilon_{osc}/k$, W_i is determined by the heating of the ions by the difference $T_e - T_i$ including the delay given by the collision frequency ν. The coupling of the equations of the ions and electrons is due to Poisson's equation. The six equations (3)to (6) determine the six variables n_e, n_i, v_e, v_i, T_e, T_i in dependence on x and the time t. Further, initial condition (variables at t = 0) and boundary conditions (time dependent indent laser field) have to be chosen. The laser field is being calculated for each time step numerically as a solution of the Maxwellian equations.

III. INITIAL AND BOUNDARY CONDITION

In the following calculation, laser pulses were chosen with a $\sin^2\beta t$ amplitude such that after realising the first maximum the laser intensity is constant. β was chosen to reach this level at a time t=0.15psec. The initial conditions were chosen as

$$T_{i,e}(x;t = 0) = 100\ \text{eV} \tag{9}$$

$$v_{e,i}(x;t = 0) = 0 \tag{10}$$

and $n_{e,i}(x;t = 0) = n_o(x)$ has been selected from the experience of the Rayleigh case[7,12,16] for neodymium glass laser radiation with $[n_o] = \text{cm}^{-3}$

$$n_o(x) = \begin{cases} 0; & x \geq 50\mu \\ 10^{21}\{1 - \frac{1}{(1-\alpha[x-50\mu])^2}\}; & 0 \leq x \leq 50\mu \\ 10^{21}\{1 - \frac{1}{(1+\alpha[x+50\mu])^2}\}; & -50\mu \leq x \leq 0 \\ 10^{18}; & x \leq -50\mu \end{cases} \quad (11)$$

to avoid total reflection[16], α has to fulfil the following restriction

$$x < \alpha_o = \frac{2\omega}{c} = 1.7 \times 10^5 \text{ cm}^{-1} \quad (12)$$

for neodymium glass laser radiation. It has to be noted[16] that the reflections at $x = \pm 50\mu$ and $x = 0$ are remarkably small in the collisionless case $(\nu^x = 0)$ if $\alpha < 0.5\alpha_o$. The case of collisions results in modifications which will be reproduced by the programme automatically.

IV. GENERATION OF INSTABILITIES

From the numerous cases calculated, we describe the one where the generation of strong reflection has been generated in an early stage. The standing wave pushes the plasma towards the modes and the generated rippling of the density is parametrically increasing the reflection. The case of Fig. 1 we find $(E^2+H^2)/8\pi$ (corresponding fairly to the intensity) with one local maximum at the time where the laser reaches the maximum intensity. It is remarkable that this maximum is not at $x = 0$, where the initial density maximum is, as the absorption and the intensity dependence of the optical constants modify the laser field. The maximum corresponds to an intensity $I = I_{vac}/|\tilde{n}|$ related to its vacuum value I_{vac} by a swelling factor $\theta = 1/|\tilde{n}| \approx 7$ only the reached plasma velocity up to this time is shown in Fig. 2. and the electron density in Fig. 3. The velocity

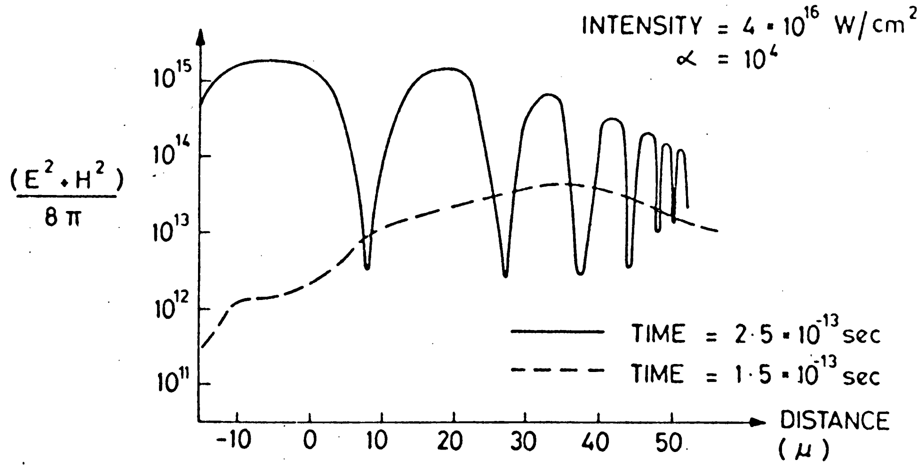

Fig. 1: Calculation of $(E^2+H^2)/8\pi$ for $\alpha=10^4$ at an intensity 4×10^{16} W/cm^2 at the times 1.5×10^{-13} sec and 2.5×10^{-13} sec.

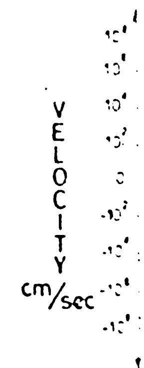

profile at t = 0.15 psec is positive from x = 50μ down to 35μ which corresponds to an expansion (ablation) of this part of the plasma corona as a thick block with velocities up to 10^7 cm/sec, while the plasma below 35μ is moved as a whole block to the interior of the plasma (towards negative x). The density at that time (Fig. 3) shows very well a similar profile as the initial one, Eq. (11), especially the Rayleigh-like decay at 40 to 50μ. But it is remarkable, that the initial maximum at x = 0 has been moved to a value of 3.8μ which is due to some internal compression of the block moving towards -x, as the velocity profile is not constant. The generation of an instability can be seen at the time t = 0.45 psec, where the $(E^2+H^2)/8\pi$ (Fig. 1) is oscillating, corresponding to a standing wave. The velocity has then changed drastically into the oscillating profile of Fig. 2. The maxima and

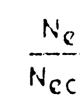

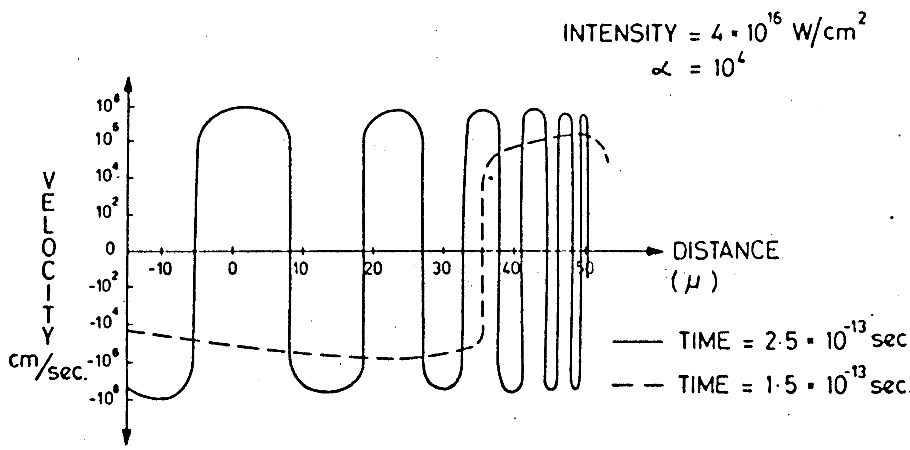

Fig. 2: Velocity profiles corresponding to the case of Fig. 1

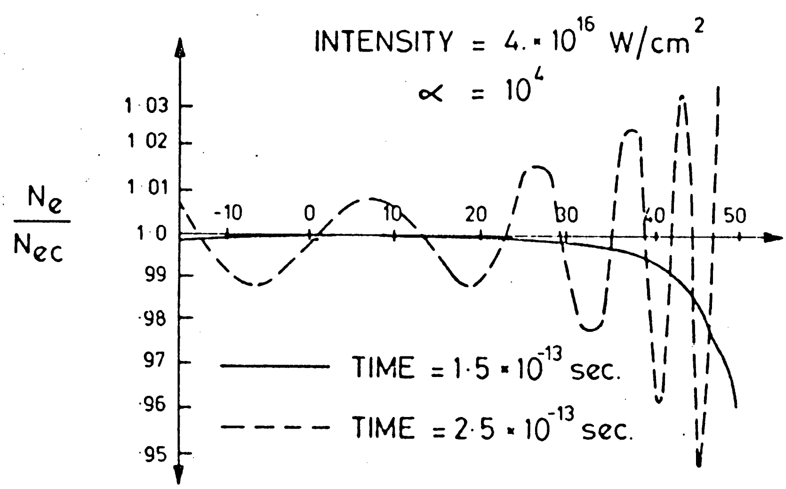

Fig. 3: Electron density (related to the cut off density) corresponding to the cases of Fig. 2.

minima correspond very close to the vacuum wave length $\lambda=\lambda_{vac}$ at $x = 50\mu$, while a swelling $\lambda=\theta\lambda_{vac}$ of $\theta=9$ around x=0 can be seen. The density (Fig. 3) shows a ripple, easily understood by the motion due to Fig. 2. The following time steps show a very high reflectivity because of this Brillouin type dynamic instability[18].

V. ACCELERATION OF BLOCKS

Compared to the cases of Fig. 1 to 3, the situation is quite different, if an $\alpha=5\times10^4$ cm^{-1} and a maximum intensity of 10^{16}W/cm^2 is used (Fig. 4 and 5). It is

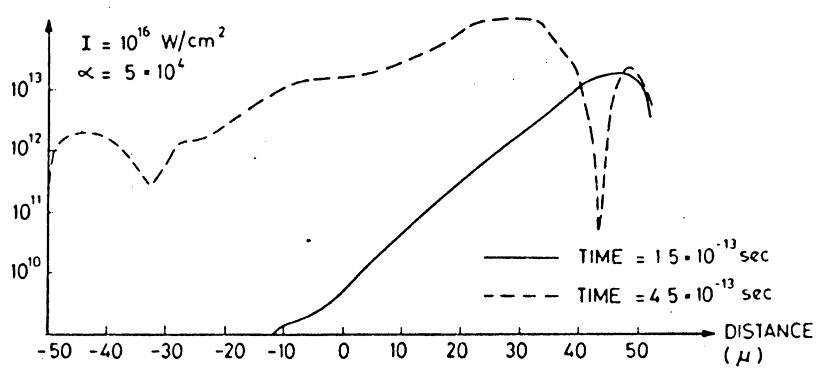

Fig. 4: Spatial profiles of $(E^2+H^2)/8\pi$ for a case with initial electron densities of Eq. (11) using $\alpha=5\times10^4$cm^{-1}, maximum laser intensity of 10^{16}W/cm^2 at the times 0.15 psec and 0.45 psec.

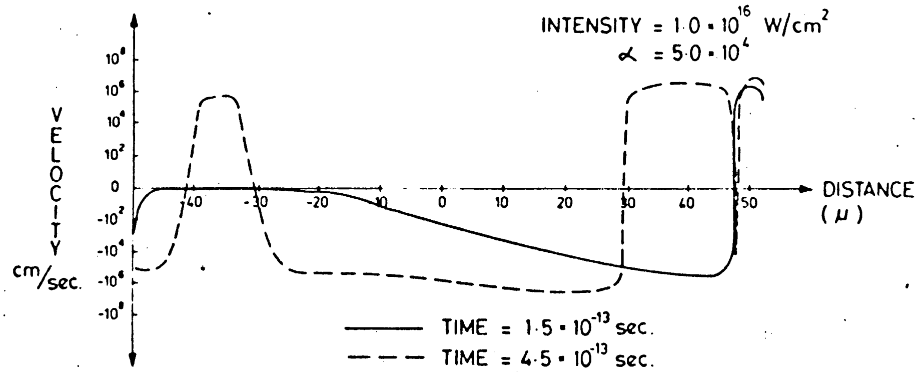

Fig. 5: Velocity profiles of the case of Fig. 4.

remarkable that at the early time 0.15 psec, the laser intensity has a maximum near 40μ (swelling 14) and then drops strongly towards x = 0. This is due to the fact that an $\alpha=5\times10^4$ cm^{-1} causes a density very close to the cut-off density, and the less intensity than the former case causes a less decrease of the collision frequency by the intensity dependent nonlinearity of ν^x in Eq.(8). Nevertheless, at t = 0.45 psec, the swelling of the intensity (θ=120) at x = 30μ lets the light penetrate through the whole plasma without standing wave pattern (these did not appear even at later times) where the plasma was then (Fig. 5) moving in two blocks, from 30 to 50μ towards +x (ablation) and far less than 30μ towards -x (compression). The modification near -35μ is understandable from the minimum of $(E^2+H^2)/8\pi$ near x = -35μ.

By a systematic search it was possible to find a series of cases where only a two block motion appeared for varying intensities and constant α with a separation of the blocks around the same depths x(±3μ).

Evaluation was made of the amount of kinetic energy E_k thathad been transferred by the nonlinear force which both the gasdynamic expansion and the thermokinetic acceleration had neglected. We have evaluated

$$E_k(I) = \frac{1}{x_2 - x_1} \int_{x_1}^{x_2} \frac{m_i n_i v_i^2}{2} \, d\xi \qquad (13)$$

for dependence on the laser intensity (Fig. 6). The

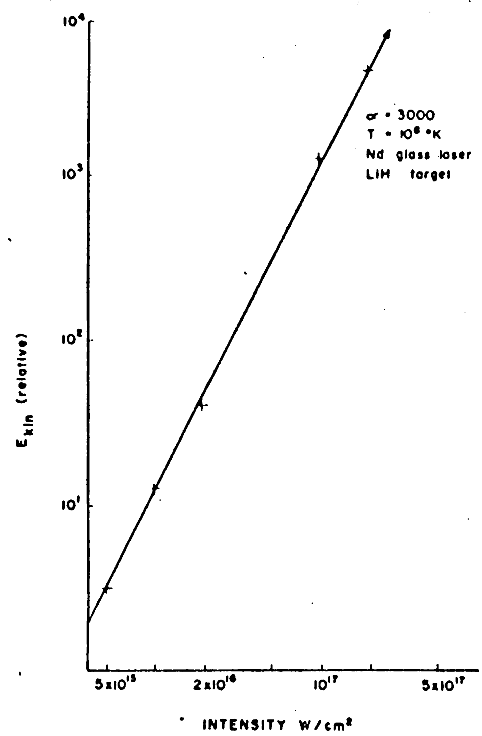

Fig. 6: Kinetic energy transferred to the plasma $E_k(I)$, Eq. (13) for $\alpha = 3\times10^3 cm^{-1}$ up to a constant time t = 0.1 psec for independent temporal laser profiles.

result is that the transferred kinetic energy is increasing nearly quadratically against the neodymium glass laser intensity,

$$E_{kin} = \text{const} \times I^{1.8} \quad (5\times10^{15} < I < 10^{18}\ \mathrm{W/cm^2}) \tag{14}$$

expressing the nonlinear nature of the interaction. The energy transfer is a nonlinear, macroscopic, electrodynamic absorption process.

VI. CONCLUSION

The nonlinear force of laser plasma interaction showed various properties from numerical calculations for neodymium glass laser radiation of more than 10^{15} W/cm^2 intensity. The generation of strong reflection and that a standing wave could be generated from an initial Rayleigh density profile where nearly no reflection is expected for collisionless plasmas is unexpected. The reason for this behaviour is understandable from the intensity dependent thermal absorption process. Other cases show a nearly ideal transfer of the laser radiation into a block moving against the laser radiation and another in the same direction. The transferred energy was quadratically increasing against the laser light intensity. The momentum of each block was just compensating the momentum of the corresponding block moving in the opposite direction. Preliminary results for times of 5 psec were similar which confirms that the neglect of the retardation of the laser field in the numerical code is not important for the kinetic processes discussed here.

REFERENCES

1. H. Hora, D.Pfirsch and A. Schülter, Z. Naturforschung 22A, 278 (1967).

2. H. Hora, Phys. Fluids 12, 182 (1969); 17, 939 (1974); 17, 1042 (1974).

3. J. Lindl and P. Kaw, Phys. Fluids 14, 2714 (1971).

4. J.W. Shearer and J.L. Eddkeman, Phys. Fluids 16, 1753 (1974).

5. J.A. Stamper and S.E. Bodner, Phys. Rev. Letters 37, 435 (1970).

6. V.A. Klima and V.A. Petrzilka, Cz.J.Phys. B22, 896 (1972).

7. H. Hora, Laser Interaction and Related Plasma Phenomena, H. Schwarz and H. Hora eds. (Plenum, New York) 1971, Vol. 1 p. 383; 1972, Vol. 2, p. 341; 1977, Vol. 4, p. 841. Laser Plasmas and Nuclear Energy (Plenum, New York, 1975).

8. J.W. Shearer, R.E. Kidder and J.W. Zink, Bull.Am. Phys.Soc. 15, 1483 (1970).

9. K.A. Brueckner, Laser Interaction and Related Plasma Phenomena, H. Schwarz and H. Hora eds. (Plenum, New York) 1977, Vol. 4, p. 891.

10. M.E. Marhic, Phys. Fluids 18, 837 (1975).

11. A.Y. Wong and R.L. Stenzel, Phys. Rev. Letters 34, 727 (1975); R.L. Stenzel, Phys. Fluids 19, 865 (1976).

12. H. Hora, Sov. J. Quantum Elect. 6, 154 (1976).

13. J. Nucholls, Laser Interaction and Related Plasma Phenomena, H. Schwarz and H. Hora eds. (Plenum, New York) 1974, Vol. 3B, p. 395

14. H. Hora, Aust. J. Phys. 29, 375 (1976).

15. K. Boyer, Astonautics and Aeronautics, Vol. 11, No. 1, 28 (1973); G.H. McCall, D.V. Giovanielli and J.F. Kephart, Proc. 8th Conf. Laser and Nonlinear Optics, Tbilissi, May 1976, p. 287.

16. H. Hora, Jenaer Jahrbuch 1957, p. 131; H. Osterberg, Jour. Opt. Soc. Am. 48, 513 (1968).

17. E. Goldman, Plasma Physics 15, 289 (1973); H. Hora, E. Goldman and M. Lubin, Univ. Rochester -LLE Rept. No. 21 (1974).

18. F.F. Chen, Laser Interaction and Related Plasma Phenomena, H. Schwarz and H. Hora eds (Plenum, New York) 1974, Vol. 3A, p. 291.

bulletin

OF THE AMERICAN PHYSICAL SOCIETY

OCTOBER 1976

1 A-16 Propagation of Laser Radiation in Inhomogeneous Plasma and Dynamic Properties.* V. F. LAWRENCE and H. HORA, Dept. Theor. Phys., UNSW, Kensington-Sydney, Australia. --In order to calculate the nonlinear (ponderomotive) forces[1] and the momentum transfer in laser irradiated inhomogeneous plasma, the exact knowledge of the solution of the Maxwellian equation for plane waves is necessary. The standard approximation of inhomogeneous plasma with steps of constant refractive index is studied numerically with high precision. The comparison with the exactly known case of Rayleigh's profiles of the refractive index, shows a clear discrepancy, which may explain the high difference in measured and calculated reflectivities of laser produced plasmas, even as long as nonlinearities and anomalies are excluded. Using the nonlinear intensity dependence of the refractive index and of the absorption, the direct transfer of laser energy into kinetic energy of plasma is calculated preferably for cases of the Rayleigh profiles for isentropic coupling and compression of plasma.

*Supported by ARGC grant no. 15-001-71

[1] H. Hora, Phys. Fluids, 12, 182 (1969).